4th POST-OPERATIONS CROSS-CALIBRATION STATUS REPORT

P. García-Lario[1]

SAI/2000-063/Rp, Version 1.0

January 8, 2001

[1] ISO Data Centre, Astrophysics Division, Space Science Department of ESA,

Document Information

Document:	4th Post-Operations Cross-Calibration Status Report
Title:	4th Post-Operations Cross-Calibration Status Report
Reference Number:	SAI/2000-063/Rp
Issue:	Version 1.0
Issue Date:	8 January 2001
Authors:	P. Garcia-Lario

Document Change Record

Date	Revision	Comments
28 Nov 2000	Version 0.1	First Draft
03 Dic 2000	Version 0.2	Chapter 4 updated
06 Dic 2000	Version 0.3	Section 3.4.7 added
07 Dic 2000	Version 0.4	Minor updates
08 Jan 2001	Version 1.0	External version

Contents

1 Introduction **1**

1.1 Scope . . . 1
1.2 Structure of cross-calibration activities . . . 1
1.3 Final Goals: General . . . 2
1.4 Final Goals: per Working Group . . . 3
1.4.1 Beam Profiles/Pointing . . . 3
1.4.2 Glitches . . . 3
1.4.3 Line profiles . . . 3
1.4.4 Photometric calibration . . . 3
1.4.5 Polarisation . . . 4
1.4.6 Spectral Matching and RSRF . . . 4
1.4.7 Transients . . . 4
1.4.8 Interactive Analysis . . . 4

2 Review of Cross-Calibration Plan **5**

2.1 Overview of Working Group activities . . . 5
2.2 Report on actions on-going and/or closed . . . 5
2.2.1 Beam Profiles/Pointing: . . . 5
2.2.2 Glitches: . . . 17
2.2.3 Line profiles: . . . 23
2.2.4 Photometric calibration: . . . 27
2.2.5 Spectral Matching and RSRF: . . . 33
2.2.6 Transients: . . . 36
2.2.7 Interactive Analysis: . . . 49
2.2.8 Polarisation: . . . 53

3 Internal and external cross-calibration **56**

3.1 The concept of cross-calibration . . . 56
3.2 Definition of standard and cross-calibration sources . . . 56
3.3 A new cross-calibration strategy . . . 57
3.3.1 Introduction . . . 57
3.3.2 Internal and external cross-calibration . . . 58
3.3.3 Comparison with models . . . 60

3.4 Cross-calibration comparisons . . . 61
3.4.1 Sources observed with SWS, CAM-CVF and PHT-S . . . 61
3.4.2 Cross-calibration of sources observed with IRAS and ISO SWS . . . 70
3.4.3 Cross-calibration of sources observed with MSX and ISO SWS . . . 75
3.4.4 Cross-calibration of sources observed with IRAS and ISO LWS . . . 77
3.4.5 ISOPHOT versus COBE/DIRBE . . . 80
3.4.6 Comparison between ISO and KAO line fluxes . . . 82
3.4.7 Cross-Calibration comparisons with models . . . 83

4 Calibration accuracies and 'Error Budget' 91
4.1 PHT . . . 91
4.1.1 Improvements in OLPv9.0 for PHT . . . 91
4.1.2 Current calibration accuracies and 'Error Budget' for PHT . . . 93
4.1.3 Future plans in PHT calibration . . . 94
4.2 SWS . . . 98
4.2.1 Improvements in OLPv9.5 for SWS . . . 98
4.2.2 Current calibration accuracies and 'Error Budget' for SWS . . . 99
4.2.3 Future plans in SWS calibration . . . 103
4.3 CAM . . . 103
4.3.1 Improvements in OLPv9.5 for CAM . . . 103
4.3.2 Current calibration accuracies and 'Error Budget' for CAM . . . 104
4.3.3 Future plans in CAM calibration . . . 106
4.4 LWS . . . 107
4.4.1 Improvements in OLPv8.7 for LWS . . . 107
4.4.2 Current calibration accuracies and 'Error Budget' for LWS . . . 107
4.4.3 Future plans in LWS calibration . . . 111

Chapter 1

Introduction

1.1 Scope

This is the fourth of a series of Reports generated every six months by the ISO Data Centre (IDC, hereafter) which tries to summarize the up-to-date status (as of November 2000) of (cross-)calibration activities during the ISO Post-Operations Phase (POPS, hereafter).

It includes information on the latest achievements in the calibration of all four ISO instruments with special emphasis on cross-calibration aspects as well as an assessment of the progress made in the last six months within the framework of the POPS Cross-Calibration Plan.

The previous Status Reports can be found respectively at:

`http://www.iso.vilspa.esa/users/expl_lib/ISO/1st_status_report_ext.ps.gz`

`http://www.iso.vilspa.esa/users/expl_lib/ISO/2nd_status_report_ext.ps.gz`

and

`http://www.iso.vilspa.esa/users/expl_lib/ISO/3rd_status_report_ext.ps.gz`

This series of Status Reports will culminate in the Final POPS Cross-Calibration Status Report to be issued in April 2001, containing, among other things, a compilation of the Final Reports provided by each of the ISO Calibration Working Groups (see below), the final status of internal and external Cross-Calibration of ISO with other ground-based and space facilities, and the final estimations made for the accuracy of OLP data products with caveats and recommendations for the users of the ISO Legacy Archive.

1.2 Structure of cross-calibration activities

The global IDC strategy for approaching cross-calibration during the Post-Operations phase, as described in the ISO POPS Cross-Calibration Plan, is based on topic-oriented Working Groups, each one of them addressing one specific calibration topic.

Working Groups (WGs, hereafter) are formed by members from the IDC and from the different NDCs. They are also open to contributions from external individuals interested in actively participating in ISO calibration activities.

Eight Working Groups (WGs, hereafter) were created during Post-Operations and seven of them are still actively working on:

- Beam Profiles/Pointing
- Glitches
- Line profiles
- Photometric calibration
- Spectral Matching and RSRF
- Transients
- Interactive Analysis

Note that the activities of the Polarisation WG (the 8th WG) are considered now completed with the release of the ESA SP series proceedings *"ISO Polarisation Observations"* ESA SP-435, December 1999. No further work is planned on CAM polarisation calibration and only update notes will be provided for PHT as appropriate.

Of course, the topics addressed by each of these WGs overlap in many cases since many cuts through the calibration issue are possible. For example, studies of *Transients* are fundamental to a full understanding of the instruments' photometric calibration, which is the main goal of the *Photometric Calibration* WG. The WG scheme provides them with a platform to exchange their knowledge and to progress with respect to their own subject.

It is the responsibility of cross-calibration manpower to maintain an overview of the work of the several Working Groups, cooperate with instrument-specific calibration manpower in efforts to understand inconsistencies of calibration relevant to more than one instrument and establish links between the different Working Groups when necessary favouring a fluid exchange of useful information.

An up-to-date overview of the composition of each of these WGs can be found at:

`http://www.iso.vilspa.esa.es/users/expl_lib/ISO/WG_COMPOSITION_3.PS`

1.3 Final Goals: General

The objectives of cross-calibration can be summarized as follows:

- Compare the results of different ISO instruments and verify the errors quoted for each instrument-specific calibration. Where these results appear to be inconsistent seek to understand and to eliminate those differences.
- Compare ISO results with external data (e.g. ground based observations, KAO data, IRAS, MSX, COBE,..). Where results appear to be inconsistent seek to understand and to eliminate those differences.
- Verify that, from a more global point of view, the calibrations of the individual ISO instruments are correct, and ensure a certain level of homogeneity and consistency of the data and how they were calibrated (e.g. compatibility of models, bandpass zero-points, and of calibration philosophy and procedures).

The intention is to have a flexible plan/strategy with these goals as a reference which is materialized in a detailed schedule of cross-calibration activities for each of the Working Groups listed above.

Responsibility for cross-calibration planning is with the IDC in close interaction with the NDCs, which are responsible for instrument-specific calibration.

1.4 Final Goals: per Working Group

1.4.1 Beam Profiles/Pointing

· Characterization of the instruments' beam profiles.

· Address common problems (asymmetries, vignetting, ghosts,..) and their possible relation to the ISO telescope point spread function (PSF).

· Allow cross-fertilisation of models available.

· Evaluation of common deconvolution tools, to apply to extended source data, once beam profile calibration files become available.

· Support improvement of ISO pointing reconstruction in OLP.

1.4.2 Glitches

· Statistical analysis and characterization of glitches in the four ISO instruments. Study of the relation with the space radiation environment.

· Compare glitch statistics and glitch height distributions with model predictions and simulations.

· Enhance the quality of the reduced ISO data, improving the de-glitching and de-tailing algorithms in the pipeline and/or IA.

· Keep the knowledge on the radiation environment and its effects on the detectors, so that it can be applied to future missions.

1.4.3 Line profiles

· Characterize the SWS and LWS observed instrumental profiles.

· Study the stability of these instrumental profiles as a function of time, forward and backward scans, detector, line strength and point-like versus extended sources.

· Analysis and interpretation of deviations found from line profile definition; recommendations and caveats.

· Comparison with theoretical instrumental profiles and resolution.

1.4.4 Photometric calibration

· Definition of the photometric system and description of calibration sources/ models used in ISO data reduction.

· Characterization of the photometric accuracies achieved by each ISO AOT (and the corresponding photometric 'error budget').

· Make periodic 4-instrument photometric comparisons on selected sample targets and extend this comparison to calibration models and to photometric results obtained with other facilities (IRAS,MSX,COBE, ground-based,..) using OLP data products.

- Make similar comparisons on a subsample of targets using data reduced with the latest available versions of the instrument IAs and compare this with OLP photometric accuracies.
- Testing of photometric improvements as new algorithms or calibration files become available stimulating their inclusion into the corresponding IAs first and eventually into the pipeline.
- Identification and analysis of photometric calibration problems affecting OLP data products providing recommendations and caveats to the users of the ISO Legacy Archive.

1.4.5 Polarisation

- Characterization of the polarimetric capabilities of ISO. Angles, detection limits, wavelength dependency, internal consistency (PHT,CAM) and comparison with external data.

1.4.6 Spectral Matching and RSRF

- Analysis of spectral matching between LWS and SWS in the overlapping region. Same with CAM-CVF and PHT-S spectra. Comparison with models.
- Identification of possible systematic errors in the measured spectral response to extended sources by comparing the observations from a variety of instruments. Effects on the determination of spectral line fluxes.
- Expansion of cross-calibration between the instruments beyond the wavelength regions which they have in common.
- Characterization of the Relative Spectral Response Function (RSRF) for all ISO spectroscopic modes.

1.4.7 Transients

- Characterize transient effects in the 4 ISO instruments and determine the best correction method as a function of detector type, observing mode and characteristics of the source, and estimation of effects on photometric accuracy.
- Stimulate the development and implementation of S/W tools to detect and correct transient effects in IAs first and eventually in the pipeline.

1.4.8 Interactive Analysis

- Coordinate the information flow between developers of the different instruments' IAs, making sure that each team is aware of what other teams are doing and that S/W tools developed by one of the teams are made available to other teams if they consider it useful.
- Stimulate the implementation of new S/W tools in the four ISO instruments' IAs.
- Raise the profile of the various IA packages as means to enhance data reduction.
- Investigate communication channels between the IA users and IA developers in both directions.

Chapter 2

Review of Cross-Calibration Plan

2.1 Overview of Working Group activities

As it is defined in the ISO POPS Cross-Calibration Plan, the WGs should:

- look at major calibration issues across instrument boundaries
- identify problems, (interim-)goals and milestones (usually linked to OLP milestones)
- trigger/recommend further work, and recognise imperatives in their area
- establish and pursue relevant contacts in NDCs
- identify good calibration sources and strategies.

2.2 Report on actions on-going and/or closed

A number of actions proposed in the last version (3.0) of the ISO POPS Cross-Calibration Plan, have been closed in the last six months. In the following, a summary of the main results found and conclusions reached is provided, sorted by WG. In some cases, the activities described below were not directly carried out by members of the WG but they are included because they are considered to be relevant for the future planning of the WG or to illustrate a progress on the current understanding of a problem under analysis by that specific WG.

Note that reports on other actions closed before June 2000 can be found in the previous issues of this document (First, Second and Third POPS Cross-Calibration Status Reports).

2.2.1 Beam Profiles/Pointing:

```
BP: Proceedings of the Workshop:  "ISO Beyond point sources:
     studies of extended  infrared emission" held at VILSPA
     (September 14-17, 1999)
```

The Proceedings of this Workshop are going to be published in volume 455 of the ESA Special Publication Series.

Before it becomes available, the final programme and abstracts of the presentations given can be found at:

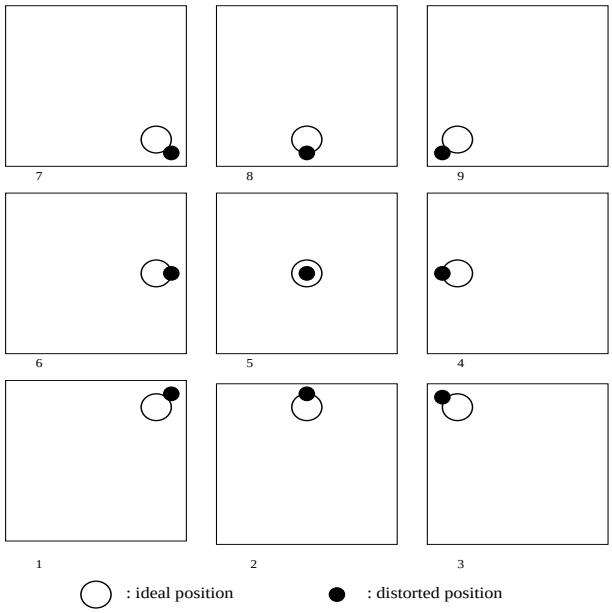

Figure 2.1: *Distorted raster observation of a point source with ISOCAM - ISO CAM Handbook*

`http://www.iso.vilspa.esa.es/meetings/isobeyond/fourth_announcement.html`

Full papers presented at the Meeting by different members of this WG are available under request at `helpdesk@iso.vilspa.esa.es`.
This includes the following presentations:

- *"The ISO point spread function and CAM beam profile"* by Koryo Okumura,
- *"An investigation of the ISO LWS beam profile and fringing"* by Chris Lloyd,
- *"ISOPHOT aperture profiles and background measurements"* by Thomas Müller,
- *"ISOPHOT aperture sequences on point- and extended sources"* also by Thomas Müller, and
- *"ISO Beam Profiles and extended source flux calibration"* by Alberto Salama.

`BP: Field distortion corrections in ISOCAM data`

ISOCAM images present a field distortion whose amplitude depends on the lens which determine the pixel-field-of-view (p.f.o.v., hereafter) of the image. The differences between the ideal positions and the real measurements (Figure 2.1) are known to occur because of all the optical elements encountered in the beam path. It is important to correct for this instrumental effect especially when co-adding maps from a raster observation.

Field distortion increases with the p.f.o.v. and has been derived for the LW channel $6''$ and $3''$ lenses, from particular CAM data sets using calibration observations of fields that contained many stars. No measurements were made for the $1.5''$ lens because the distortion is in general cases small and the measurements too difficult to perform as the amplitude of the satellite jitter is of the order of the quantities to be measured.

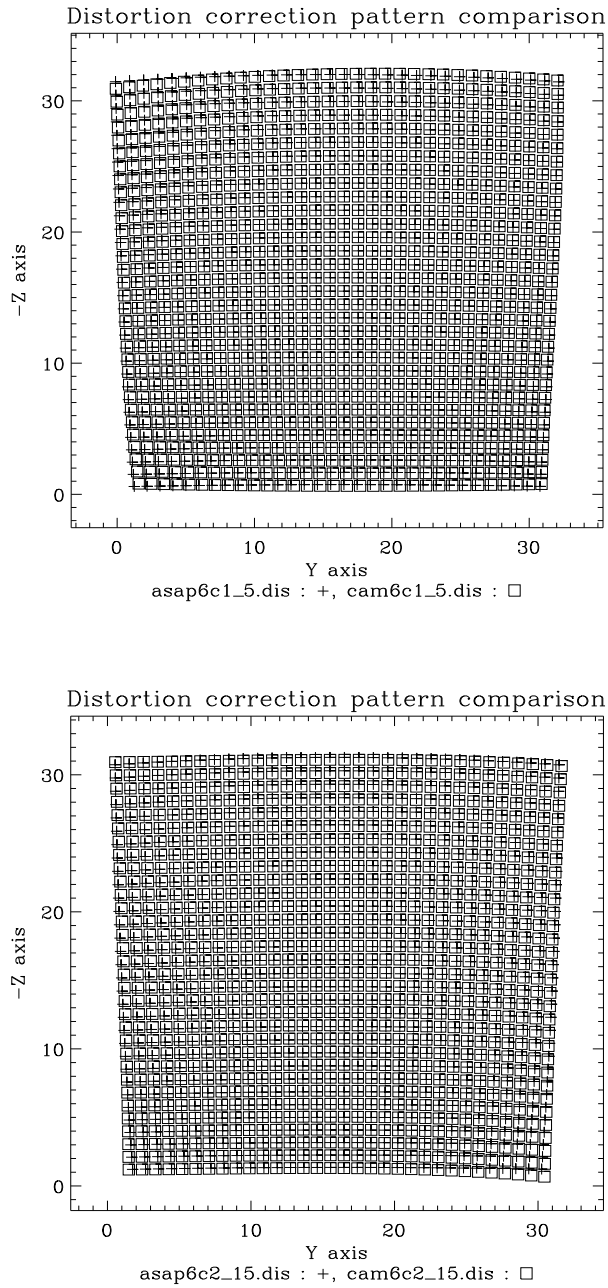

Figure 2.2: *Comparison between observations (squares) and model (crosses) for CVF1 at 5 μm (top) and for CVF2 (bottom) at 15 μm both through 6″ pixel field of view - Koryo Okumura*

The raster pattern size also increases with wavelength (∼4.5 % from 4 to 15 μm) and can be modelled with a suitable choice of the refractive index of germanium, which is the main constituent of the lenses of the LW channel and a part of filters. Its refractive index is not known with a good accuracy at the operational temperature of ISOCAM.

For CAM images taken with the $6''$ and $3''$ p.f.o.v., third order polynomial coefficients have been derived which are able to reproduce the distortions observed (see Figure 2.2). Currently, a distortion correction is implemented in CIA which uses the coefficients corresponding to the nearest configuration. However, the distortion seems to be different also for different filters with the same configuration, suggesting a wavelenght dependence, as already mentioned.

Optical models can help to derive a complete set of polynomials taking this into account, even when no calibration observations are available. We know that there are several elements playing a role in creating distortion effects. First, the field mirror tilt, which creates a deformation with trapezoidal form; second, the lens aberration, which creates a pin cushion distortion; and third, the filter width, which has an effect on the magnification.

The final goal of this investigation is to develop a tool based on this optical model able to correct quantitatively for field distortion for any CAM configuration. For this, new data sets were analysed by a group of CAM experts (B. Ali, R. Gastaud, K. Okumura and S. Ott) during a dedicated workshop at VILSPA, including 46 CAM exposures of a crowded field (originally intended to detect a Gamma-Ray Burst) which were compared with 2MASS images of the same field and combined, providing an almost uniform coverage of the field. As a consequence of this analysis, the distortion files were reviewed and upgraded for the filters LW1, LW2, LW4, LW5, LW6, LW8 and LW9 in the internal NOV00 version.

Efforts are currently on-going trying to describe the distortions observed at different wavelengths by a single parameter K and determine the effect of lens wheel positioning uncertainty. This 'distortion intensity' K depends on the choice of the origin of coordinates of the polynomials and represents the standard deviation of the distorted image from the distortion-free image computed over the detector surface. Other parameters can be defined to describe the distortion in a way which does not depend on the global offset of the origin of coordinates based on the determination of the divergence and rotational of the vector field which represents the distortion. The current situation is that although observations and model now basically agree, some further fine tuning is still required.

During the photometric analysis performed, it has been confirmed that the model PSFs used for automatic PSF fitting of point sources are sharper than the observed ones at short wavelengths. The shorter the wavelength, the larger the deviations found are. As a consequence, inconsistencies are found between the point source flux measured by the automatic PSF fitting routine and that measured using standard manual aperture photometry. The reason for this deviation may be cross-talk in the detector, which is more important for a sharp structure (point source at short wavelengths) and a low background emission (also at short wavelengths). The difference between the two photometries can reach 40% around 5 μm.

In addition, a new aspect of the above mentioned PSF deviation was discovered: the fitting routine using computed PSFs gives a biased position of the point source, which results in detections preferentially at the corner of each pixel. This is currently limiting the accuracy of the distortion correction. Note that the OLP uses the observed Cal-G PSFs and so does not suffer from this bias effect. This will be further investigated. Improvements are expected in the understanding of the distortion problem once this effect is removed.

For an updated description of the current status of the distortion problem the document *"ISOCAM Field Distortion Report"* by Koryo Okumura is available at:

`http://www.iso.vilspa.esa.es/users/expl_lib/CAM/dist_rep.pdf`

`BP: Implementation of SWS beam profile calibration files in SWS IA`

The SWS beam profile model generated by Douwe Beintema (see Figure 2.3) has been used as input for the production of the corresponding calibration files. They were generated by covering an area of $12' \times 12'$ with a spacing of $1''$. These new Cal-G files are expected to be of extraordinary help in the calibration of extended sources and bad-pointed observations. They have already been implemented in SWS IA and will be made available as part of OSIA v2.0.

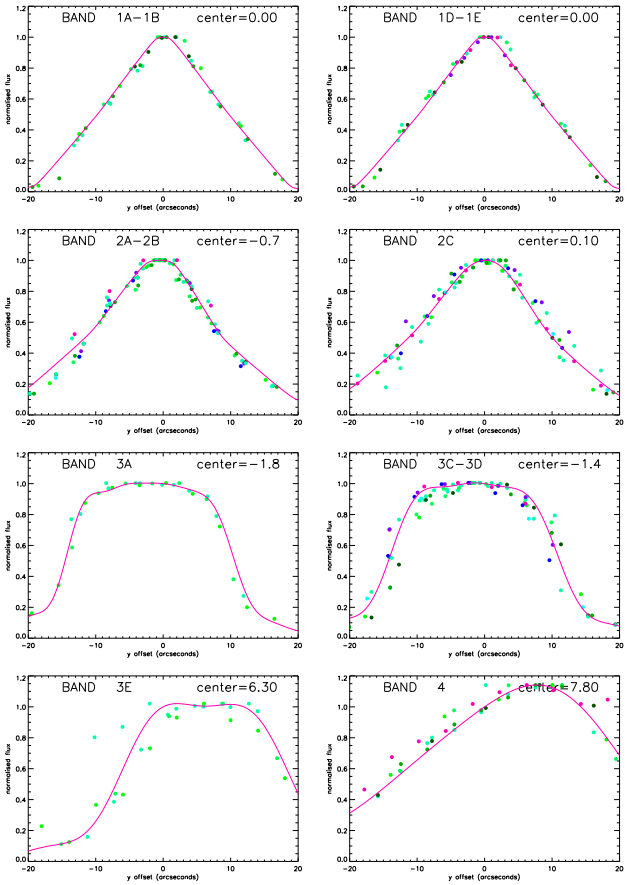

Figure 2.3: *SWS beam profiles. Comparison between model and observations in the y-axis for the different SWS bands - Douwe Beintema + Rosario Lorente*

A comparison has been made between this SWS beam profile model and the telescope PSF model provided by Koryo Okumura (based on CAM data) in order to check for consistency.

The result of this comparison is that the PSF cores are the same (difference in brightness ∼0.2% of central peak). At the first diffraction ring the differences are of the order of 5% and in the outer field they are of the order of 10%. At wavelengths shorter than 6 μm the comparison fails because of pixel size effects. The major difficulty in both models is the sampling (typical array sizes are ∼1000×1000, resulting in no more than two points per spider legs), alleviated by the introduction of a random jitter on the pupil contours in Beintema's model. The model developed for CAM cannot easily be plugged-in into the SWS model, which is set-up to propagate further into the SWS optics. Also, for the SWS the correction for the instrument displacement with respect to the the telescope axis is disabled, and there is no tilt correction, but the effect on the beam profile is insignificant. Beintema noted that in the design phase of SWS, when the computer capabilities were much less than today, the quantitative effect on the beam profile of the internal diffraction losses were not fully assessed. During instrument level testing, ghosts

were observed, caused by internal reflections between the many flat surfaces. This was solved by moving back the gratings (the so-called 'balcony solution'), with the introduction of another 20% diffraction loss. The aperture stop was too small with respect to the specifications. It could have been made bigger at the expense of instrumental resolution. It is interesting to note that similar problems are expected with HIFI on FIRST, which will have the additional constraints imposed by a coherent beam.

```
BP: Implementation of SWS pointing correction tool in SWS IA:
      appliation to SSO tracking correction
```

The SWS beam profiles, as can clearly be seen in Figure 2.3, are in many cases far from flat-topped. This makes SWS very sensitive to small pointing offsets. In addition, there are internal detector misalignments which can reach up to $8''$ and produce mismatches between different bands.

To correct for the effects produced in SWS spectra by these detector misalignments and peaked profiles, a pointing correction tool was generated and will be soon implemented in SWS IA and later in OSIA v3.0. It is able to correct for absolute pointing offsets up to $10''$ with a resolution of $0.1''$.

In order to illustrate the goodness of this tool, we show in Figures 2.4 and 2.5 an example of its application to Solar System Observations which need to be corrected for tracking effects.

In Figure 2.4 we show the offsets (of up to 4 arcsec) deduced from the comparison of the ISO-centric ephemeris now available for all SSO's by the JPL facility HORIZONS with the coordinates stored in the IIPH file during the observation of the asteroid Ceres with SWS (mode 06; detector 26) in revolution 256. As we can see, as a consequence of the fact that Ceres was a moving target to ISO, corrected coordinates were updated every few hundred seconds in order to move back the target to the centre of the aperture.

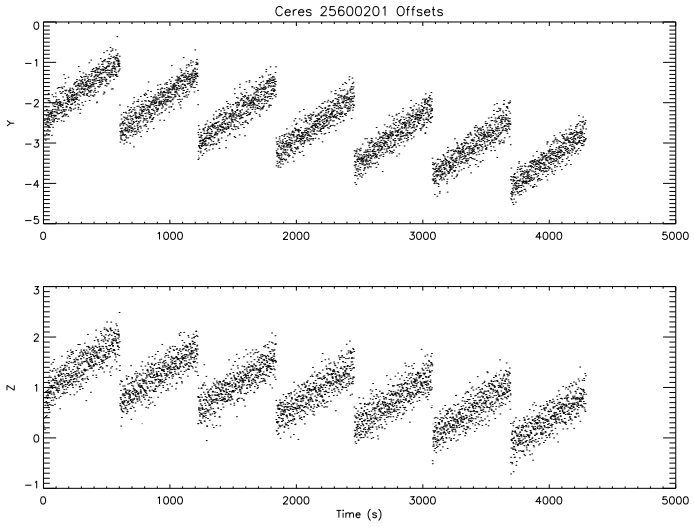

Figure 2.4: *Estimated (y,z) offsets in units of arcsecs between the centre of the SWS aperture and the actual position of Ceres as observed with SWS06 in tracking mode during revolution 256, derived from the comparison of the ISO-centric ephemeris provided by the JPL facility HORIZONS with the coordinates stored in the IIPH file -Alberto Salama.*

If the actual (y,z) offsets are accurately known it is possible to determine the correction which needs to be applied to the recorded flux for each grating position as a function of time in order to account for beam profile effects.

Figure 2.5 shows a comparison of the SWS spectrum corresponding to this measurement before and after the pointing correction tool is applied showing how the mismatches observed between the SWS bands are almost completely removed.

It is foreseen to expand the routine to an IA tool soon. In addition, investigations have been proposed to study the effect of this pointing correction in relation with the previously found 0.7 sec shift between science and pointing data.

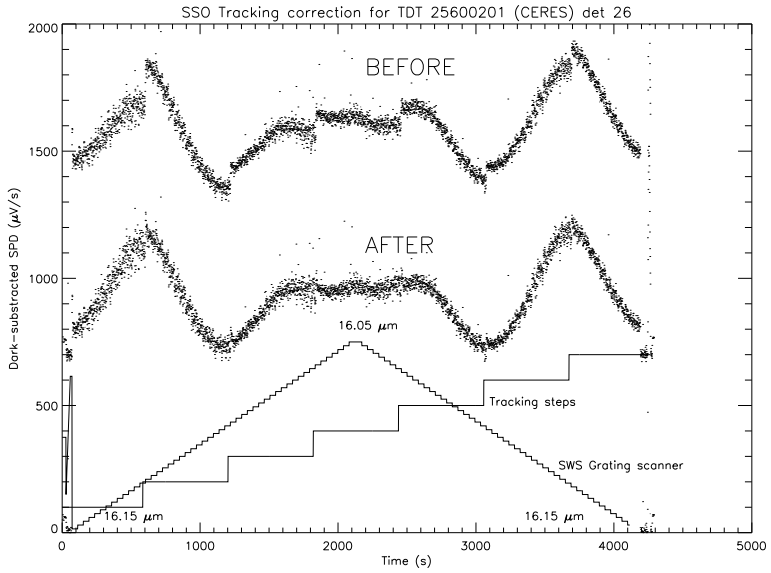

Figure 2.5: *SWS06 spectrum of the asteroid Ceres (detector 26) observed in revolution 256 where the spectrum obtained is shown before and after the pointing correction tool is applied to every grating position as a function of the offset estimated in Figure 2.4. Note how the band mismatches are almost completely removed after the correction - Alberto Salama.*

`BP: Characterisation of LWS beam profiles`

As SWS, a comparison has also been made between the adopted LWS beam profile model and the telescope PSF model provided by Koryo Okumura (based on CAM data) in order to check for consistency.

The result of this comparison is that there are only minor differences, mostly in the outer field, but the resulting extended source correction factors are the same.

As it was already mentioned in previous Status Reports, the basic problem with LWS beam profiles is the understanding of the core beam width, found to be narrower than expected ($40''$ instead of the previously assumed $50''$). Now this discrepancy is believed to be caused by the Winston cones located in front of the detectors. A small misalignment of the M2 mirror causes

the off-axis rays to hit a field stop. It is not clear if this is responsible for any of the asymmetry in the beam or the reduction in the beam size.

Concerning fringing, it is now well established that it is always observed in the case of extended sources and sometimes when point sources are observed off-axis, with the amplitude of the fringing increasing towards longer wavelengths. The most recent version of the optical model by Bruce Swinyard and the optical group at RAL includes the substrate on which the entrance mirror M2 is mounted. This reproduces the basic parameters of the observed fringe pattern, although not the intensity of the fringes. However, the results found are consistent with the interpretation that the fringes are due to interference between the light reflected from the M2 mirror and its substrate.

Regarding the fracturing of the spectra on one side of the Mars scans (observed together with an apparent simultaneous reduction in fringing) one plausible interpretation is in terms of specular reflections on the M2 mirror system for off-axis incoming radiation.

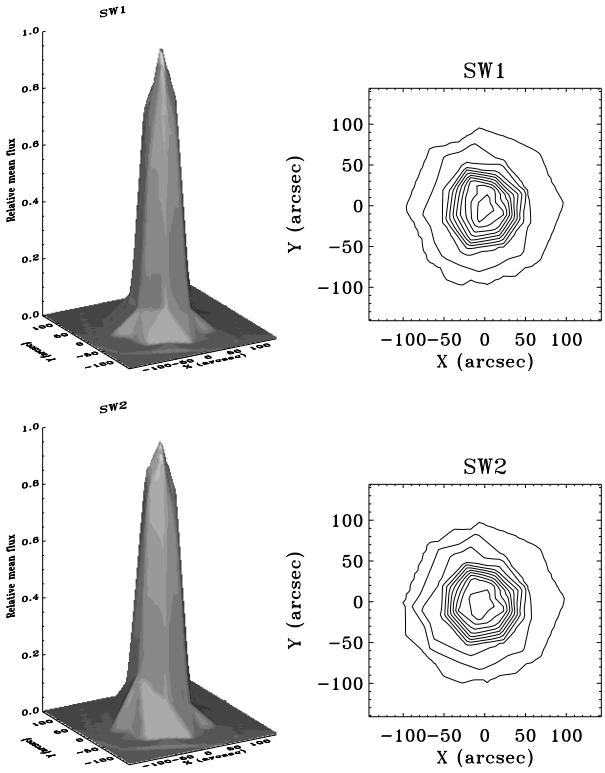

Figure 2.6: *3-D and contour plots of the beam profile of the LWS detectors SW1 and SW2 - Chris Lloyd*

BP: Characterisation of ISOPHOT aperture profiles: new PSF factors available for PHT-P and PHT-C arrays

PSF factors (the intensity fraction of a point source entering an aperture) and solid angles for PHT-P and PHT-C arrays have been recalculated by B. Schulz using the basic telescope model by K. Okumura, now including the tripod. The most recent model, which includes the instruments displacements in the ISO focal plane has also been used but the results are basically the same (at the expense of a factor of two in CPU time). Thus, it has not been used further.

The PSF factors for PHT-P, calculated with the new PSF model have been compared with values from earlier reports and the ISOPHOT calibration tables. They tend to be smaller by a few percent, i.e., more energy is falling outside the central maximum due to diffraction by the tripod. The new data available is used to analyse also the influence of source colour.

Theoretical PSF factors have also been determined for the PHT-C arrays. where the field lenses are taken as detector entrance apertures. In this case, given the dimensions of the Airy disk at these wavelengths of 42"to 88" for C100 detectors and 101" to 168" for C200, the PSF is just matching the pixel size and it is not expected to see a flat plateau on top of a beam profile, as it would be the case for shorter wavelengths. This leads to strong flux losses in the case the source is placed in the centre of the C200 array, because of the existing gap in the middle of the four pixels and make corrections for this effect very difficult. To be less vulnerable to pointing errors and achieve a better S/N, the calibrated fluxes of the four pixels are summed up, and the corresponding PSF factors in this case describe the fraction of the flux of a point source which observed this way enters any of the pixels of the entire array. Similarly, a successful adjustment of parameters also for the C100 array is proposed. Through comparison with real observations of point sources located at different offet positions it is possible to compare the predicted *vs* observed fractional PSFs and establish the quality of our model description. It is found that the previously reported disagreement between the empirical and theoretical PSF factors in PHT-C detectors can be better explained by small misalignments between pixels in the array (larger distances between pixels) rather than by a reduced pixel size (smaller effective areas).

BP: Characterisation of ISOPHOT-P aperture profiles: standard/non-standard aperture photometry

PHT-P photometric calibration was established with 'default' apertures and is based on point-sources (stars, asteroids and planets). But many observational programmes were performed with other apertures and the scientific targets are not always point-like. The question is then to know how do different apertures change the calibration and whether point- and extended sources show the same trends.

Results from relative and absolute aperture photometry in 3 PHT-P filters (12, 25 and 60 μm) have been recently analysed by Thomas Müller. Relative signal sequences taken with the same filter and different apertures show the same trends for the FCS and for the sky background measurements as expected. It can therefore be concluded that the illumination from the FCS is flat. However, aperture sequences on bright background positions show that the linearized signals do not scale with the aperture area. The same deviations can be found for FCS signals using different apertures.

A comparison of absolute sky photometry with COBE/DIRBE measurements (see plots in Section 3.4.5) indicate, that the apparent solid angles of PHT are off by 15% at 12μm, 40% at 25 μm and about 30% at 60 μm in the default apertures (52", 79" and 180", respectively) with respect to the currently implemented ones and for the P2 filter centred at 25 μm, they also depend on the brightness level (signal linearity problems of the order of 30% in the brightness range from 15 to 50 MJy/sr), although the scatter is high and contradictory results have been obtained by responsivity analysis performed at MPIA. With the results obtained it is now possible to calculate the effective solid angles for a large range of apertures for all 3 filters. Point sources, on the other hand, are found to be consistent with the theoretical PSFs values for medium (23") to large apertures (180").

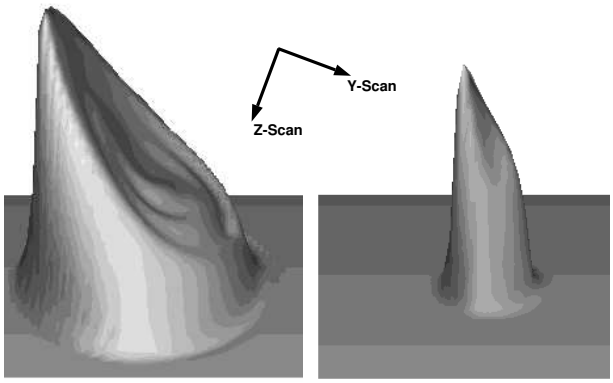

Figure 2.7: *Constructed 3-D aperture profile at 12.0 μm for the 180$''$ aperture (left) and for the 52$''$ aperture (right) from two perpendicular scans parallel to the S/C y and z-axis - Thomas Müller*

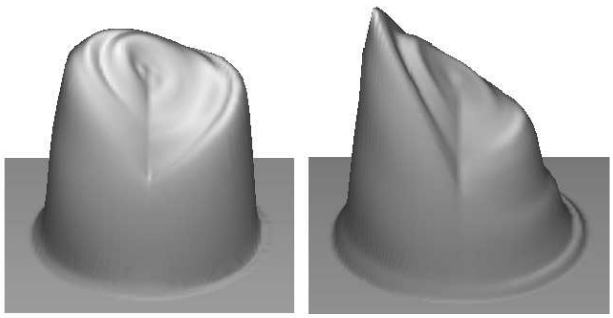

Figure 2.8: *Constructed 3-D aperture profile at 7.3 μm (left), and at 16 μm (right), using the 180$''$ aperture from two perpendicular scans parallel to the S/C y and z-axis- Thomas Müller*

These results have the following consequences:

- The default responsivity is strongly biased towards the default aperture. This means it may not be applicable in non-default apertures.

- To obtain reliable photometry of extended sources (the intermediate case) the default aperture as well as non-default aperture measurements have to be analysed carefully and the trends, offsets and uncertainties estimated correspondingly.

- Faint point-sources on a strong background fall under the category of sky background measurements, where the solid angles are more important than for bright sources. Photometry in non-default apertures has to be handled with care.

- The combination of on-source and off-source measurements in different apertures is difficult and strongly affected by the wrong solid angles.

- Aperture sequences on strongly structured extended sources will be extremely difficult to analyse. On the other hand, aperture sequences can be used to distinguish between point- and extended sources. It is also possible to determine quantitatively the source extension from PHT04 sequences, in excellent agreement with ISOCAM results.

The full report on *"PHT Apertures and Absolute Photometry"* was prepared by Thomas Müller and it is available at

`http://www.iso.vilspa.esa.es/users/expl_lib/PHT/TM_aperture.ps.gz`

`BP: Description of final status of ISO Pointing and improvements during Post-Operations`

In the first months of the ISO mission it was found that errors up to 4 arcseconds could be present in the ISO pointing, depending on the target observed. The pointing appeared to be much better than the specifications (Absolute Pointing Error of $11.7''$, but it was suspected that some systematics could be present, which could therefore be corrected for.

Thus, a specific calibration programme was designed and executed in revolution 137, by which a number of point-like sources were observed with ISOCAM. 79 stars were selected from the Ground-Based Preparatory Programme (GBPP) list of calibration standards and observed in the LW9 filter (at 15 μm). The centroids of all these images were derived with good determinations in 54 cases. These were correlated with (i) the position of the guide star in the STR (Star TRacker), (ii) star ecliptic and galactic coordinates, (iii) the Solar Aspect Angle, and (iv) guide star magnitudes. A possible correlation was found only with the position of the guide star in the STR field of view, indicative of a possible improvement in the ISO pointing.

A second attempt was done in revolution 264, with a more accurate star selection procedure based on the improved Hipparcos star catalogue coordinates and an ad-hoc empirical colour-colour relation between visual magnitude and the expected flux in the CAM LW9 filter. After analysis of the results obtained, the correlation between pointing offset and position of the guide star in the STR was confirmed.

An independent investigation was then initiated based on the absolute pointing reconstruction as given by the confirmation star, a second guide star used at the start of every revolution. It appeared that a recalibration of the STR was possible, via the introduction of a focal length dependence on the angle of incidence of the visible radiation coming from the guide star. The model was applied to predict the offsets measured in revolution 264 with excellent results.

A verification exercise was performed in revolution 368, based on a series of SWS02 observations on and around HR 6705. With the new calibration, the measured offsets were decreased substantially, being only $+2.4''$and $-1.0''$ along the Y and Z axis respectively. Further to this,

the go ahead was given to the uplink implementation of the STR recalibration which became operative as of revolution 369.

A second, but lower magnitude, improvement in the ISO pointing was obtained by increasing the sampling of the Sun ephemerides as used by the onboard software of the AOCS. As of revolution 453, a new so-called Sun model was introduced, and the improved algorithm was also introduced in the downlink in OLP v6.1.

The most recent ISO Pointing model now considers the effects of differential aberration, proper motion and parallax of the guide stars used.

While aberration was thought to be corrected for ISO observations by the fact that guidestars are always close ($\leq 2.5^0$) to the observed target, the differential aberration effect can cause pointing errors up to $0.9''$ (if ISO's velocity is considered as well, this can become even larger).

On top of aberration two other significant sources of residual pointing errors were addressed, parallax and proper motion of guidestars. The effects are smaller ($\leq 0.4''$) but still significant in some cases, fortunately only affecting few nearby guidestars.

New Cal-G files were generated which correct for the Pointing Correction effects above refered and they have already been implemented in OLP v8.6.

Now, after all these improvements have been introduced in the pipeline and in order to get a quantitative assessment of the ISO Pointing Accuracy, a scientific validation exercise has been carried out, using the stars observed in revolution 264 experiment as test cases. The main conclusion obtained is that the Absolute Pointing Error for ISO is found to be $1.4''$, a value which exceeds all expectations.

A minor limitation still exists which comes from the fact that the CAM PSFs used for the determination of the centroids of the stars observed is sampled with a step of $0.5''$, resulting in an uncertainty in the determination of the position of the stars in the CAM images which could be slightly improved in the future.

The full story is documented in *"The ISO Absolute Pointing Accuracy"* by Alberto Salama and Andy Pollock, available at

`http://www.iso.vilspa.esa.es/users/expl_lib/ISO/pointing.ps.gz`

Soon, a full "OLPv9 Pointing Validation Report" by A. Pollock, A. Salama and T. Müller will be issued and posted in the ISO public web server.

`BP: Pointing improvements in OLP v9.0`

OLP v9 has seen some recovery procedures introduced into the derivation of IIPH files. The IIPH gives real-time estimates of the pointing direction of the prime instrument every 0.5 sec derived from those parts of the telemetry reserved for the AOCS system. Very occasionally, for operational reasons, some parts of the pointing telemetry were not available, notably the RPID that shows which part of a raster is currently in execution. Any missing values are now recovered by comparison with the expected pointing schedule. There are also new allowances for unexpected delays in the schedule. Improvements have also been introduced to ensure the accuracy of individual 0.5 sec pointing data as the telescope's position is adjusted between the successive apertures or raster points in an observation. The combination of these measures was designed to guarantee, even under difficult circumstances, the completeness and reliability of the pointing files delivered with observers' data.

2.2.2 Glitches:

`GL: Glitches Working Group: General status`

The overview paper on the effect of glitches in ISO Detectors with the title *"The ISO Detectors and the Space Radiation Environment"* by Ana Heras et al. has finally been published in *Experimental Astronomy* (vol. 10, p. 177 - August 2000).

It presents a statistical study of the glitch rates and glitch characteristics as derived from the data of the four instruments on board of ISO, and compare the results obtained for each instrument and for different detector materials with the available models. The evolution of glitch rates and some instrument performance parameters are analysed as a function of time in the mission and ISO's position in orbit.

The observed glitch rates are found to be 1.5−4 times higher than the value predicted by the CREME96 model for the cosmic ray integral flux. Moreover, when comparing the deposited energy distribution associated with the observed glitches and the results from ray-tracing simulations including only direct cosmic rays, it is found that the contribution from the lower deposited energy hits is larger than in purely cosmic-ray based models (although there is a good agreement for the higher energies in Ge detectors).

It is concluded that between 30% and 75% of the observed glitches are caused by δ-rays and other secondary particles produced in the detector and in the instrument and satellite shields.

The production of secondaries has been modelled more recently by Hervé Dzitko and Arnaud Claret (CAM) and by Petteri Nieminen (LWS) using the GEANT3.21 Monte-Carlo particle transport simulation code.

With respect to CAM (Figure 2.9) the glitch size, glitch rate and energy properties were predicted this way and compared with in-flight data.

Counting rates induced by secondary nuclear interaction particles can be estimated through an analytical approach, assuming the geometrical interaction cross section and the average multiplicity of the interaction, and considering also the secondary particles emitted by the shield near the detector.

A mean number of 8.48 $\pm$ 0.46 pixels/glitch and a glitch rate of 0.83 $\pm$ 0.12 glitches/sec were derived.

Experimentally, $\sim$1 glitch/sec is detected, close to the mean value (if we consider the errors) of $\sim$0.83 glitches/sec derived.

The results derived from Monte-Carlo simulations were presented at the NSREC (Nuclear and Space Radiation Effects Conference) last July in Grenoble (Proceedings book not yet available).

The full report concerning LWS is contained in the internal document *"GEANT simulation of ISO LWS detector energy deposit distribution"* by Petteri Nieminen.

The discrepancies in LWS glitch statistics with models that were reported in the past (contribution from high energy impacts lower than for other instruments) are now finally understood. According to Martin Burgdorf, who revised the calculations made, the discrepancies were due to the use of an inadequate database for deriving the glitch height distribution statistics. Instead of using all observations, it seems that when only bright sources are selected from the database to perform the calculations the number of strong glitches in the distribution increases with respect to the number of small glitches, which makes the observed distribution similar to what it is expected from the models and more consistent with the results obtained for the other instruments. The glitch height distribution histograms are expected to be affected through the conversion factors from glitch height to energy deposited. The largest uncertainty here is the

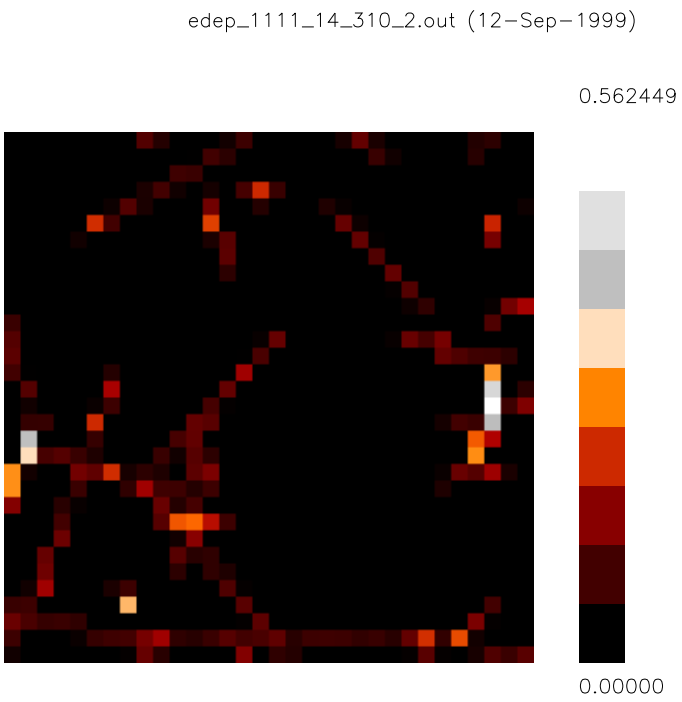

Figure 2.9: *Example of synthetic glitches produced using the GEANT code applied to CAM data - Arnaud Claret*

photoconductive gain G. Apparently, when the faint sources are considered, the strong glitches are systematically underrepresented, probably because the analogue amplifier gain is set to a higher value for observation of weak sources and therefore drives stronger glitches beyond the limit with which the cold electronics can cope. The new results are promising and although pending a more detailed analysis they seem to indicate that the reported discrepancy between LWS glitch statistics and models is solved and both are now consistent.

Details on improved de-glitching techniques per instrument are given below.

`GL: PHT status: Implementation of the two-threshold de-glitching method in OLP v10.0`

Concerning PHT de-glitching, and as already mentioned in the previous Status Report, no additional improvements are expected in PIA.

With regard to pipeline data products, the idea of implementing in the pipeline the more sophisticated, two-threshold de-glitching method which works at ERD level has not been abandoned, but it has slightly been modified in order to facilitate its implementation in version 10 of the OLP. In its original form, the application of this de-glitching algorithm required a quite different approach to the problem (the correction is applied at read-out level and not at ramp level) and the changes needed to fit it into the structure of OLP were far from simple.

Now it is proposed that, following the detection of a glitch along the sequence of read-outs of a ramp, the sigma for determination of the glitch detection threshold is reduced to a lower value giving a second and hence more efficient threshold level.

The description of the original two-threshold de-glitching method can be found in the document *"De-glitching methods by the ISOPHOT Interactive Analysis (PIA)"* by Carlos Gabriel and José Acosta available at:

`ftp://astro.estec.esa.nl/pub/aheras/iso_gwg/PHT_degl.ps`

`GL: SWS status: Improvements of glitch detection in SWS data`

A list of modules have been updated or added to SWS OLP v9.5 pipeline processing. Some of them, especially the pulse-shape correction, have a direct impact on glitch detection since they lead to a better linearization of the SWS integration ramps.

The new glitch detection and removal is now extremely efficient. However, a side effect of the high sensitivity of glitch detection/removal is that spectral lines observed at fast speed with the SWS01 observing mode can be removed or swallowed. For OLP v9.5 it has been decided to warn the archive users retrieving observations that might be affected by this problem. For OLP v10, a solution has been proposed by Fred Lahuis who is now awaiting validation. As a fall-back in case of unforeseen problems in the implementation the option remains to detect glitches but not fix them. The provisional tests made so far indicate that most false glitch detections are suppressed thanks to the normalization of the first derivative before the glitch detection. In the few cases where there are still glitches detected they have no noticeable effect on the derived

signal. This thanks to the combined effect of the normalization and the adapted slope fitting. There, for low resolution data, no combined slope and glitch fit is made anymore but instead a glitch repair is done before a single slope fit.

The details of the new deglitching method are given in the document "Degliching of SWS Low Resolution Data" by Fred Lahuis, available at:

`http://sws.ster.kuleuven.ac.be/documents/low-resolution-deglitching.ps`

De-tailing SWS glitches in band 2, by using the 'dynadark' module, which models the memory effects in these detectors, is still under study. Concerning the study of the statistics on SWS tails, and due to manpower limitations, it has been postponed after the delivery of next OLP v10.0. Thus, possible improvements in de-tailing derived from this analysis will only be implemented in OSIA at a later stage.

`GL: CAM status: Improvements of glitch detection in ISOCAM data`

Concerning OLP v9.5, the deglitching is now performed using the Multi-Resolution Median Transform method [Starck et al. 1998; *"Image Processing and Data Analysis: The Multiscale Approach"*, Cambridge University Press, Cambridge (GB)]. This method is useful to deal with glitch structures of different sizes, and particularly for structures with large dynamics and perform an efficient automatic detection. The idea is the following: as we observe the same position in the sky during n exposures, we cannot have any structure in our signal which has a temporal size lower than n * *tint*. This means that all the significant structures (i.e. not due to noise) at small scales are due to glitches. The method consists in taking the MMT for each pixel It is a non-linear multi-resolution median transform (x, y), to set to zero all structures higher than a given level (determined from a noise modeling) in the smaller scales, and to reconstruct the deglitched temporal signal. Figure 2.10 shows the results of such a treatment. Figure 2.10 (top) shows the values of a pixel of the camera as time elapses. The x-axis represents the frame number (time / integration time), and the y-axis is the signal in ADU per second. These data were collected during a raster observation, and the satellite remained at the same position for about 20 frames, and the integration time was equal to 2.1 s. A source is at the limit of detection (frames 130 to 150). All peaks are due to cosmic ray impacts. Figure 2.10 (middle) shows the same data after the glitch suppression. The third plot (Figure 2.10 (bottom)) shows both data and deglitched data overplotted. We see that the noise and the signal are not modified during this operation.

The method is robust and works for non-stabilized data. The only real limitation is that we cannot detect glitches which last for a time longer than or equal to $n * tint$. That means that the more frames we have per camera configuration, the better the deglitching will be. Some "special" glitches introduce a gain variation with a very long time duration. These special glitches can be separated in two types: 1) the pixel value decreases slowly until a stabilized value is reached (see Figure 2.11); 2) the pixel value decreases first below the stabilized value, and then increase slowly until the stabilized value is reached (see Figure 2.12). In both cases, the stabilization can be very slow, and the deglitching method presented here does not correct for this effect. As a result, pixels where a glitch has been detected are not used when averaging values corresponding to the same sky position and same configuration.

As already mentioned in our last Status Report, several other de-glitching methods have been developed by Stephan Ott for application to ISOCAM data in special cases.

The idea is to take advantage of valuable information about ISOCAM's current configuration, glitch distribution, flux level and redundancy in the raster or beam-swith observation, ignored

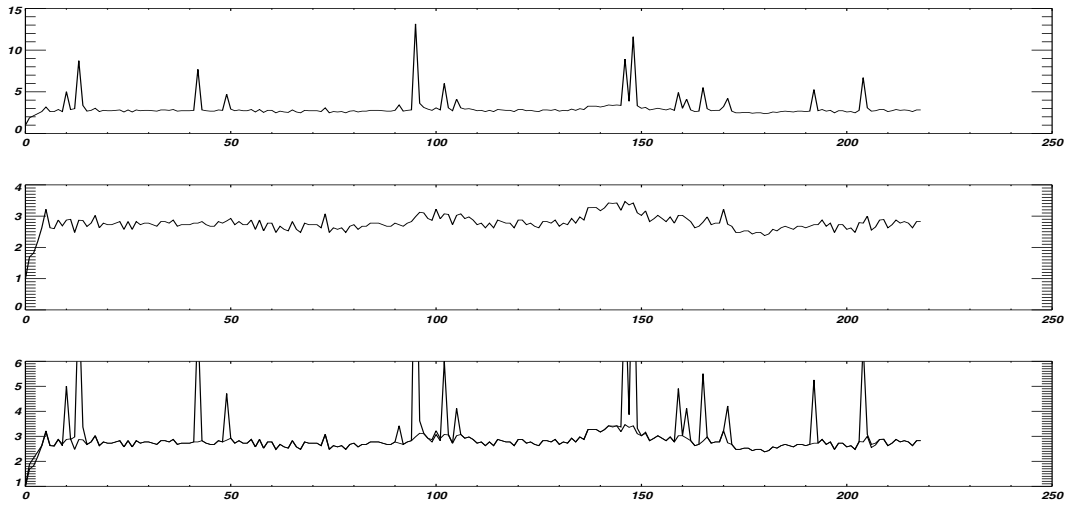

Figure 2.10: *An example of deglitching; original data (top), deglitched data (middle), and both overplotted (bottom) - ISO CAM Handbook*

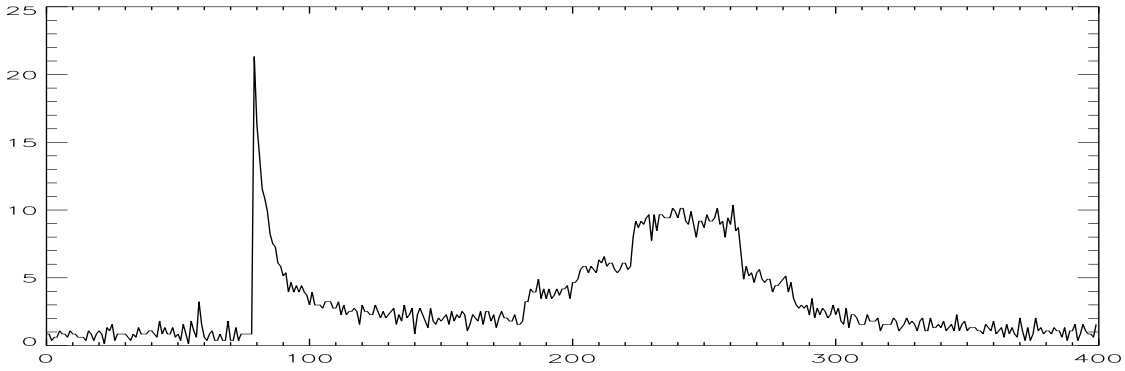

Figure 2.11: *Glitch with very long duration. The flux in ADU is plotted against time given by the exposure index - ISO CAM Handbook*

by currently existing standard de-glitching techniques (multi-resolution, sigma clipping,..). This leads to badly chosen thresholds, which result in too high noise level due to un-suppressed glitches, masked out sources or gradients and no deglitching for observations with few read-outs. In the last few months some of these new de-glitching methods have been improved (like those used for faint sources and low redundancy data in CAM parallel) giving very satisfactory results. A detailed description of all these techniques, together with examples of results obtained and a list of application fields and caveats to take into account in each case can be found in the document *"ISOCAM Faint Source Report"* by Bruno Altieri et al. available at:

`http://www.iso.vilspa.esa.es/users/expl_lib/CAM/fs_report.ps.gz`

and in the document *"Innovative Cosmic Ray Rejection in ISOCAM data"* by Stephan Ott et al. which can be found at:

`http://www.iso.vilspa.esa.es/science/pub/2000/cosmic_ray.ps.gz`

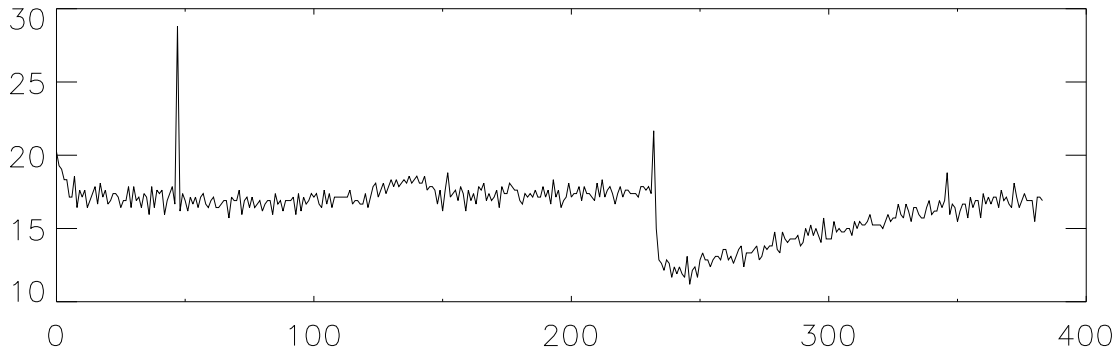

Figure 2.12: *Glitch with a negative tail. The flux in ADU is plotted against time given by the exposure index. Note the gain variation of about 5 ADUs which appears after the second glitch - ISO CAM Handbook*

All these de-glitching tools are available with CIA v4.0 or will soon be made available in CAM v5.0 (expected release in mid 2001).

The possibility of implementing a more sophisticated glitch detection algorithm (specially conceived for the detection of very faint sources) in the browse product generator of the ISO Data Archive through the use of a post-processor script (not coupled with OLP) is being investigated.

`GL: LWS status: improved de-glitching techniques`

As already mentioned in the previous Status Report, no further efforts are foreseen to improve de-glitching in LIA and OLP v10. SPD processing was slightly modified in OLP 8.7, leading to a better glitch detection and, with this, the recognition of glitches in the LWS pipeline can be considered to be in its final form.

`GL: ISOCAM de-glitching and the detection of near-earth objects`

Thomas Müller has investigated the possibility of discovering near-earth objects with ISO. These are very fast moving objects in the ISO field of view, with an apparent speed of up to 2° per hour. His calculations show that objects of only 100 m diameter can be considerably bright (around 1 mJy) in the wavelength range 12-15 μm, which means that they would be detectable by ISOCAM. Actually, some elongated features have been detected (see one example in Figure 2.13) in CAM images which are associated with relatively slow moving Solar System objects. However, fast moving near-earth objects might be more difficult to detect, since they probably present signatures in the CAM field of view which are identical to those produced by glitches. Therefore, they might have been removed by the automatic de-glitching algorithm in the CAM data processing. In order to avoid these objects to be confused with glitches an intelligent modification of the current de-glitching algorithms would be needed, which needs to be carefully meditated and designed. Thus, any systematic search of this kind of astronomical objects will have to wait until the Active Archive Phase.

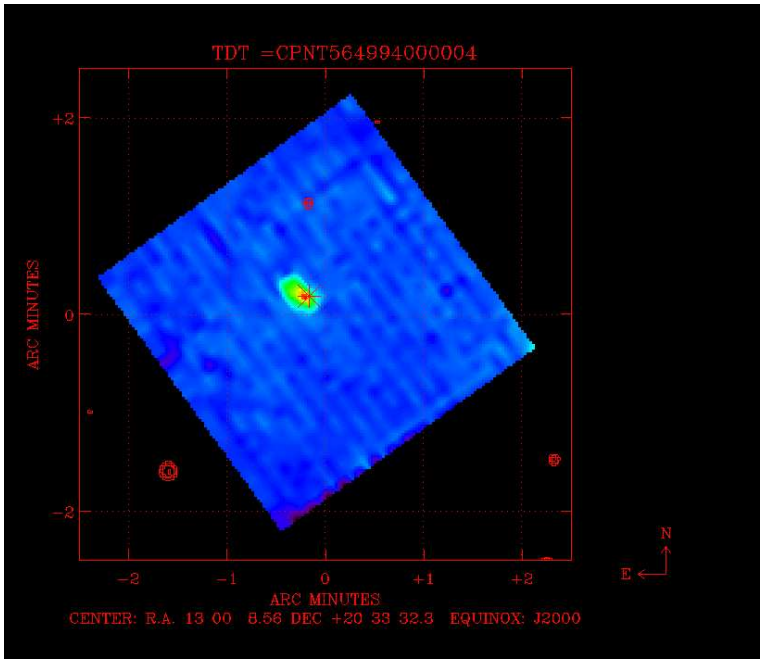

Figure 2.13: *The Amor asteroid (3671) Dionysus, as seen by the CAM parallel mode. The marks the predicted ISOcentric position, the overlaid contours are the corresponding DSS sources. An elongation due to the apparent speed of about 120″/hour during the 11 min integration time is clearly visible - Thomas Müller*

2.2.3 Line profiles:

```
LP: Determination of the SWS spectral resolution and instrumental
     line profiles.
```

The document *"Spectral resolution of SWS AOT 1"* by Rosario Lorente, describing the SWS AOT01 spectral resolution as a function of the scanning speed and the instrumental line profiles is available as an internal document.

Summary tables with the most relevant numbers concerning spectral resolution of this mode are provided in Section 3.3.4 of the *"ISO SWS Handbook"*, available at:

```
http://www.iso.vilspa.esa.es/manuals/HANDBOOK/VI/sws_hb
```

The speed 4 resolutions vary between 800 and 1700 increasing with wavelength. This is approximately half of the AOT 2 resolution, matching expectations, and slightly better than expected for extended sources. The FWHM remains nearly constant.

Additional information on the grating instrumental profile and resolution can be found in Section 6.11 of the ISO SWS Handbook above refered and in van den Ancker et al. (1997), accesible at:

```
http://www.iso.vilspa.esa.es/users/expl_lib/SWS/doc/sws_ip/
```

where possible instrumental effects on emission line profiles observed with SWS are discussed.

Ground-based tests showed that the SWS01 Instrumental Profiles have a gaussian shape up to accuracies of a few percent and this is confirmed by the analysis of in-flight data, with the

exception of a slight 'shoulder' on the blue side of the base of the profile and a depression on the red side, possibly dependent on the position of the source in the slit.

The last version of the document *"ISO-SWS grating resolution and instrumental line profile as measured by the full resolution modes SWS02 and SWS06"* by D. Lutz, H. Feuchtgruber and J. Morffin can be found at:

`http://www.iso.vilspa.esa.es/users/expl_lib/SWS/SWS02-06.ps.gz`

It includes a description of the database used and existing models for the determination of SWS spectral resolution in these two observing modes. In addition, an analysis of the effect of rebinning and extension of the source observed on the spectral resolution is presented. The reproducibility, observed trends with time and the possible dependence of resolution on detector, line flux or continuum flux are also investigated.

For most practical purposes, it is completely adequate to assume that an SWS instrumental profile is intrinsically a gaussian. The document gives a formula to estimate the expected line width as a function of source extent.

Other effects like mispointing, ghosts and transients are also discussed in the document.

Future plans include the extension of the analysis to other sources increasing the database and the implementation of a cross-talk correction which might explain the broad wings observed at a few per thousands level.

Resulting FWHM values have already been implemented in SWS IA, via an update in the 'resolution' module.

With respect to SWS Fabry-Pérot modes, the FWHM as measured with the internal calibrators can be found in Section 6.3.1 of the *"ISO SWS Handbook"*. Esentially, the spectral resolution decreases towards the short wavelength ends of the wavelength ranges covered by the two Fabry-Pérots, where the wavelengths corresponding to the resonances of the reflective meshes are approached. The Fabry-Pérot spectral resolution depends on precisely parallel F-P plates.

Measurements of the Fabry-Pérot spectral resolution in-orbit suffered from the lack of bright, narrow lines. Three lines were measured and lower limits found to the spectral resolution that were very close to expectations. This is reported in Valentijn et al. (1996, A&A 315, L60.)

`LP: Progress on the analysis of LWS line profiles`

The study of the LWS grating profile was completed for point sources and short wavelength detectors by Rosario Lorente. The result is a single profile valid for all SW detectors (Figure 2.14). Unlike SWS, LWS line profiles deviate slightly ($\sim$4%) from a gaussian shape, as expected. The error made on the flux determination by using a gaussian fit is only of the order of 2%, however.

The asymmetry found in the 57 μm line in the SW2 detector is probably related to the presence of a ghost feature in the Fabry-Pérot spectra.

The line profile analysis was later extended to the long wavelength (LW) detectors and completed by Cecile Gry, resulting also in one single mean profile for all the detectors.

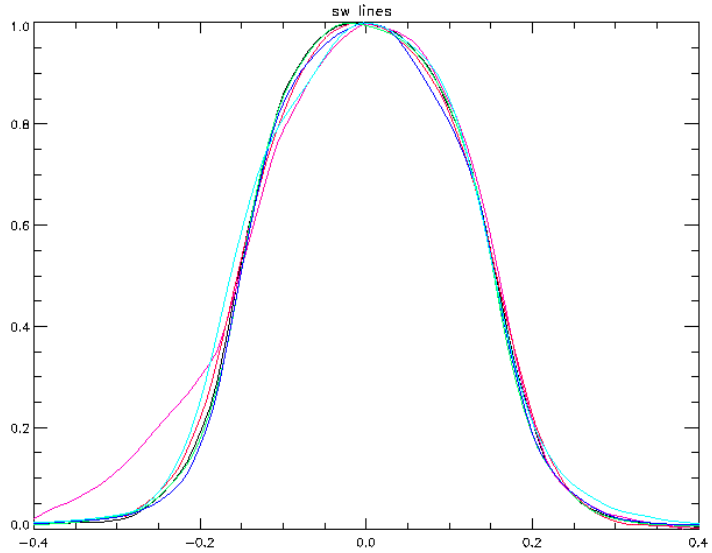

Figure 2.14: *LWS line profiles observed in NGC 6543, NGC7027 and NGC 6826. The plot includes the mean profiles observed at 52 μm (as observed on the SW2 and SW3 detectors), 57 μm (on SW2 and SW3), 63 μm (on SW3) and 88 μm (on SW5). The only discrepant assymetric profile corresponds to the 57 μm line detected on the SW2 detector - Rosario Lorente*

The line profile analysis has also been applied to extended sources, with the result that there is no profile distorsion coming from the off-centering of the source or from their spatial extension.

Meanwhile, the mean profiles are available in numerical form for profile fitting via a module in the SWS IA, and it will also be made available in ISAP v2.1 via a 'smoothing' routine. The intention exists to find an analytical function (e.g. a combination of a lorentzian and a gaussian function) to fit the numerical values. This function will eventually be also implemented in LIA or as part of the 'multi-fit' module in OSIA.

The LWS grating profiles have also been compared to pre-launch ray-tracing results at 45 μm by Anna di Giorgio. The agreement found is very good at the top of the line although the base of the line is wider than predicted.

The full report on *"LWS grating resolution and line profiles"* by Cecile Gry and Rosario Lorente is also available as an internal document.

Concerning the LWS Fabry-Pérot profiles, they have been derived by Emmanuel Caux for several lines (52 μm, 57 μm, 63 μm, 88 μm, 122 μm, 145 μm and 158 μm) on three objects (G0.6−0.6, NGC 7023 and NGC 7027), observed with the standard AOT LWS04. They compare very well with the theoretical profiles apart from an asymmetrical widening probably due to memory effects, although a misalignment (if the tilt has been changing during the scan) could also produce a similar effect (see Figure 2.15).

The origin of this asymmetry is currently being studied by Anna di Giorgio using special calibration observations performed with both forward and backward scans which will be compared with standard LWS04 observations (for which only one scan direction was used) of the same object.

It is confirmed that the resolution at short wavelengths seems significantly lower than expected from ground-based measurements. Definitive results, however, will have to await for the results of the memory effects analysis which is still being carried out.

It is foreseen that a tool will be provided in LIA to fit the Fabry-Pérot spectra with the derived

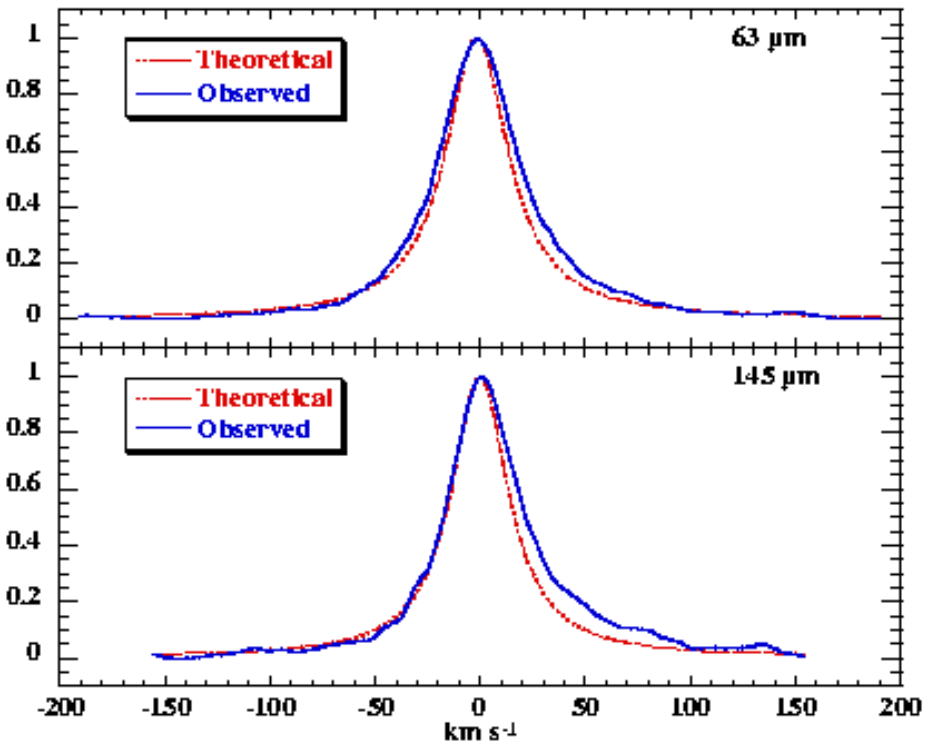

Figure 2.15: *Theoretical and observed Fabry-Pérot line profiles at 63 and 145 μm. Note the asymmetries probably due to memory effects. - Emmanuel Caux*

profiles.

`LP: PHT-S line profiles`

The PHT-S line profiles were measured in laboratory during ground calibration assessment. The spectral range was scanned with a monochromator (bandwidth 4 nm for SS and 8 nm for SL) with fixed step sizes of 4 nm and 8 nm, respectively. The results of these measurements have been publised in : *" Report on calibration of the ISOPHOT-S-FM (upgraded) Subexperiment IAC Report"*, Doc.No. IAC.FMC.002, Issue 2, 20-June-1992 by F. Garzón and J.M. Rodríguez-Espinosa.

The profiles exhibit a gaussian shape to good approximation. For the PHT-SS pixels the FWHM is 42±4 nm, for SL 97± nm. The physical distance between adjacent pixels is 350 μm which corresponds to 38.3 nm and 91.8 nm in wavelength for SS and SL respectively, assuming a linear scale. The physical size of a pixel in dispersion direction is 310 μm which corresponds to a width in wavelength of 33.9 and 81.3 nm for SS and SL, respectively.

```
LP: CAM-CVF line profiles
```

The Full Width Half Maximum (FWHM) values of the CAM-CVF have been measured from the ground and the resulting resolution values were listed in the ISOCAM Observer's Manual :

- for CVF SW, R=41
- for CVF1 LW, R=37 at 5 microns to 43 at 9.5 microns
- for CVF2 LW, R=35 at 9 microns to 49 at 16.5 microns

Although the profiles were originally given as gaussians, the shape of the profiles is actually not known.

D. Cesarsky has measured the width of the profiles on observations. Table 2.1 shows the results of gaussian fits performed on strong and narrow ion lines in M16 :

Table 2.1: *CAM-CVF line profiles*

species	λ (μm)	FWHM (μm)	σ(FWHM) (μm)	resolution (λ/FWHM)	ground-based FWHM
[Ar II]	6.98	0.16	0.02	44	0.18
[S IV]	10.51	0.26	0.03	40	0.28
[Ne III]	15.56	0.34	0.01	46	0.33

2.2.4 Photometric calibration:

```
PH: ISO Calibration web pages available as part of the ISO Data Archive
```

The old *Calibration Liaison* web pages, used during the mission for posting cross-calibration information originally intended for internal use only by the ISO Calibration Team were updated by Pedro García-Lario and made available to the ISO users community as part of the ISO Data Archive.

The new *ISO Calibration* web pages (see Figure 2.16) can be found at:

```
http://www.iso.vilspa.esa.es/users/expl_lib/wwwcal/
```

These pages contain detailed information on the calibration standards on which the absolute flux calibration of ISO is based. This includes a description of the ISO Ground Based Preparatory Programme (GBPP) and the Cohen, Walker, Witteborn et al. (CWW) absolute calibration programme, as well as information on the asteroid and planet models that were used for the calibration at longer wavelengths as well as the specific list of astronomical sources used in the calibration of each ISO observing mode. Photometric and spectral data are provided together with model spectra of the different ISO calibrators and the definition of the system zero-points.

These pages will regularly be updated with additional information and improved data as it becomes available.

```
PH: Organisation of the Workshop: "ISO Beyond the Peaks", held
     at VILSPA (February 2-4, 2000)
```

ISO Calibration

ISO Calibration Documents

List of contents:

The calibration of ISO data. I (General)

- Definition of ISO calibration standards: stars, asteroids and planets
- Photometric and spectral data
  - Results from the ISO Ground-Based Preparatory Programme (GBPP)
  - Results from Cohen et al.'s (CWW) Absolute Calibration Programme
- Model Spectral Energy Distributions (SEDs)
  - Model SEDs of stars in the GBPP
  - Model SEDs of stars from M. Cohen et al.
  - Model SEDs of asteroids from Mueller and Lagerros
  - Model SEDs of Uranus and Neptune
- Definition of the system zero-points

The calibration of ISO data. II (per instrument)

- Absolute Flux Calibration of CAM
- Absolute Flux Calibration of LWS
- Absolute Flux Calibration of PHT
- Absolute Flux Calibration of SWS

Other documents

The calibration of ISO data. I (General)

Definition of ISO calibration standards

Figure 2.16: *The introductory new ISO Calibration web page*

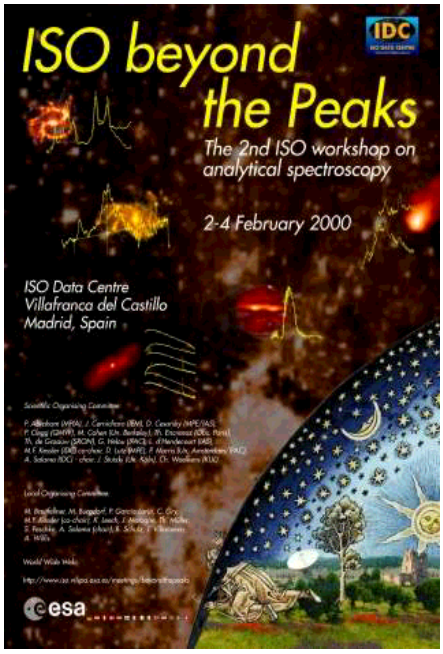

Figure 2.17: *Poster announcing the Workshop "ISO Beyond the Peaks", held at VILSPA on February 2−4, 2000*

The 2nd ISO Workshop on analytical spectroscopy with SWS, LWS, PHT-S and CAM-CVF took place on February 2−4, 2000 (see Figure 2.17) in Villanueva de la Cañada, very close to the ISO Data Centre (VILSPA, Madrid).

This Workshop was aimed at highlighting theoretical and empirical methods impacting the detailed analysis and interpretation of ISO spectra, assessing the data quality and calibrations. More than 130 astronomers gathered at VILSPA to discuss ISO observations and associated scientific interpretation, two years after the end of the ISO mission.

A broad range of observational and theoretical branches relevant to ISO were covered through specific topic-oriented sessions including Solar System Observations, Interstellar Medium and Star Formation, Stars and Galaxies, as well as specific sessions devoted to the latest data analysis techniques, theoretical models and laboratory experiments. Finally, the impact of these results in the design of future missions and instruments was also briefly addressed.

The abstracts of the (more than 80) contributions presented at the Workshop are available at:

`http://www.iso.vilspa.esa.es/meetings/beyondthepeaks/`

As for its predecessor, the proceedings will be published in volume 456 of ESA Special Publications series.

```
PH: Organisation of the "ISO Legacy Conference", to be held at
     VILSPA (February 5-9, 2001)
```

As a continuation of the series of Workshops and Conferences organised by the ISO Data Centre, a new conference is now scheduled in the week 5−9 February 2001 on *"The Calibration Legacy of ISO"* (see Figure 2.18).

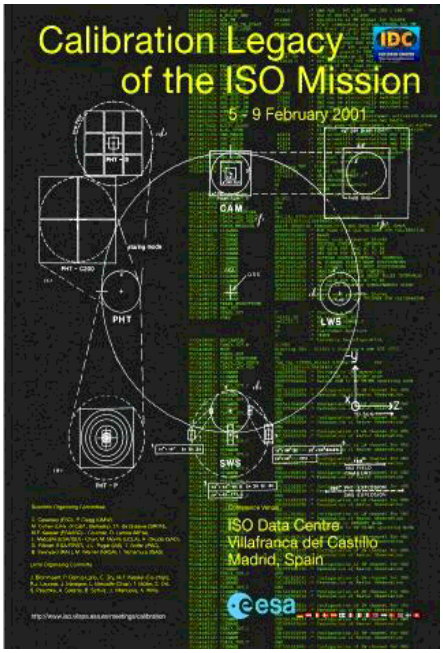

Figure 2.18: *Poster announcing the Conference "The Calibration Legacy of ISO", to be held at VILSPA on February 5−9, 2001*

The programme of the conference will reflect the wide range of astronomical and instrumental calibration issues which have been tackled during the history of the ISO project to-date. Topics range through:

- the establishment of major databases of reference astronomical calibration sources;
- lessons learned relevant to the design of future instruments;
- actual techniques developed, and problems encountered, in the ground-based and in-flight calibration of the ISO instruments.

Particular emphasis will be placed upon the relevance of the ISO experience to calibration of future space missions. So far more than 90 people has already registered for this Conference.

A preliminary summary of the invited programme can be found at:

`http://www.iso.vilspa.esa.es/meetings/calibration/legacy_invited_programme_summary.txt`

The Proceedings of this Conference, as usual, will also be published as an independent volume of the ESA Special Publications series.

```
PH: Evaluation  of calibration improvements recently achieved
     and investigation on internal cross-calibration problems
```

Following the new *statistical* Cross-calibration strategy described in the First Cross-Calibration Status Report, every six months we perform an analysis of the calibration improvements achieved either in the OLP pipeline or in IA, based on the evaluation of the effects observed in the

spectrum of a few hundred sources which had been observed in at least two of the following AOTs: SWS01 (low resolution spectroscopy), PHT40 (PHT-S staring or chopped measurements), or CAM04 (CAM-CVF spectrophotometry).

The goal is to evaluate the internal consistency of ISO calibration for sources observed with these three instruments in the overlapping region from 2 to 15 μm. The sample includes a variety of blue and red objects, faint and bright, and of course point-like and extended sources, which makes it ideal for studying the various calibration problems affecting each type of observation made with ISO as a function of the characteristics of the astronomical source observed.

In this Fourth Status Report we present (see Chapter 3) an updated analysis of the most recent calibration improvements implemented in the pipeline by comparing the new OLP v9 data products with the previous OLP v8.

The same kind of analysis will be extended to longer wavelengths. In this sense, objects observed with both PHT-C filters (photometry beyond 60 μm) and LWS01 containing a few hundred different pointings have already been selected from the ISO Data Archive. The main problem is, in this case, that cross-calibration comparisons are difficult in many cases because the dynamic range of PHT and LWS is very different. Thus, there is a minimum overlapping region in flux level at which both PHT and LWS are of enough quality to derive reliable cross-calibration comparisons. In spite of this, we estimate that a minimum number of 50 cases will probably remain as useful. The results from this comparison will be presented in the Final Status Report.

```
PH: Cross-Calibration comparison of ISO Data with other ground-
     based and space facilities
```

One of the goals of this WG is to assess the validity of ISO calibration by comparing ISO data products with data obtained with other ground-based and space facilities using the same or completely different calibrators.

Work has concentrated in the last few months on the cross-calibration comparison of ISO SWS data with IRAS photometry at 12 and 25 μm and photometric data obtained with MSX (The Midcourse Space Experiment), as well as on the cross-calibration comparison of ISO LWS data with IRAS photometry at 60 and 100 μm. The preliminary results are presented in Chapter 3 of this Status Report.

In addition, we have also presented in previous Status Reports some examples of cross-calibration checks made against ground-based UKIRT observations and other space facilities like COBE/DIRBE, as well as examples of scientific results derived from ISO cross-calibration results.

```
PH: Progress reports on absolute flux calibration
```

The latest progress reports on absolute flux calibration of individual instruments were also presented at the last meeting of the Photometric Calibration WG.

PHT:

PHT-S dynamical calibration, already very successfully applied in PIA, is now implemented in OLP v9.0. In previous versions it was noticed that, in some cases, the use of late type reference stars for which the models did not reproduce well the SiO and CO absorption features caused artificial emission features in the calibrated science spectra. Thomas Müller has investigated whether this has now completely disappeared in OLP v9.0 with the new way in which this

calibration method has been implemented in OLP v9.0, which uses now an interpolated spectral response function for the calibration of the signals instead of individual reference stars.

Figure 2.19 shows the SWS spectrum of the asteroid Hygiea, divided by the assumed thermo-physical model , where we can see that the new dynamical calibration works well, but it seems that there are still residual features present in the spectrum at 3-5% level, due to the influence of the imperfect modelling of late type stars. Spectral features in the wavelength range of the CO (4-6 μm) and SiO (7.5-10.5 micron) bands have to be checked manually to see, if the observed flux level agrees with the flux levels of the late type stars (10-100 Jy at 4-6 μm, 5-30 Jy at 7.5-10.5 μm).

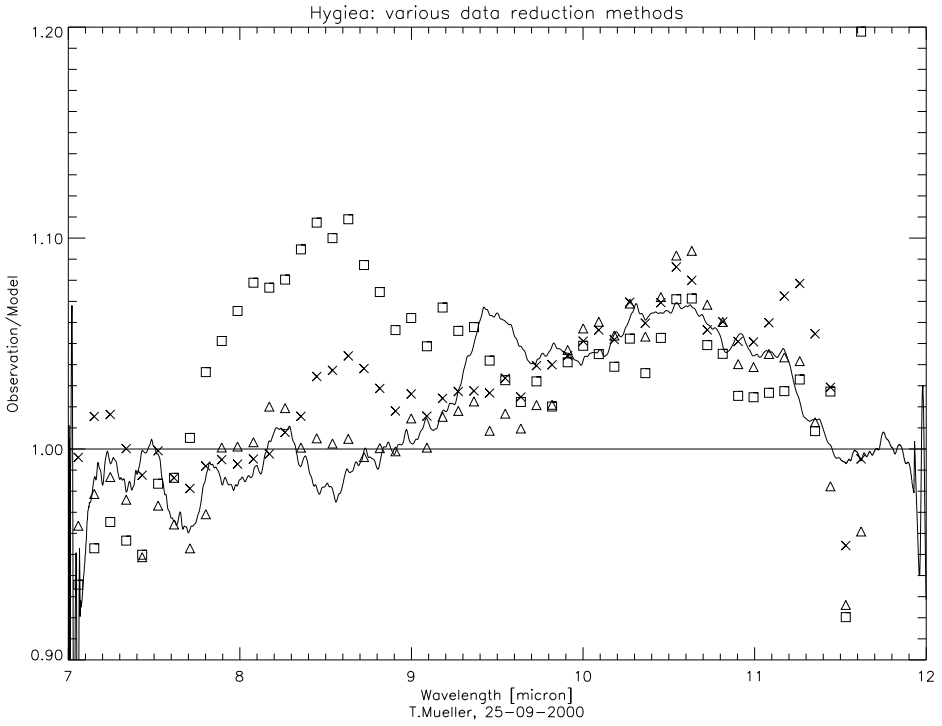

Figure 2.19: *SWS spectrum of the asteroid Hygiea (solid line), divided by its thermo-physical model calibrated with PHT-S measurements of the same asteroid calibrated using the old method using all standard stars (squares), excluding 4 late type standard stars in the reference list (triangles) and with the new method, as it has been implemented in the pipeline since OLP v9.0 (crosses) - Thomas Müller*

In addition, new linearisation tables were included in the OLP9 CAL_G files, as well as upgraded default responsivities and FCS calibration tables. Chopped photometry has also been improved with the new C100 pattern analysis and the upgrading of the signal correction CAL_G files.

LWS:

The most important changes expected for OLP v10 are: illuminator data processing improvements, a more 'intelligent' approach to dark current subtraction, a new RSRF based on LWS01 data and not on COIF data, as well as better uncertainty calculations and absolute flux uncertainties. Some other changes are being considered like detector stitching for faint sources. A strong source correction tool will be implemented in LIA (not in OLP) which will improve the flux accuracy to the 10% level.

Details on most of these calibration aspects will be given in Chapter 4.

CAM:

The main problem for the absolute flux photometry of point sources detected with ISOCAM remains the transient correction. Whether a useful routine to handle it will come out by the end of this year remains uncertain.

An analysis of the ghost reflection in CAM-CVF and how it impacts the Spectral Response Function (SRF) shows that the SRF is only marginally affected in comparison with the existing CAL_G SRF.

In addition, the impact of new available reduction routines (new de-glitching method, Fouks-Schubert transient correction) in OLP v9.5 on the SRF was also analysed. The result is that only the effect of the Fouks-Schubert transient correction can be important on the SRF at the start of the CVF measurement and especially for low fluxes.

The whole analysis lead to a further investigation on different methods to perform photometry. It was found that the current PSF-fitting routines can considerably underestimate the flux, especially at the smaller p.f.o.v. images. Aperture photometry can also be quite dependent on the radius of the aperture used (10% effect). The problems all arise from the fact that the theoretical PSF which is used for the fitting does not perfectly match with the observed one.

The conclusion at the moment is that we still stick to the old method used for SRF determination. But the SRF is only usable in limited case, because of the strong dependence of observation/reduction. A report is in preparation by Joris Blommaert and Koryo Okumura with a description of all these effects in detail.

SWS:

SWS will use a completely new, simplified flux calibration strategy in OLP v10, which takes advantage of the extremely high stability of the SWS detectors over the full lifetime of ISO. The current flux calibration performs 3 functions: 1) flat-fielding of the different detectors; 2) apply the gain determined from the internal calibrator; 3) apply signal to flux conversion.

The document *"Modification of SWS Flux Calibration"* by Russ Shipman and Fred Lahuis describing in detail this new strategy and containing the full list of observations and models used for the absolute flux calibration of SWS is available as an internal document.

Memory effects correction is now being tested for implementation in OLP v10.

New model SEDs for 16 sources were delivered by Leen Decin (KUL) which will provide a more homogeneous set than the original Cohen ones and will be used in the OLP v10 calibration.

2.2.5 Spectral Matching and RSRF:

`SM: Uranus models and the absolute flux calibration of LWS and PHT`

The Relative Spectral Response Function (RSRF) and the absolute flux calibration of LWS grating observations are based esentially on Uranus as primary calibrator. The reason for this is that Uranus is the only 'flat' bright source with a well modelled spectrum in the full LWS spectral range.

The RSRF of LWS was derived from a single 5.7 hour 36 full scan LWS01 observation of Uranus interleaved with dark current measurements which took place in revolution 317 on the 28th

September 1996. The whole observation was followed by a series of illuminator operations to establish the baseline for correcting any drift in detector responsivity with time.

All previous and subsequent observations are referred to the photocurrent to flux relationship derived from Uranus by taking the ratio between the signal measured when the illuminators are operated during an observation, and that measured when they were operated during the calibration observation of Uranus. To ensure that the power from the illuminators did not change during the course of the mission, weekly observations were made of a series of astronomical sources and the signal from these were compared to that from the illuminators.

In order to determine the conversion from photocurrent to absolute flux densities a Uranus model provided by Griffin and Orton is used as of OLP v8.7. The accuracy of this model is estimated to be better than 7% at all wavelengths.

Uranus is also used as one of the standard calibrators in the long wavelength range by ISOPHOT. However, in this case the Uranus model was provided by Abbas at an early stage of the mission and was never updated.

A quick analysis of both model spectra shows that their consistency is better than 10-15% in the wavelength range from 30 to 240 μm, although at shorter wavelengths the models become less certain (see Figure 2.20).

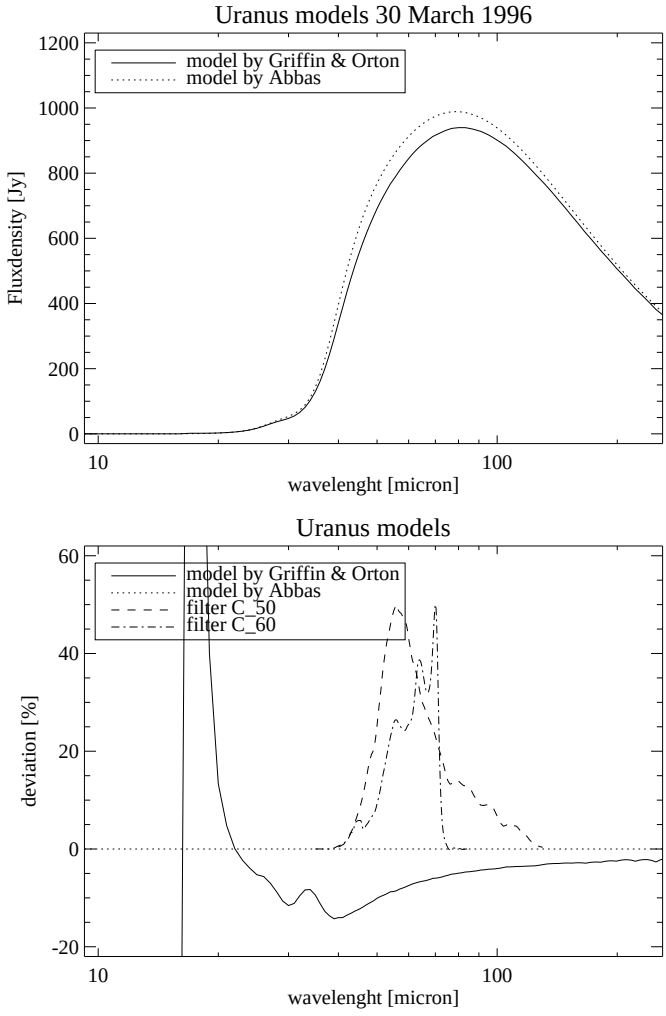

Figure 2.20: *Comparison between the Uranus models used by LWS (Griffin & Orton) and PHT (Abbas) - Bernhard Schulz*

`SM: Development of an SWS vs PHT-S convolution tool`

Bernhard Schulz has recently produced a small IDL routine named 'convolve2phts.pro', available at:

`ftp://ftp.iso.vilspa.esa.es/pub/idc/bschulz/convolve_phts/`

which convolves high resolution spectra within the 2.5 to 12 μm wavelength interval to the spectral resolution of PHT-S.

The program might be of interest for people trying to compare emission line profiles and intensities in spectra of sources observed both with SWS and PHT-S.

`SM: Stitching between detectors in LWS`

The ratio between neighbouring detectors for all LWS01 observations was calculated some time ago from OLP v7 browse products. Table 2.2 shows the results obtained (rejecting a few obvious outliers where the overlapping detectors differ by more than a factor of 2). Obviously, the numbers given in this Table may be slightly obsolete. A re-calculation of these stitching factors is expected for OLP v10 data products.

Table 2.2: *Mean flux ratios from overlapping LWS detectors - Martin Burgdorf*

Detectors	Mean ratio
SW1/SW2	0.956
SW2/SW3	1.010
SW3/SW4	1.005
SW4/SW5	1.008
SW5/LW1	1.048
LW1/LW2	1.074
LW2/LW3	1.040
LW3/LW4	0.986
LW4/LW5	0.901

The following conclusions can be extracted:

- Detectors SW2-SW5 stitch better than 1%, therefore it appears that they define the absolute flux level in a more reliable way than SW1.

- Only two detectors differ by more than 5%.

- Detector LW5 appears systematically high with respect to LW4. Calculating the mean value of LW4/LW5 for nine different sets of 100 revolutions always give a value significantly lower than 1. This is the case even though one would expect the opposite effect from the contribution of extended sources which might be included in the sample.

- No obvious trend with time is found in the quality of the stitching.

2.2.6 Transients:

`TR: Applicability of Fouks-Schubert transient correction to the various types of detectors on-board ISO`

The applicability of the Fouks-Schubert method to the various types of detectors on-board ISO (see Table 2.3) can be discussed in terms of the E_j parameter which basically measures the quality of the contacts in the detectors under study.

	detector name	type	wavelength (μm)	pixels
CAM	SW	CID In:Sb	2.5 – 5.5	32×32
	LW	Si:Ga	4 – 18	32×32
PHT	S1 & S2	Si:Ga	15 (peak)	two 1
	P1	Si:Ga	15 (peak)	1
	P2	Si:B	25 (peak)	1
	P3	Ge:Ga	100 (peak)	1
	C 100	Ge:Ga	100 (peak)	3×3
	C 200	Ge:Ga (stressed)	180. (peak)	2×2
SWS	band 1	In:Sb	2.4 – 4.1	1×12
	band 2	Si:Ga	4.1 – 12	1×12
	band 3	Si:As	12 – 29	1×12
	band 4	Ge:Be	29 – 45.2	1×12
	FP band 5	Si:Sb	11.4 – 26	1×2
	FP band 6	Ge:Be	26 – 44.5	1×2
LWS	SW1	Ge:Be	43. – 50	1
	SW2-SW5, LW1	Ge:Ga	50 to 110 (10)	five 1
	LW2-LW5	Ge:Ga (stressed)	110 to 190 (20)	four 1

Table 2.3: *List of the IR detectors on-board ISO with indications of type, operating wavelengths (peak or range) and detector topology (individual pixel, linear or matrix array).*

It is found that for the Si:Ga ($\sim$4$-$15 μm) detectors on-board ISO (PHT-S, CAM, SWS) we have $E_0/E_j >> 1$ while for the Ge:Ga ($\sim$40$-$150 μm) detectors (PHT-C, LWS) we have E_0/E_j $\sim$1 or $<< 1$. Fouks-Schubert model can be used only when $E_0/E_j >> 1$.

The consequence is that for Ge:Ga detectors the Fouks-Schubert model does not seem appropriate. No accurate analytical models can be derived from the set of equations which describe the problem. Numerical models (Haegel et al. 1999 Appl. Optics, 38, 1910) exist but need big computing resources and are very difficult to compare with data, and they cannot be used like analytical models to do transient corrections. At the present time only empirical models properly reproduce them but with a limited exactness.

For uniform illumination, the response of Si:Ga detectors is precisely described by one non-linear model. The problem of non-uniform illumination (point sources) is, however, more complicated.

In a recent contribution made by Alain Coulais et al. to the SPIE 45th Annual Meeting held in San Diego (California) this year a complete review of the physical and empirical models that were actually developed for the ISO detectors together with some dedicated inversion techniques. The document *"Transient response of IR detectors used in space astronomy: what we have learned from ISO satellite"* can be found at:

`http://www.iso.vilspa.esa.es/science/pub/2000/Coulais_SPIE45.ps.gz`

The problems encountered with ISO detectors are obviously extremely useful in order to test and improve the Si and Ge detectors to be used in future space projects.

`TR: Implementation of pulse shape corrections in the SWS pipeline`

The so-called SWS 'pulse shapes' are small detector voltage jumps visible at SPD level which affect the calibration of SWS spectra leading to flux shifts of up to 10 Jy in the worst cases.

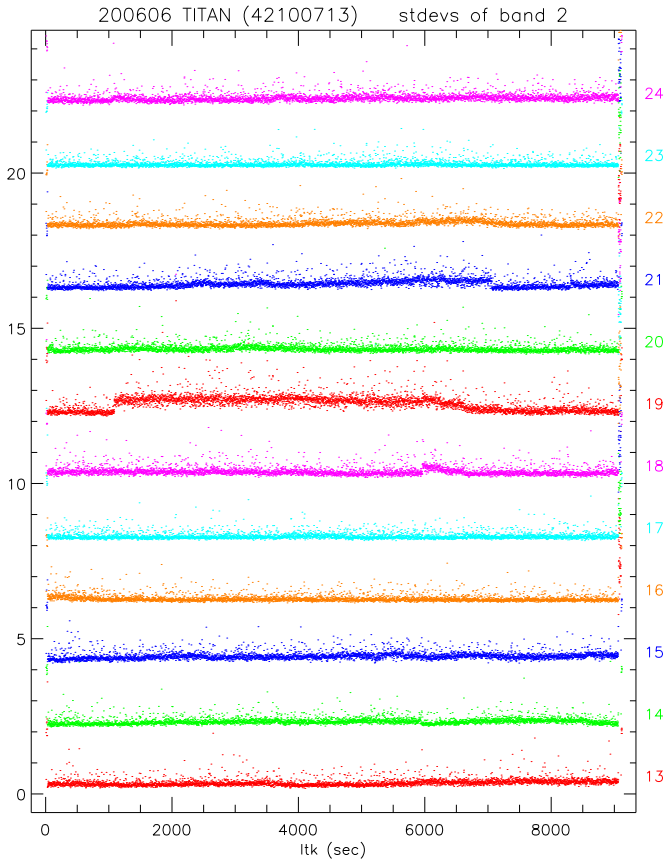

Figure 2.21: *Example of pulse shapes detected in the SWS spectrum of Titan at SPD level - Fred Lahuis*

They occur in only one detector at a time and can be generally described as a sudden decrease or increase of the signal, which then remains constant or has a long recovering time (>> 10 s) after the jump. These jumps are normally seen at low signal levels and there are typically a few of them per hour randomly distributed in time (see Figure 2.21).

There are indications of a relation between the signal jumps and a residual after reset pulse effect.

A tool has been developed by Fred Lahuis which corrects for these voltage jumps by adjusting a baseline to the affected portion of data which remove almost completely the effect on the calibrated spectra. As a byproduct, the tool also corrects for glitches since they have a similar effect on the signal. This way most of the detector jumps are removed with very high efficiency (although not all and not always up to the 100% level).

This correction tool has already been implemented in OLP v9.5.

For a more detailed description of the problem the document *"Pulse-shape Correction"* by Fred Lahuis is available at:

`http://sws.ster.kuleuven.ac.be/documents/PULSE_SHAPES/pulse-shape.ps`

`TR: Transient corrections in band 2 SWS data`

The application of the adapted Fouks-Schubert method to correct band 2 (Si:Ga) detectors for memory effects developed by Do Kester is currently implemented in SWS IA and, soon, in OLP v10. Later it will be incorporated into OSIA. The recently improved version of the so-called 'dynadark' IDL module is, in addition, now much faster (a factor of 4).

The detector parameters $\beta = 0.82$ and $\Lambda = 63$ V^{-1} finally adopted for the pipeline are the same for all detectors, after a detailed analysis of possible dependences with revolution number, flux level or temperature, which were finally discarded.

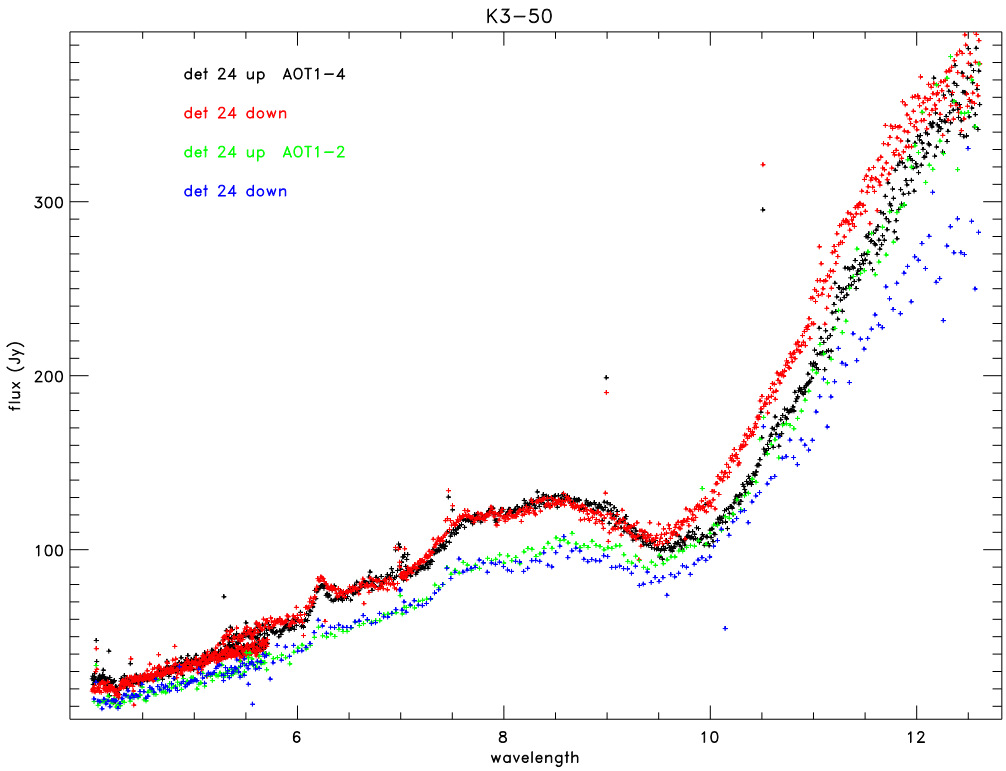

Figure 2.22: *The K3-50 spectrum as processed with the standard pipeline. Only detector 24 is displayed. The up and down scans are different and the measurements with different speeds give different results - Do Kester*

In Figures 2.22 and 2.23 we show an example of the application of this method to two observations made with SWS on the compact HII region K3−50, an AOT1 speed 2 and a four times as long AOT1 speed 4. As memory effects live in the time domain, and not in the spectral domain, the measured signal is quite different. Standard pipeline processing does not address memory effects yet. So the resulting spectra are quite different. Figure 2.22 displays the up and the down spectral scan of both AOTs for detector 24 only. The AOT1 speed 2 is generally below

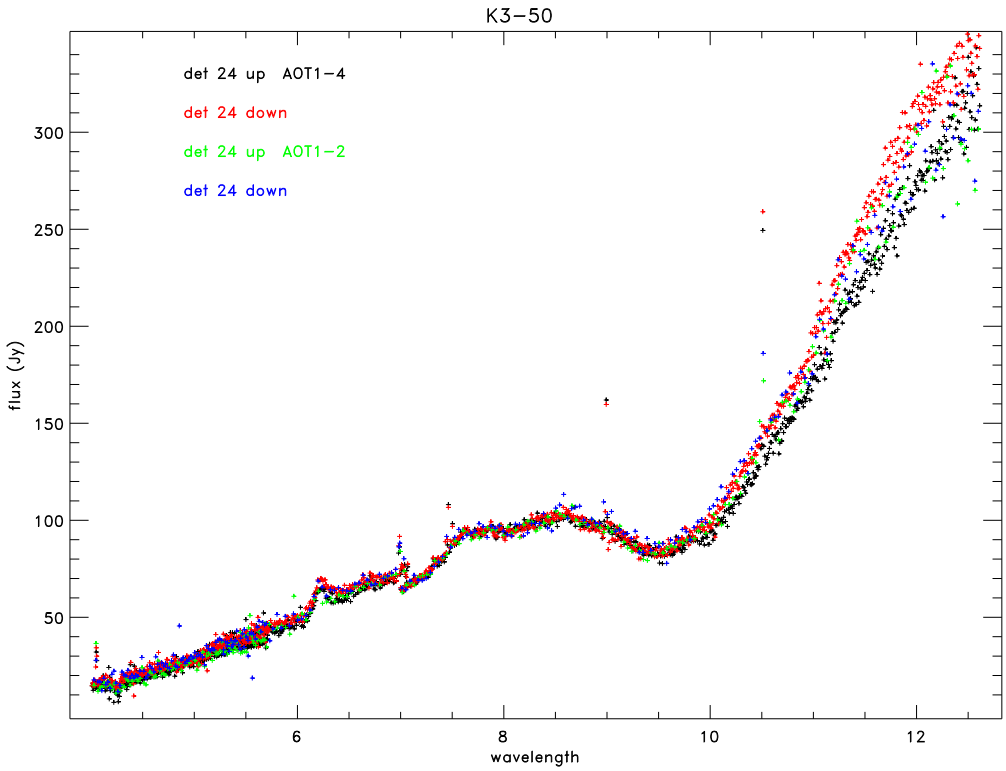

Figure 2.23: *The K3-50 spectrum as processed using the memory model. Only detector 24 is displayed. The AOT1 speed 2 and the AOT1 speed 4 overlap. Note that the formal end of band 2 is at 12 μm. Band 3 starts there.*

the speed 4 points. Also the up and the down scans are not on the same level, more so in the speed 2 than in the speed 4. The speed 4 has had more time to relax to the final signal levels.

In Figure 2.23 the memory model has been applied. Now both AOTs give the same final spectrum. The up and the down legs also overlap much better.

The other processing steps, after application of the memory model, were exactly the same as in the standard pipeline. This is not as it should be. It can be seen that the total flux goes down when applying the memory model. We have to derive new flux calibration tables yet. Small effects of this can be seen at the band edges. They don't line up completely.

Note the discrepancy in the black crosses after 10 μm. This is a so-called detector jump (see previous subsection). It can hardly be noticed in the SPD as it is masked by the flux of the source itself. But here we can clearly see it. The memory model is so good that these other effects stick out like a sore finger.

A detailed description of the way in which the Fouks-Schubert method has been adapted to SWS band 2 data and how the detector parameters have been chosen is contained in the internal document *"Memory Effects and their Correction in SWS Si:Ga detectors"* by Do Kester.

Unfortunately, for SWS band 4 there is no working model yet. Fouks-Schubert method simply does not work in this type of detectors, as we have already mentioned. Efforts are, however, still on-going trying to find an alternative method, although it will certainly not be possible to implement any solution for this problem in OLP v10.0.

`TR: Transient effects in ISOCAM: progress status and plans`

The Fouks-Schubert correction has now been implemented in the processing of OLP v9.5 data products.

A general description of transients in ISOCAM LW detectors can be found in *"Transient correction of the LW-ISOCAM data for low contrasted illumination"* by Alain Coulais and Alain Abergel (A&AS, 141, 533)

available at:

`http://www.iso.vilspa.esa.es/science/pub/2000/ds8869.ps.gz`

This document shows that, for uniform (low gradient) illumination, the Fouks-Schubert model allows us to describe the LW response to upward and downward steps of flux with an accuracy of better than 1%. For each pixel, only two parameters have to be used, which are found to be constant over the whole life of ISO. However, the approach is not valid for non-uniform (high gradient) illumination, which is typically the case of point sources.

Alain Coulais, in collaboration with Boris Fouks, is still trying to find a possible solution to the problem of describing the transient behaviour of point sources in ISOCAM data.

Efforts are concentrated on in-flight data taken with CAM with the $1.5''$ lens and filters LW10 and LW3 (largest PSF) where the lowest spatial gradients on individual pixels are expected.

Unfortunately, none of the empirical models tested so far give correct responses (closer than 10% for each pixel and each readout).

Recently, an innovative 3-D approach is being tried which looks promising. First attempts were based on an inaccurate knowledge of some important parameters of the detectors (both geometrical and electrical). Part of these missing parameters were unknown, others were not published because they were not considered useful in the past. The new model takes into account the true geometry and good parameters of the detectors in order to derive an adapted semi-analytical model (only recently it was found that between each contact there is another electrode which can have an important effect on the model, and the sizes of bottom and upper contacts have been determined).

Additional tuning of the model is still on-going (taking into account the reflecting plane, for instance, or the rectangular geometry of the pixels, so far considered circular). This is needed in order to obtain satisfactory quantitative results (may be up to the 5-10% level of accuracy). Still there are problems not solved, like how to deal with the different behaviour in the transient response as a function of the precise part of the pixel which is illuminated by a given point source (the behaviour is not the same if the point source falls at the centre of the pixel or at the edges).

The new 3D equations have been obtained with the current conservation condition (1D) replaced by the continuity equation (3D) and some new boundary conditions. The kernel so created is the 3D equivalent to the 1D description of the problem and shows how the field of the charges created under a flux change in one point of the (x,y) plane penetrates through the bulk and spreads to all sides creating 3D picture of the force lines of the field. This effect is strong because the screening length for the charges, created in the bulk of low-background detectors under a time-variable irradiation, is very long, creating cross-talkings (current spreading). A pixel is illuminated, but the charge from it creates currents in neighbouring pixels (see Figure 2.24). Under homogeneous irradiation, the influence of the 3D field effects on the transient current in the detector can be described with a good exactness in one dimensional (1D) approximation

with the use of the field averaged along the contact planes and with the re-normalization of the contact parameter E_j. For highly inhomogeneous irradiation such approach is impossible, and 3D equations must be used.

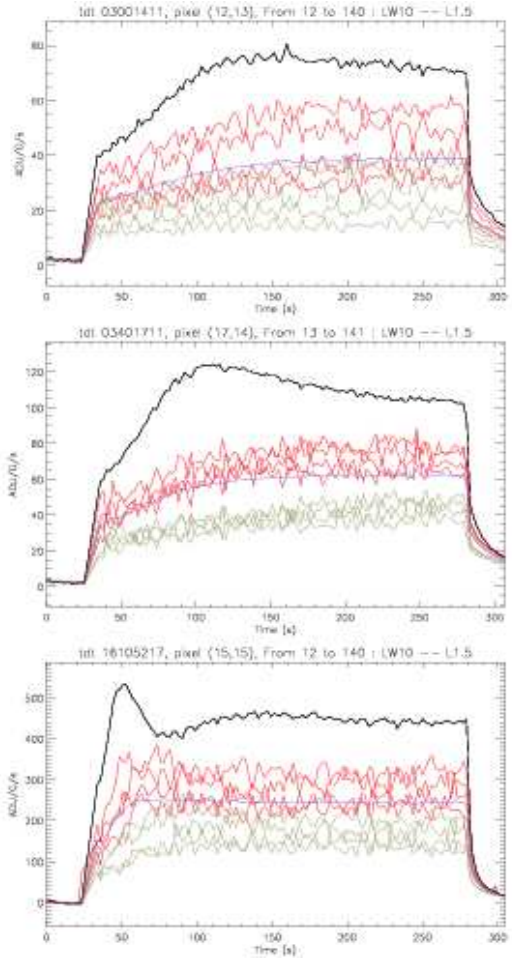

Figure 2.24: *Signals coming from the 3x3 pixels around point sources detected with CAM are shown in the left panels for three different flux levels. The central pixel is plotted in dark; in red, the four closest neighbour pixels; in yellow the four pixels in the corner; the blue line is the mean of the 9 pixels - Alain Coulais*

The computed results derived from the currently simplified 1D model (see Figure 2.25) illustrate the current spreading (the appearance of the current in dark regions neighboring to the illuminated ones) that results from the spreading of field lines and the current overshooting that results from a high current density in the region under a high-density flux. The presented results give rather good qualitative description of the transients under point-source illumination. In order to get an exact quantitative description of the transients the theory has to take into account the real 3D topology of the detectors and their conductive surroundings.

Unfortunately, the amount of work pending is considerable and it will not be possible to include any tool to correct point source fluxes for transients in the ISOCAM pipeline.

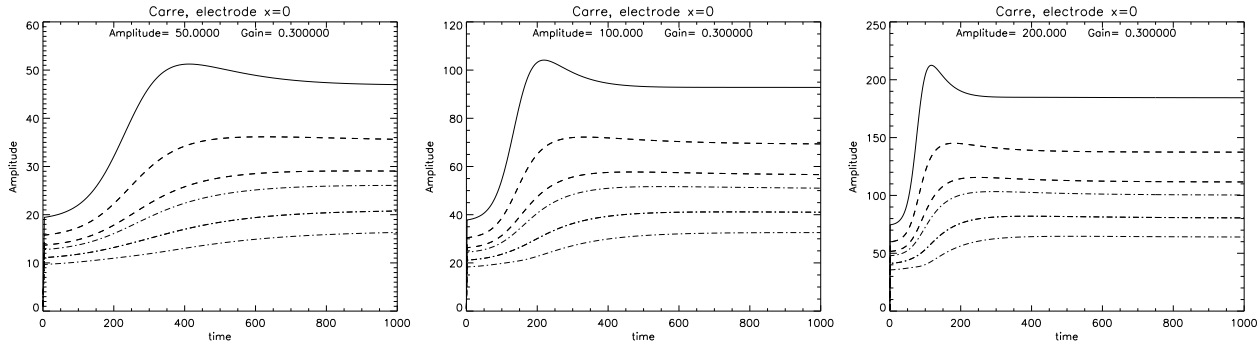

Figure 2.25: *Three model transient responses for the same point spread function profile with three different amplitudes. The source is off-centered by (1/4,1/4) of pixel size. The continuous line shows the transient response for the central pixel, the dashed lines are for the the 4 adjacent pixels (only 2 lines because of symmetry) and the dot-dashed lines are for the diagonal pixels (3 lines). Note the similarities with real observations shown in Figure 2.24 - Alain Coulais*

`TR: Transient effects in ISOPHOT: general status and plans`

Full transient correction methods are, in the case of ISOPHOT, restricted to PIA in most cases, where several corrections are available. The main reason for this is that, because the quality of the fit must be checked, these methods are usually highly interactive.

The corrections available in PIA include empirical solutions based on exponential functions for the Ge:Ga type detectors (P3, C100 and C200); or a Fouks-Schubert correction that can be applied to P1 and P2 filters (Si-based) and PHT-S measurements. However, the detector specific constants of P1 and P2 filters have not been fully determined and the model cannot reproduce the often appearing hook responses in the signals of these detectors while the model seems to work well with the chopped PHT-S mode.

In OLP, a routine has been implemented which detects the presence of a significant signal transient in the case of staring PHT-P and PHT-C observations. When a transient is detected, a range of unreliable signals is flagged. The algorithm is iterative and is applied until either no significant systematic variation can be detected in the remaining signals or a minimum number of signals is left.

In the case of chopped PHT-P and PHT-C observations, non-stabilized signals cause significant losses on the true difference signal. The present signal derivation in OLP relies on the analysis of signals from pairs of consecutive readouts rather than signals per ramp. This gives better statistics of the signals per chopper plateau, since in many chopped measurements each chopper plateau covers only a few (typically 4) ramps. To increase further the robustness in determining the difference signal, the repeated pattern of off-source and on-source chopper plateaux yields a *generic pattern* in a chopped measurement which consists of only 1 off- and 1 on-source plateau. The generic pattern is generated using an outlier resistant averaging. The shape of the generic pattern determines the correction factors with regard to stabilized staring measurements.

Since OLP v8.4, an empirical model is used to correct PHT-S chopped data for transients which is based on the comparison of behaviour with respect to reference stars, while for PHT-S staring observations the so-called 'dynamic calibration' method is prefered and used as part of OLP since version 9.0. The calibration is performed by comparing the signal time evolution of the target star with a that of a set of standard stars at similar flux levels.

Previously, the dynamic calibration method was implemented in PIA (since version 7.3), where the signal time evolution for each pixel was fitted with a Chebyshev polynomial and stored in a

database, together with the equivalent flux assigned by comparing the behaviour observed with that of the best matching calibrator. This way an accuracy in general better than 10% can be achieved and the spectral shape is well preserved. The goodness of the correction method is based on the high reproducibility of behaviour of every PHT-S pixel (same time constants) for a given illumination level.

In OLP v9.0 the method has been automated by creating surfaces which describe the temporal behaviour of each PHT-S detector pixel under different illumination conditions which are just the result of the interpolation of all different calibration observations.

An example showing the extraordinary improvements that can be achieved with this method is shown in Figure 2.26.

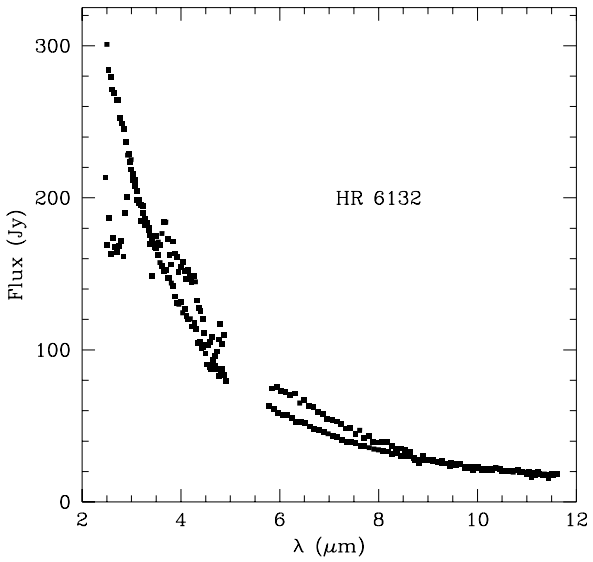

Figure 2.26: *PHT-S (staring) spectrum of the star HR 6132 before (black squares) and after (red squares) the dynamic calibration method to correct for transient effects is applied to the spectrum*

`TR: Transient effects in ISOPHOT: P32 chopped raster maps`

Work in the last six months has mainly concentrated in the correction for transient effects in PHT32 chopped raster maps.

During the ISO mission, the ISOPHOT instrument has collected more than 1100 observations in oversampled mapping mode (AOT PHT32) in the wavelength range of 45 to 240 microns. The observations comprise mapping of small and large extended regions, but also faint point sources. In this case the mapping approach was adopted in order to minimize confusion noise.

PHT32 observations are still not scientifically validated because of strong signal transients due to flux changes generated by the relatively fast chopper movement which produces never-stabilized signals. The effect is a decrease in the source flux measured (up to a factor of 3, depending on the flux contrast between source and background), problems with the determination of PSFs for point vs extended sources and the presence of ghosts (90 arcsec away in the y-axis direction).

The transient behaviour observed cannot be modelled (over- and under-shooting effects are usually observed). Richard Tuffs has tried to approach the problem by making use of the redundancy given in the PHT32 mode. The method applies an iterative drift correction assuming

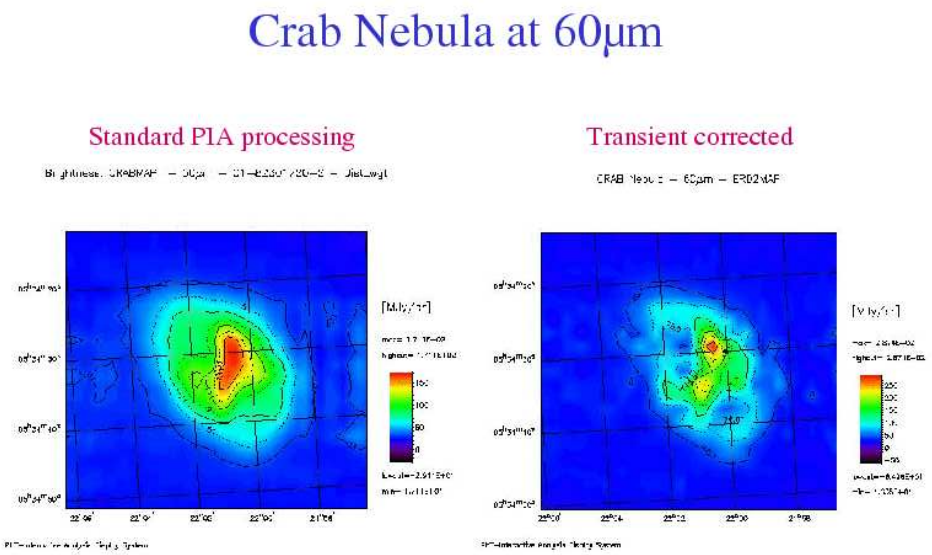

Figure 2.27: *PHT32 map of the Crab Nebula at 60 μm with standard processing (left) and after application of the new transient correction (right) - Richard Tuffs*

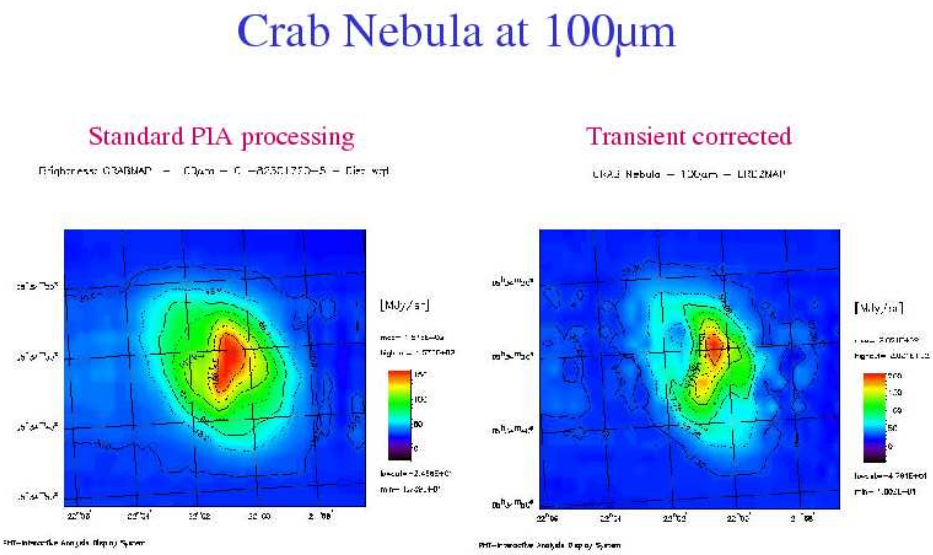

Figure 2.28: *PHT32 map of the Crab Nebula at 100 μm with standard processing (left) and after application of the new transient correction (right) - Richard Tuffs*

a 2 exponential drift curve and, as we have already mentioned, uses data redundancy, deriving the initial drift constants from calibration targets.

The results obtained are quite satisfactory now (see Figures 2.27 and 2.28) and an interactive correction tool has been implemented succesfully in PIA (no hope of including this correction in OLP v10.0). The algorithm used, however, is highly interactive and requires a considerable level of expertise from the user. Since the algorithm cannot be released with a large amount of initial support, hands-on workshops on PHT32 processing have been organized at VILSPA and IPAC in order to support data reduction (see Section 2.2.7).

`TR: Transient effects in ISOPHOT: C100 detectors`

A preliminary analysis has been made also concerning transients in PHT C100 Ge:Ga detectors by J. Sée at IAS. After testing different models (linear and non-linear, empirical or physical from Fouks' team), it was concluded that only an empirical non-linear model with a non-symmetrical behaviour can reproduce the observations:

- downward incoming flux steps results in an instantaneous decrease of $J_n(t)$ down to J_n^∞

- upward incoming flux step results, after an instantaneous jump β in an exponential increase of $J_n(t)$ up to J_n^∞.

Moreover, the memory effect from the block $n-1$ into the n-th one is taken into account (in an approximated form) and, as seen in the data, the memory effect is reset when a downward step occurs.

To correct for these transients effects a block by block inversion method has been developed by F. Belleux and implemented locally into the framework of PIA.

Two kinds of information are available:

1. the sought incoming flux is positive and

2. "by construction" a piecewise constant signal.

The idea developed is to account for these informations in order to make the inversion robust. This kind of 'a priori' knowledge can be captured mathematically.

Simulations show that the proposed method properly inverse the system and correct the transients and the reconstruction error is less than 1%. In the case of real data analysis the method seems to work as well as for the simulated data but the presence of glitches tends to slightly overestimate the stabilized value.

In addition, there are still problems with the method because of the known limited accuracy in the FCS, the limited accuracy in the determination of the (β,λ) maps for the 3×3 detectors (using median value at this moment) and the non stationary noise of the detector, whose impact on the method is still under study.

In parallel, comparison of ISO maps taken with C100 detectors are being made against IRAS maps of the same fields which show that the consistency in relative flux level is within 5%.

`TR: Transient effects in LWS: status and plans`

All LWS detectors exhibit transient behaviour. This falls into two main categories, a long term transient due to the steady accumulation of particle hits during each revolution and a short term transient caused by changes in flux. In terms of calibration the transients cause two problems, the correct determination of line strength and wavelength and the determination and application of a steep edged spectral response function.

Figure 2.29 shows the response of the three detector types in LWS to a illuminator sequence. The Ge:Be detector SW1 has a long time constant (several minutes) in response to illuminator 1 and this is also apparent when the illuminator is switched off. The unstressed detectors have a fairly flat response whereas the stressed detectors have a hook response.

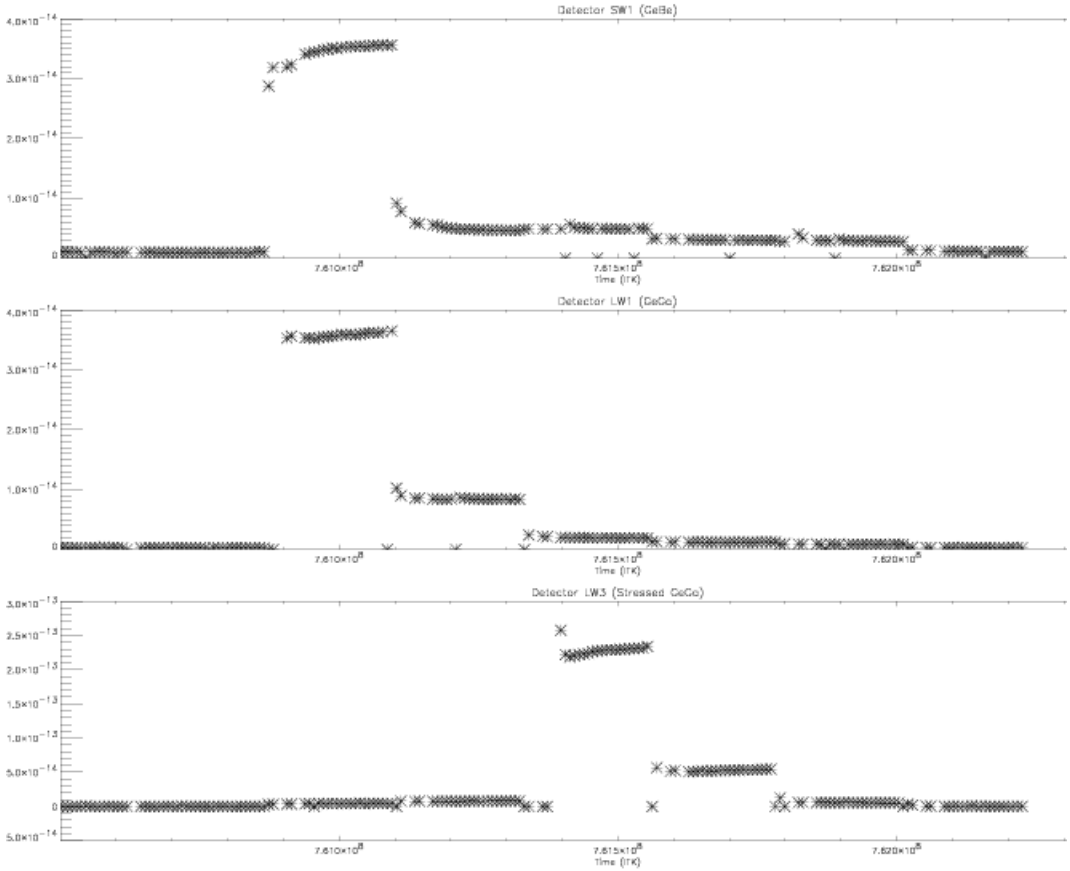

Figure 2.29: *The response to an illuminator sequence of the three detector types used by LWS: Ge:Be SW1 (top); unstressed Ge:Ga LW1 (middle); stressed Ge:Ga LW3 - Tanya Lim*

One of the major effects of transient behaviour is in the determination and application of the relative spectral response function (RSRF). LWS is operated in a mode where the grating is scanned forward and backward through the spectral range. For most detectors the scans pass through steep sided RSRFs and the resultant profiles are clearly split with the photocurrent dependent on scan direction. The calibration stategy up to now in the derivation of the spectral response function has been to average all data before dividing by the Uranus model. However when this averaged RSRF is applied in the pipeline it leads to scan dependent behaviour in the resultant spectra. Figure 2.30 shows a spectrum of Uranus for the two worse affected detectors SW1 (Ge:Be) and LW2 (Ge:Ga(s)). In the case of SW1 the response function is triangular leading to a cross over effect at the top of the response function (around 48 μm). LW2 has a steep sided response at the long wavelength side and has a relatively long time constant (a few seconds). One possible approach is to use two RSRF functions, each derived only from scans in one direction. Attempts at this calibration stategy have so far led to promising results.

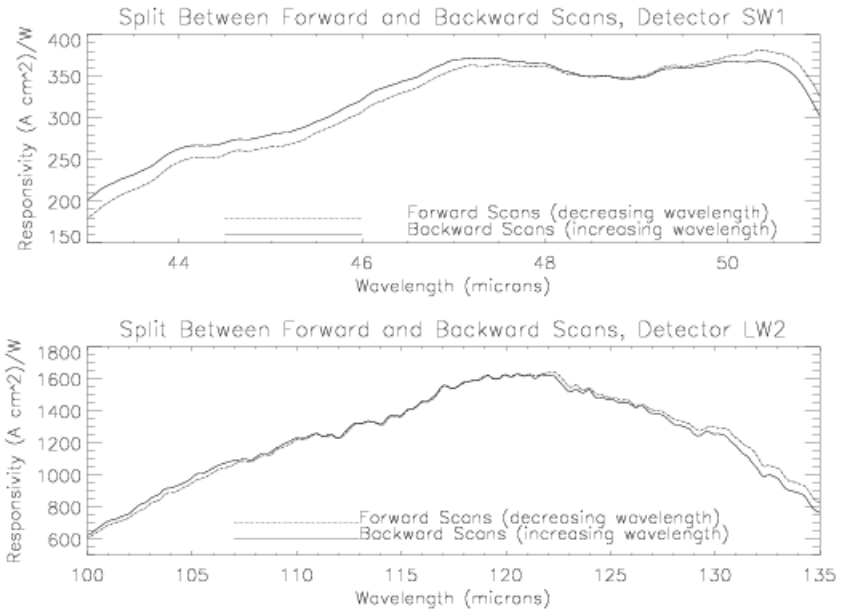

Figure 2.30: *Spectrum of Uranus showing split between forward and backward scans for the two detectors worse affected by transient behaviour - Tanya Lim*

Emmanuel Caux is working on the correction for memory effects in LWS data applying a correction based on the Fouks-Schubert model adapted for LWS data.

Although the Fouks-Schubert model, as we have already mentioned, is in principle not applicable to Ge-based detectors (with the exception may be of LWS parallel mode observations), memory effects can be at least partially removed for LW detectors which are based on Ge:Ga (note that the stronger memory effects are observed in the stressed Ge:Ga detectors LW2 to LW5) by the application of this correction (see Figure 2.31)

Satisfactory results are obtained in all cases where the modified Fouks-Schubert method was applied. The method also consider overshooting effects for big flux jumps.

The situation is worse for Ge:Be detectors (the case of SW1) where Fouks-Schubert model simply does not work.

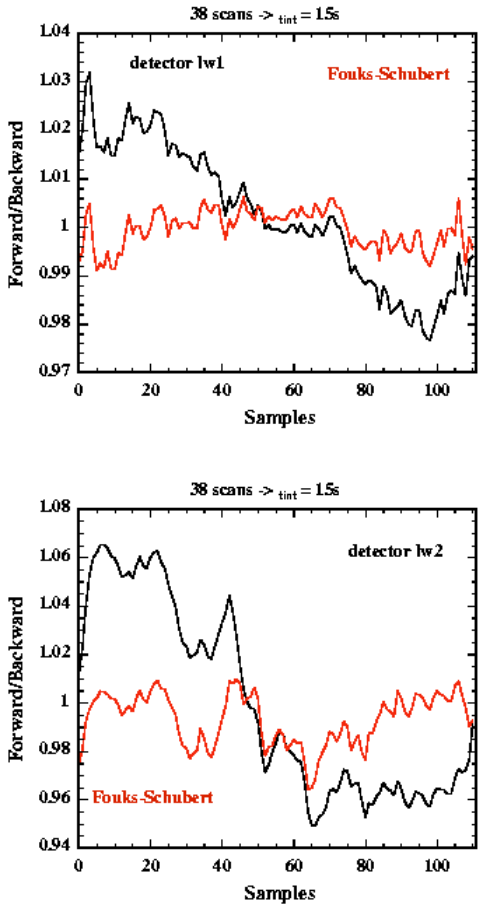

Figure 2.31: *Ratio of LWS forward/backward scans before and after the application of the transient correction based on the Fouks-Schubert model - Emmanuel Caux*

At the last LWS OLP 10 Review Meeting held at RAL in March this year it was decided to support the generation of transient corrected RSRFs (at least for LW detectors) using the adapted Fouks-Schubert model, which are now being produced at CESR by Emmanuel Caux. The new RSRFs so obtained differ by just a few percent with respect to the old ones. The impact on the whole LWS calibration will be investigated by Tanya Lim at RAL. The improved RSRF, however, will only be implemented in LIA, but never in OLP v10.

Exploring all space parameters for α, β and E the analysis performed so far leads to the following conclusions:

1. β is rather constant (0.74 to 0.95, depending on the detector considered)
2. α and E are not independent (α = a − b x log(E))

The routine used to find the Fouks-Schubert parameters is stable, but it still remains to check posible dependences on the spectral shape of the source.

The quadratic difference of forward/backward scans is more important for detectors presenting a large memory effect (SW1, LW2 and LW3). This gain depends also on the type of source observed; extended sources with large fringing lead to a much more important effect than point sources observed with the same detector and similar photocurrent on the detector.

The transient behaviour of the LWS detectors also affects the line flux accuracy. The effect is dependent on both the line flux and illumination history, and at this time no correction is done. The effect however is minor with the worst case stressed Ge:Ga detectors only affecting the line flux by a few percent. The unstressed Ge:Ga detectors although exhibiting transient behaviour have very short time constants and have a negligible effect on line fluxes. The detector most affected is the Ge:Be detector which has time constants of the order of minutes, however very few bright lines have been observed in this wavelength range (43-51 μm).

2.2.7 Interactive Analysis:

`IA: Distribution of questionnaires on IAs`

In order to improve the communication flow with the users, the decision was taken by SWS, PHT and LWS members of the WG to follow the initiative of CAM and send an e-mail questionnaire out to users soliciting thoughts on their IAs. PHT has already sent out its own questionnaire to PIA users (over 100 identified) last February while SWS will soon do the same with a similar questionnaire adapted to the specific characteristics of this instrument to be sent to OSIA users.

In both cases answers were received from about 25% of the people to which the questionnaire was sent.

In general users were very happy with both IAs. The major lesson learned from this exercise was that users should be asked for their comments early on in the S/W development cycle, rather than near the end when few addition can be made.

`IA: Recent IA releases: major improvements and future plans`

A summary of the implementation status and plans per IA can be found below together with a list of major improvements contained in the more recent versions released with respect to previous ones.

- **PIA v9.0:** (released July 7, 2000)

  This was a small update of PIA v8.2, released in April 2000, which fix some identified bugs and include minor improvements. The release note is available at:

  `http://www.iso.vilspa.esa.es/manuals/PHT/pia/latest_version/rel_notes.txt`

One of the recent improvements implemented in PIA is the Map Simulator. This is a mapping simulation system released already with PIA v8.2 which allows the user to simulate sky (background + point/extended sources) and what the detectors PHT-C100 or PHT-C200 should have seen from it in any of the different observation modes (PHT22 or PHT32), including glitches and transient effects. The data derived can be ingested as normal measurements into PIA.

A detailed description of the capabilities of this simulator can be found in the document *"Map coadding and simulation techniques with the ISOPHOT Interactive Analysis (PIA)"* by Carlos Gabriel and Min Hur, available at:

`http://www.iso.vilspa.esa.es/users/expl_lib/PHT/cgabriel-SP455.ps.gz`

Another interesting tool recently implemented under the PIA environment by Richard Tuffs and Carlos Gabriel is the PHT32 map processing for C100 and C200 arrays, which correct chopped raster maps for transient effects applying an iterative drift correction assuming a 2 exponential drift curve and uses data redundancy, deriving the initial drift constants from calibration targets. This is a highly interactive tool which requires a considerable level of expertise from the user. Since the algorithm cannot be released with a large amount of initial support, hands-on workshops on PHT32 processing have been organized at VILSPA and IPAC in order to support data reduction.

Thus, two workshops on *"Processing PHT32 Oversampled Mapping"* will be organized at VILSPA in the weeks of February 12-16, 2001 and March 12-16, 2001 and another one at IPAC in the week of March 26-30, 2001. They will consist of lectures and talks in the mornings and hands-on work tutored by experts in the afternoons. The last day of each workshop will be dedicated to small presentations of results achieved during the week. As of November 21, more than 15 people have registered.

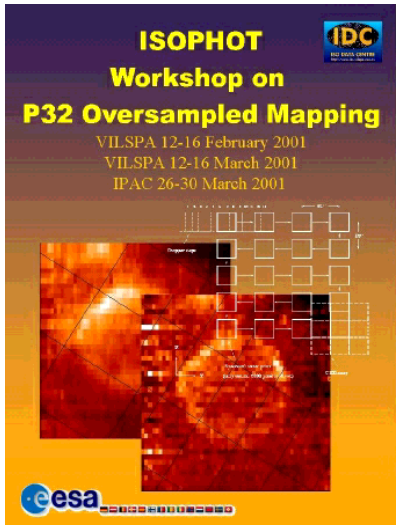

Figure 2.32: *Poster announcing the Workshop on "PHT32 Oversampled Mapping"*

Currently it is planned to release PIA v10 in March 2001 in conjunction with OLP 10. The main addition will be this PHT32 software.

- **CIA v4.0:** (released April 11, 2000)

  - CIA v4.0 includes an improved implementation of the Fouks-Schubert transient correction leading to better results and to a reduction in processing time up to a factor of 20. Obsolete algorithms used for transient correction and de-glitching were removed.

  - an improved dark correction using a second-order time-dependent correction which reduces the dark uncertainty by up to 30% is included.

  - access to long-term transient correction and variable flat-field algorithms routines via the SLICE package (see previous Status Report for a description) is now possible.

  - 'back_project' module allows the possibility to back project a raster mosaic to a set of exposures to verify stability and de-glitching.

  - 'raster_scan' module offers now the option '/weight' to use the weighted mean to create a mosaic.

  - CIA v4.0 allows the handling of Solar System Object and polarisation observations.

  - 'ximage' provides improved functionality for astronomical image display, especially for the analysis of data from raster observations.

  - 'xcvf' provides an interface to the spectral analysis package ISAP.

  - users are warned of saturations in the data. The position of the saturated pixels can be obtained and masked out.

  - new algorithms to treat faint sources in CAM-CVF observations are included

  - v5.0 of CIA is expected in June 2001 (will include error propagation)

- **OSIA v2.0:** (to be released in December 2000)

  - it will basically contain the same routines that are used in the SWS 9.5 version of the pipeline.

  - the 'dynadark' module to correct band 2 SWS data for transient effects will not be available yet in this version since its implementation in the pipeline has been postponed to OLP v10

  - beam profiles will be made available with OSIA v2.0.

  - OSIA v3.0 will only be released after OLP v10.0

- **LIA v8.0:** (released May 4, 2000)

  - A new tool has been written for Interactive Fabry-Pérot Multi-Gaussian Fitting of blended lines. The input data should be averaged LWS spectra produced by the ISAP 'average'.

  - Another tool has been made available with LIA v8.0 which can be used for interactive defringing of LWS data (LWS01, LWS03 and LWS04 modes).

  - An option has been added in the 'short_aal' module to include data following glitches in the output LSAN file.

  - LIA v8.0 is valid for LWS OLP v8.7 data products only

- **ISAP v2.0:** (released May 3, 2000)

  - ISAP v2.0 is now able to cope with standard ISO LWS, SWS, PHT-S and CAM-CVF spectra.

  - the transmission profiles for the SIRTF instruments: IRAC (InfraRed Array Camera) and MIPS (Multiband Imaging Photometer for SIRTF) are now available in their preliminary versions in the 'Synthetic Photometry' package.

  - now it is possible to read in simple ASCII spectra, and many routines have been modified to operate in such spectra which require few or no keywords.

  - the internal 'Feeder-merger' routine is now used for the advanced routines: 'Average', 'Clip', 'Smooth', 'Norm', 'Rebin'. 'Feeder-merger' strips away the YAAAR data structure before processing arrays, and reassembles the structure afterward. Thus, these advanced routines now process simple arrays, and in principle, may be used independently of ISAP.

  - for LWS data, the user may now apply a 'Small source to Large source Correction' which consider the shape of the LWS beam profile.

  - also for LWS data only, the user may now apply an aperture vs. wavelength correction, as a refined correction to the standard pipeline processing.

  - the Zodiacal light predictor (based on J. Good's IRAS model) has been generalized to handle spectra from ISO or any other mission, as long as FITS keywords for RA, DEC and DATE are present in the headers and it can re-introduce the FIR offsets found in the IRAS data set, as a function of wavelength.

  - Lorentzian fitting is now supported (useful for PAH's in CAM)

  - the enhanced line list in 'line-fit' now includes many mid-IR Unidentified Bands (PAHs) and some FIR Unidentified Lines.

  - multiple lines can now be fit freeing one λ and constraining a fixed $\Delta\lambda$ to exist between fitted components.

  - Flux per steradian (Intensity) is now allowed as a unit and is carried through routines.

  - the user can now convert between intensity and flux, by specifying aperture.

  - there is an enhanced 'shift' routine that handles lines and scans as desired (to obtain mean values, overlap values, etc.) - a convenience for SWS and LWS processing.

  - the user may clip many sigma data points without averaging using the standalone graphical Clip routine.

  - there is now convenient merging of groups of spectra.

  - improved reduction recipes for LWS and SWS have been delivered in the /isap/doc/recipes area.

  - a further final update of ISAP (v2.1) is foreseen to be released very soon containing a few minor improvements. Among them, it will contain the MSX transmision profiles as part of the 'Synthetic Photometry' package and the mean LWS profiles in numerical form for profile fitting via a 'smoothing' routine.

Short recipes have been written by the ISO instrument scientists residing at IPAC (except for SWS) for data reduction of ISO data. Recipes are available for the four ISO instruments and most of the observing modes. They can be found under the IPAC ISO web pages at:

`http://www.ipac.caltech.edu/iso/recipes.html`

Quick reference cards for data reduction, checklists and short descriptions of routines frequently used in the interactive calibration of ISO data can be found in this web page.

2.2.8 Polarisation:

`PO: Polarisation infrared emission from the starburst NGC 1808`

A mid to far IR polarisation study on the starburst galaxy NGC 1808 has been performed by R. Siebenmorgen, E. Krügel and R. Laureijs. At 6 μm extended emission was found with ISOCAM on scales of $23'' \times 15''$ and an integrated flux density of 1.13Jy, whereas the 170μm flux of 103.6Jy detected with ISOPHOT is not resolved.

Mid infrared polarisation was detected with ISOCAM showing symmetry with the major axis of the galaxy. The fractional polarisation is small in the disk but approaches $\sim 20\%$ in the outer parts. The emission observed is most plausible of thermal origin by partly aligned, spinning and non-spherical dust particles. Knowledge of the polarisation mechanism allows to derive the magnetic field structure in the disk. In the ISO beam a far infrared polarisation of $p_{170\mu\mathrm{m}} = 3.6 \pm 0.4\,\%$ at a polarisation angle of $\theta_{170\mu\mathrm{m}} = 101^\circ \pm 3^\circ$ is found which is interpreted as being caused by emission of elongated grains. By comparing with radio data the magnetic field seems to have both horizontal and vertical components. It is concluded that at least a fraction of the dust particles in the interstellar medium must have elongated grain shapes.

This is the first observational evidence for the presence of polarised thermal emission in an external galaxy.

The ISOCAM images were made using the observing template CAM05. A 3×3 raster with a raster step size of $123''$ was adopted with the $3''$ pixel field of view. The read out time of each exposure was 2.1s. After a background measurement, 15 exposures on the source were taken to stabilize the detector and then a raster was taken through the free hole of the entrance wheel. On each raster position another 15 science exposures were taken. Then similar rasters were also taken for each of the three polarisers. The polariser rasters were repeated in 2 cycles. The data were reduced with the ISOCAM interactive analysis (CIA v4.0). Only basic reduction procedures such as dark current subtraction, removal of cosmic ray hits and transient correction were applied to the data. The coadded images at each raster position were projected on the sky and corrected for field distortion to derive the final mosaics. The mosaics have a pixel scale of $1''$. The polarised signal is found to be consistent between the cycles, so that an average of all cycles gives the final mosaic image for each polariser. We derive the polarisation image shown in Figure 2.32 after correction of the instrumental polarisation.

Observations of linear polarisation at 170 μm were performed with the ISOPHOT C200 2×2 detector array. The polarisation was obtained by measuring several cycles of the 0, 120 and 240 degrees polarisers eventually followed by an open (sky) measurement and a measurement of the internal reference calibrator. Four different pointings were commanded such that each of

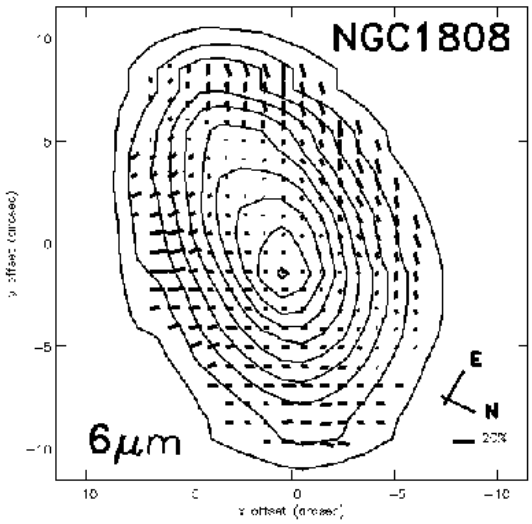

Figure 2.33: *Polarisation image of NGC1808 at 6*μm *(ISOCAM filter lw4) observed with angular resolution of* $\sim 5''$ *(FWHM) and* $3''$ *pixel field of view . The observed E-vectors and the contours of the total emission are shown in detector coordinates. The celestial North-East orientation is indicated - R. Siebenmorgen et al. (2001)*

the 4 detector pixels measured the polarisation of the centre position in succession. In addition, the observations on the source were bracketed by two background observations to determine the zero signal level and to monitor instrumental variations.

The sky measurements were processed and calibrated using the standard procedures for photometry. After coaddition of the 4 pointings of the C200 array, a small map was obtained which indicated that the brightness distribution of the galaxy is not significantly different from that of a point source. Then, as it was already mentioned, it was concluded that NGC 1808 was not resolved with ISOPHOT at 170 μm. The galaxy is much brighter than the background and a flux of $F_\nu(170\mu\text{m}) = 103\pm10$ Jy was derived with an adopted uncertainty of 10% based on the estimated uncertainty in the ISOPHOT absolute photometric calibration.

Since the galaxy is a point source at 170 μm we determined the polarisation only for the 4 pixel-position combinations centred on the galaxy. The polarisation measurements of the other positions in the map are not relevant as they were pointed on the wings of the beam profile of the galaxy. The processing of the signals were carried out according to the procedure described in Laureijs and Klaas (1999; "ISO Polarisation Observations", R. Laureijs and R. Siebenmorgen, ESA-SP435) using their instrumental polarisation values.

The resulting fractional polarisation degree (p) and polarisation angle (θ) with respect to the equatorial North per C200 detector pixel are presented in Table 2.4. The polarisation vector obtained from pixel 3 is significantly diffferent from the other pixels, and has a somewhat lower accuracy. This measurement was therefore rejected. The last line of Table 2.4 gives the polarisation after taking the weighted average of the stokes parameters of pixels 1, 2, and 4

Table 2.4: *Polarisation of the centre position of NGC 1808 at 170 μm for each pixel of the ISOPHOT C200 array. Due to the 180 degrees ambiguity, the angles in the first two quadrants were chosen.*

pixel number	P [%]	θ degrees
1	4.1±0.9	75±6
2	5.3±1.2	116±6
3	2.2±1.1	3±14
4	5.0±1.0	114±6
mean	3.6±0.4	101±3

after subtraction of the instrumental polarisation. Uncertainties introduced by the instrumental polarisation of the pixels are not included. They are estimated to amount to less than 1% in the final polarisation degree.

Chapter 3

Internal and external cross-calibration

3.1 The concept of cross-calibration

Cross-calibrations can be used (i) as consistency checks, and (ii) as true calibrations. In the first instance observations of a source by a pair of instruments are compared to evaluate internal consistency: if the results do not agree (to within the stated uncertainties) then the calibration procedure of one of the instruments (though possibly both) is incorrect. In the second instance, results from the less accurate instrument(s) can be calibrated against data from the more accurate one(s).

In the case of ISO, the above concept can be applied both to pairs of ISO instruments that overlap in wavelength range and also to ISO instruments vs other non-ISO instruments.

3.2 Definition of standard and cross-calibration sources

The absolute flux calibration of three of the four ISO instruments (CAM, PHT - at short wavelengths - and SWS) is based primarily on results of the Ground-Based Preparatory Programme (GBPP, Jourdain de Muizon and Habing, 1992 Les Houches Series: Infrared Astronomy with ISO, p. 129) and of the Cohen, Walker, Witeborn et al. (CWW) absolute calibration programme (Cohen et al. 1992a AJ 104, 1650, 1992b AJ 104, 2030 and 1995 AJ 110, 275), though the long wavelength filters of PHT also use planets and asteroids to cover the bright and intermediate part of their dynamic range. The absolute flux calibration of LWS is currently based on Uranus as primary source.

For cross-calibration purposes a small set of astronomical sources was used during operations, composed by a few bright stars (like HR 7310, HR 7341, HR 6436, γ Dra or α Boo), planetary nebulae (NGC 7027 and NGC 6543), galaxies (Mrk 279), asteroids (Cybele, Hygiea) and planets (Neptune) on which most of the cross-calibration comparisons were carried out. For most of them, observations exist taken throughout the whole ISO mission with more than one instrument and in many cases covering a wide range of wavelengths.

Note that, because of the limited common dynamic range between the ISO instruments, not all kind of inter-comparisons are possible. Stars are too faint in the long wavelength range of ISO to be used for cross-calibration analysis in the spectral region beyond 100 μm and asteroids and

planets have to be used instead. While the results of the CWW and the GBPP programmes, based on stars, are believed to be accurate to ±5% or better and are consistent with one other, the uncertainties in asteroid and planet model spectral energy distributions are larger (10−15% level). In the case of asteroids their characterization is additionally complicated by their variability. Thus, the cross-calibration of LWS in the long wavelength range is especially difficult, since the comparison has to be made against PHT measurements, and the dynamic range overlap between PHT and LWS is limited.

Another important limitation is imposed by the fact that calibration problems do not necessarily affect all the cross-calibration sources in the same way. Thus, some comparisons do not shed any light on the understanding of a given problem if we restrict our analysis to the small sample of objects listed above.

3.3 A new cross-calibration strategy

3.3.1 Introduction

In order to take into account all the limitations and caveats considered above a new cross-calibration strategy was activated in Post-Operations based on the statistical analysis of large data sets of sources.

The following aspects need to be considered:

- cross-calibration data sets must be able to ensure proper handling of differences in beam sizes, filter profiles and spectral resolution, as well as the use of differing absolute calibration systems and of different sets of astronomical standard sources.

- the detailed investigation of specific calibration problems may require the selection of dedicated subsamples of targets. Thus, cross-calibration data sets should contain a combination of bright/faint, red/blue, point/extended sources. This way it will always be possible to draw a complete picture of the impact on ISO data of an existing problem or evaluate recent achievements in ISO calibration properly.

- calibration data sets should satisfy at least one of the following conditions:

  - they have been observed with more than one instrument/configuration at least once during the ISO mission (for internal cross-calibration purposes)

  - infrared data from non-ISO instruments exists (for external cross-calibration)

  - accurate models exist against which ISO data can be compared (for absolute flux calibration).

3.3.2 Internal and external cross-calibration

The short wavelength range ($\lambda < 45$ μm)

Internal cross-calibration:

A total number of 277 different positions in the sky have been identified using the ISO Data Archive where spectra were taken during the mission with at least two of the following AOTs: SWS01, CAM04 (CAM-CVF) and PHT40 (PHT-S staring or chopped).

Unfortunately, not all the observations are suitable for a direct cross-calibration comparison. In some cases there are slight pointing offsets which, as we have already mentioned in this document, can account for strong variations in flux. For this reason, only pointings of a given astronomical source which differ by less than $3''$ have been considered for direct cross-calibration. Note, however, that the subsample of bad pointed observations so defined is not useless, since it constitutes an excellent database of test cases for checking the pointing correction tools now available in PIA and SIA for PHT and SWS data, respectively.

In addition, some of the sources in this large cross-calibration sample are known to be extended. They were also identified and considered as a different subgroup. Again, the subsample of extended sources observed with various instruments so defined constitutes an excellent database to be used for the analysis and comparison of beam profile models, the test of aperture size corrections, or to study the effects induced by the extension of the sources on line profile resolution, fringes, etc.

Last, but not least, there is a further aspect to consider in cross-calibration and this is variability. We know that many of the stars observed by ISO are characterized by their strong variability. They are in many cases pulsating stars in the Asymptotic Giant Branch (AGB) phase evolving into planetary nebulae (young stellar objects are also variable but usually the amplitude of the variations in the ISO spectral range is not that large). These variable sources were also removed from the initial sample (note, however, that observations of variable sources with different instruments can still be used for internal cross-calibration if they were taken sufficiently close in time).

After all, if we restrict our analysis to the subsample of non-variable, point sources, not affected by pointing problems, and bright enough to provide reliable data, we end up with a much smaller database compared to the initial one, but which still includes a between 100 and 150 different positions of the sky observed either with SWS or with PHT-S and around 10 to 20 different sources observed with CAM04.

Note that the smaller number of CAM-CVF observations available for cross-calibration is just the natural consequence of the predominant use of this observing mode to observe faint extended sources which otherwise cannot be detected and/or spatially resolved by SWS or PHT. Thus, there is only a small overlap of observations between CAM-CVF and SWS or PHT-S.

External cross-calibration:

For external cross-calibration, specific observations in the ISO database have been compared with observations of the same sources made with ground-based facilities like UKIRT, or with other space facilities, like IRAS, COBE/DIRBE, KAO or MSX (see Section 3.4).

A cross-calibration analysis of sources observed both with SWS and PHT-S, as well as with UKIRT was presented in a previous Status Report.

A special effort has recently been spent in the generation of a large cross-calibration database of sources selected from the ISO Data Archive to be statistically compared with IRAS in the SWS range. The idea is to compare the ISO observations made with SWS with IRAS photometry at 12 and 25 μm. The preliminary results from this analysis were presented in the previous Status Report and in Section 3.4.2 in this Report we present an update based on the analysis of the same sample of sources but now with OLP v9.5 data products.

Other comparisons have also been performed between IRAS and PHT photometry at 25 μm (see previous Status Report) or between PHT-S and COBE/DIRBE photometry. In this latter case, the results obtained at 4.9 and 12 μm were also presented in the previous Status Report. In Section 3.4.5 of this Report we present additional results this time concerning PHT background measurements at 12, 25 and 60 μm which are compared to COBE/DIRBE results.

The long wavelength range ($\lambda > 45$ μm)

Internal cross-calibration:

With respect to the internal cross-calibration of the long wavelength spectral range covered by ISO, a similar exercise was performed as for the short wavelength range. This way, it has been possible to select a few hundred different positions in the sky from the ISO Data Archive where ISO observations taken both with PHT-C filters (photometry beyond 60 μm) and LWS01 are available.

The main problem again is that cross-calibration comparisons between PHT and LWS are difficult because of the very different dynamic range of the two instruments. Thus, there is a minimum overlapping region in flux level at which both PHT and LWS observations are of enough quality to derive reliable cross-calibration comparisons. In spite of this, we estimate that a minimum number of 50 cases will probably remain as useful. The results from this cross-calibration comparison will be presented in the Final Status Report.

External cross-calibration:

Concerning external cross-calibration, efforts are concentrated in the generation of a specific cross-calibration data set of observations selected from the ISO Data Archive to be compared with IRAS photometry at 60 and 100 μm. This work is being carried out by Josephine Chan at RAL and the preliminary results are also presented in Section 3.4.4.

In addition, we also presented in a previous Status Report the results obtained from a cross-calibration comparison of LWS and raster scans performed on two different fields showing complex extended emission at 100 μm with IRAS maps obtained at the same wavelength, between ISOPHOT IRAS photometry at 60 μm and a cross-calibration analysis of ISOPHOT C100 and C200 maps with COBE/DIRBE data. In addition, in Section 3.4.6 of this Report we will also show the results from a cross-calibration comparison made between ISO observations of a number of compact HII regions with LWS and observations taken with the Kuiper Airborne Observatory (KAO).

Connecting the short and the long wavelength range

In order to give consistency to the results obtained in the short and the long wavelength range, an internal cross-calibration analysis was also performed between SWS and LWS observations,

whose results were already presented in the previous Status Report.

The mean value of the LWS/SWS ratios so obtained was <LWS/SWS> = 1.02, very close to unity. This is remarkable, if we consider that LWS and SWS were calibrated in a totally different way (LWS calibration is based on Uranus as primary calibrator while SWS band 4 calibration is mainly based on ground-based ILT experiments using blackbody sources).

A revision of this analysis is foreseen to be included in the Cross-Calibration Final Report using OLP v10 data products.

3.3.3 Comparison with models

The short wavelength range ($\lambda < 45$ μm)

In this Status Report we present a few examples of spectra taken with SWS and how do they compare to models and/or template spectra available, most of them the result of the CWW and the GBPP programmes, believed to be accurate to ±5% or better.

It is important to consider that one has to be careful in the interpretation of the results obtained, since some of the stars for which the most accurate models/templates are available have been used as standard calibrators by ISO. In this case, a nice fit of the observations with the model just confirms the internal consistency of the calibration system but does not help too much in determining the quality of the absolute flux calibration.

The intention is to expand the number of test cases under analysis in the Final Status Report giving emphasis to comparisons made against models corresponding to stars not considered as standards by ISO and using the latest available models.

Other comparison with models are shown for CAM and LWS. In the case of PHT, many of these comparisons can be found in the *"Report on the PHT Scientific Validation for OLP Version 9.0"* by U. Klaas et al. (see Section 3.4.7).

The long wavelength range ($\lambda > 45$ μm)

In previous Status Reports we have already shown comparisons of the LWS spectrum of Uranus with several available models. In addition, we have also reported on a number of consistency checks which have been made between LWS observations and model spectra of Neptune, Mars and Callisto.

Unfortunately, the uncertainties in asteroid and planet model spectral energy distributions are larger (10−15% level) than for stars and usually several models exist for the same source, which are basically the consequence of the selection of different input parameters for the model.

Thus, in this case, an important aspect to consider is to determine among the various models available, which one is the more accurate one, and this is not always a simple task.

In Section 3.4.7 we will show the results obtained from a recent cross-calibration comparison of LWS02 measurements made on Ceres with a model of the same asteroid.

A summary report on the different analysis made with a description of the models selected and the reasons on which we based our selection will also be presented in the Final Status Report.

3.4 Cross-calibration comparisons

3.4.1 Sources observed with SWS, CAM-CVF and PHT-S

A summary of results derived from the analysis of the sample of astronomical sources observed at the short wavelength range of ISO (between 2 and 15 μm) with SWS01, CAM04 (CAM-CVF) or PHT40 (PHT-S) was presented in the previous Status Report. At that time, the analysis made was based on 'simulated' OLP v9 data products which were compared with the by then existing OLP v8.4 data products, since the 'real' OLP v9 ones were not yet available.

Now we have the possibility to compare 'real' OLP v9.5 data products with the previously existing OLP v8.4 data products. However, unfortunately, the comparison has to be restricted to a few number of cross-calibration test cases specifically selected for this purpose in advance to the general release of this new version of the pipeline, which is taking place on the same date this report is being completed (November 28).

To remind you, the main changes in OLP v9 with respect to OLP v8 data products are expected to be a consequence of: (i) the application of the dynamic calibration method in PHT-S staring observations to correct for transient effects; (ii) the use of the Fouks-Schubert model in ISOCAM data to correct for transient effects; and (iii) new absolute flux calibration improvements and better detection of glitches in SWS.

SWS versus PHT-S

Figure 3.1 shows a number of examples of OLP v8.4 data products corresponding to a few sources in the short list of cross-calibration test cases as as they were retrieved from the ISO Data Archive. The examples shown include representative cases of 'red' sources [AFGL 2999 and S Per] (upper panel), 'blue' sources [HR 6132 and HR 7310] (middle panel) and 'faint' sources [PV Cep and IRAS 21434+4936] (lower panel), all of them observed with PHT-S in staring mode, with the exception of IRAS 21434+4936, for which the triangular chopping mode was used, and it is here included for comparison.

As we can see, there is a general good agreement in the overall shape of the OLP v8.4 spectra. However, strong discrepancies of the order of 20% to 40% are observed in some cases which are far from acceptable.

Some of the problems that might be affecting the data in the most discrepant cases are well known. Others have been discovered only very recently.

First, they are in a high percentage related with transient effects in PHT-S data taken in staring mode (especially at the shortest wavelengths), for which no correction was applied in OLP v8.4. This is clearly reflected in the fact that the only chopped observation shown in Figure 3.1, that of IRAS 21434+4936, shows an excellent agreement with SWS data even at a very low flux level (chopped PHT-S observations are corrected for transients in OLP v.8.4 using a different, empirical method which gives quite satisfactory results and, thus, they are not affected by this problem).

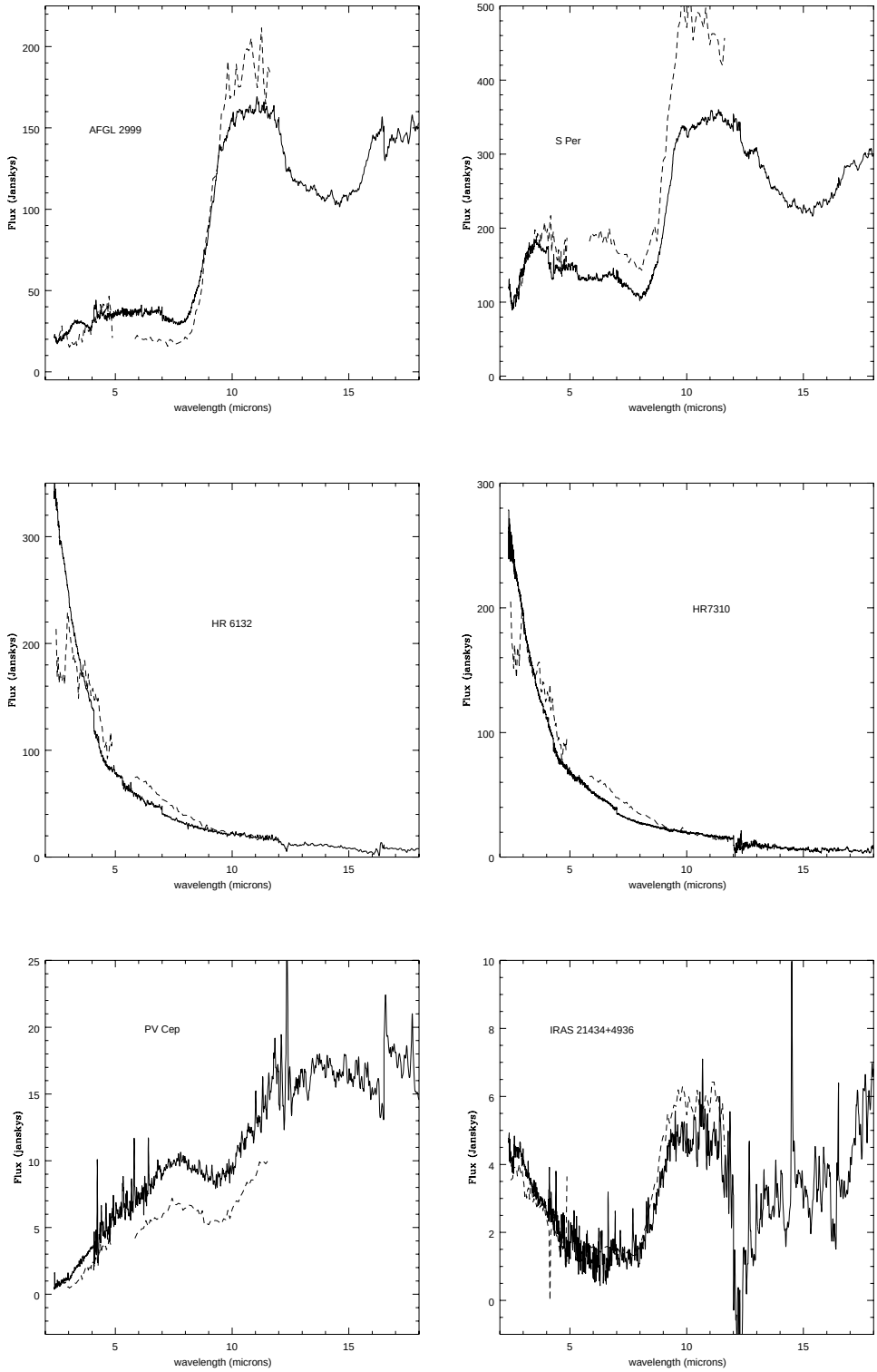

Figure 3.1: *SWS (solid line) versus PHT-S (dashed line) OLP v8.4 spectra of a few sources in the cross-calibration sample of test cases as they are retrieved from the ISO Data Archive*

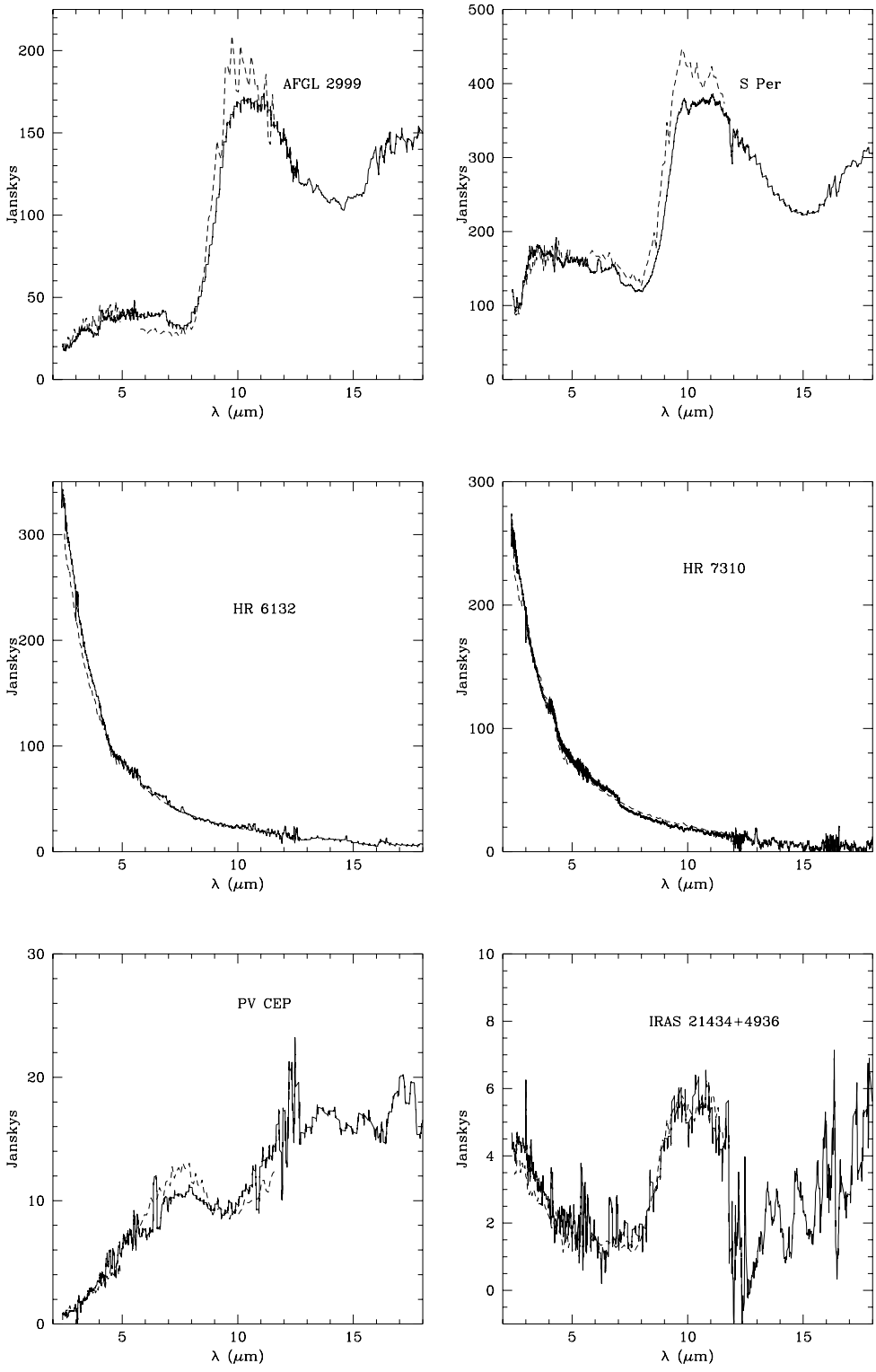

Figure 3.2: *SWS (black solid line) versus PHT-S (red dashed line) OLP v9.5 spectra of the same sources shown in Figure 3.1*

In addition, a bug in the absolute flux calibration of SWS has recently been detected (see Section 3.4.2) which lead to a systematic ∼10% underestimation of the OLP v8.4 ISO fluxes in band 2.

If this is the case, one should then expect to strongly improve the level of agreement of PHT-S data with SWS in OLP v9.5, where the dynamic calibration method is implemented and the calibration bug in SWS has been removed.

Figure 3.2 show the same set of sources this time processed with OLP v9.5 of the pipeline. As we can see, the improvement is significant in all cases and the level of agreement reached is found to be better than 10-15% in most cases in the overlapping wavelength range.

However, there are still minor discrepancies (of the order of ∼10%) which especially affect the two red sources, AFGL 2999 and S Per, showing the strong flux jump produced by the silicate emission detected at 10 μm. Since this is the spectral region which in SWS is known to be mostly affected by transients we consider the possibility of this remaining discrepancy being originated by memory effects in band 2 SWS data as a potential explanation for the discrepancies observed, but confirmation of this will have to wait until OLP v10 data are available.

Considerable discrepancies between SWS and PHT-S data of the order of ∼20% are also detected around 10 μm in the spectrum of PV Cep, which is a much fainter star, as we can see in Figure 3.2. This is surprising since for faint sources like PV Cep memory effects are not expected to be strong in SWS band 2 data.

In this case, it is possible that the still remaining discrepancies between PHT-S and SWS might be due to the fact that the PHT-S spectrum of PV Cep was slightly overcorrected whith the application of the dynamic calibration method. This is supported by the strong transient correction that was needed, suggesting that the signal was originally far from stabilisation, which always makes the results of the transient correction more uncertain.

Other minor problems are also evident in Figure 3.2. They consist mainly in small flux jumps observed between bands in some of the SWS spectra there displayed. As we have already mentioned, most of them might be due either to the possibility that the source was observed slightly off-centred or to an incorrect dark current subtraction. In both cases, manual intervention is needed using IA. In the first case, a major improvement has been achieved in the last few months with the availability of the new SWS pointing correction tool which will soon be available under SIA to be implemented late in OSIA v3.0. With respect to the second problem, it is always possible to try a slightly better dark current subtraction using IA.

The typical effect of an incorrect dark current subtraction appears quite clear in the case of the SWS spectrum of the faint source IRAS 21434+4936, where a strong flux jump is observed between bands 2C and 3A at 12 μm, bringing the flux into negative values at the short wavelength edge of band 3A.

SWS versus CAM-CVF

Figure 3.3 shows two examples of CAM OLP v8.0 and SWS OLP v8.4 data products as they were retrieved from the ISO Data Archive. They correspond to the bright star HR 7310 and the faint star HD 179218, two sources contained in the cross-calibration sample which are considered to be representative of the general behaviour observed for CAM and SWS OLP v8 data products.

As we can see, there is a general good agreement between SWS and CAM, within the 15% level,

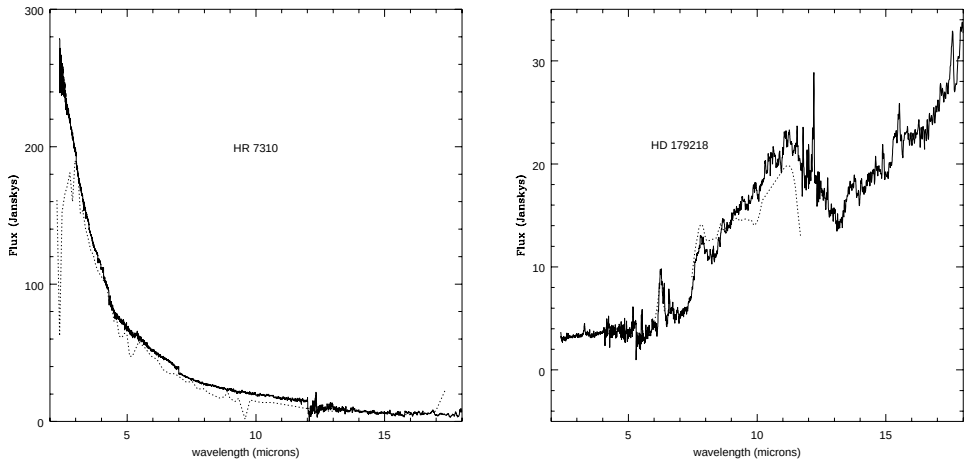

Figure 3.3: *SWS OLP v8.4 (solid line) versus CAM-CVF OLP v8.0 (dotted line) spectra retrieved from the ISO Data Archive of two of the sources in the cross-calibration sample*

both in the overall shape of the spectra and in the absolute flux level, with the exception of the edges of the CAM-CVF scan on HR 7310, which strongly disagree with SWS data, and some small jumps which look like absorption features in the CAM-CVF spectra of both stars. In addition, a small jump between bands 2C and 3A is also observed at 12 μm in the SWS spectrum of HR 7310. It closely resembles the one we have just described in IRAS 21434+4936 and can be attributed to an incorrect dark current subtraction in band 3A by OLP v8.4.

We know that the small jumps observed in the CAM-CVF spectra are quite probably due to the automatic PSF fitting tool used by OLP to extract individual CAM-CVF spectra of point sources detected in the field. In order to get rid of these artifacts (for which a solution is planned to be implemented soon with the definition of a new extraction procedure and a the use of a better sampled PSF), we performed manual aperture photometry in the CAM-CVF fields with the help of CIA v4.0. This way we were able to obtain a much better agreement with SWS data, as it is shown in Figure 3.4.

With respect to the discrepancies still observed at the blue and red ends of the CAM-CVF spectrum of HR 7310, we know that they are probably due to the effect of transients. Unfortunately, the transient correction based on the Fouks-Schubert model which has been implemented in OLP v9.5 is in principle only valid for low gradient illumination conditions. Thus, only the photometry of extended sources and of very faint point sources is expected to improve significantly.

Figure 3.5 shows the same spectra, this time reduced with version 9.5 of the pipeline and extracted from the CVF fields using 'manual' aperture photometry. As we can see, there is no significant change in the spectrum of HR 7310 with respect to OLP v8.4, nor even at the edges of the spectrum.

However, it is interesting to note the small but significant impact that the Fouks-Schubert correction had on the spectrum of the faint emission features present in the spectrum of HD 179218. If we compare this spectrum before and after the correction we can see that the emission features detected at 6.2, 7.7 and 8.6 features appears now sharper and in better agreement with the detections made by SWS. This is a nice example of the kind of improvements that the application of the Fouks-Schubert transient correction might produce in OLP data products.

In order to show this effect more in detail we have considered another example. This time, a

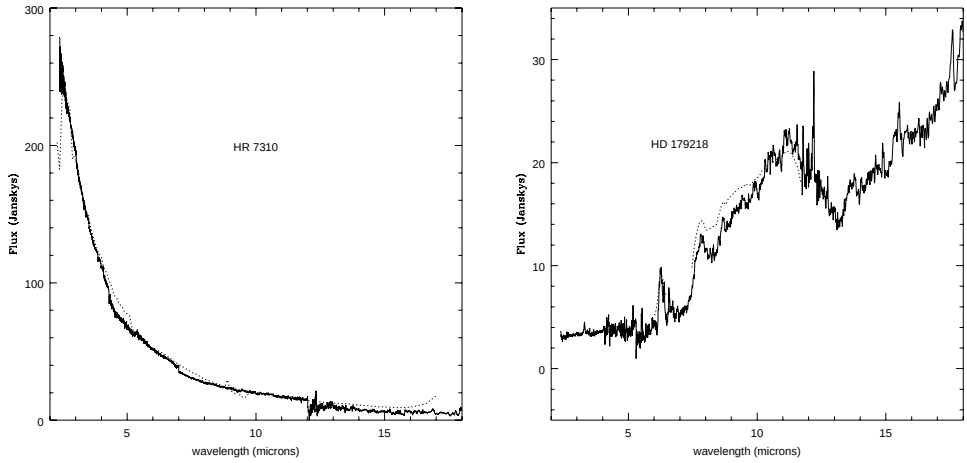

Figure 3.4: *SWS OLP v8.4 (solid line) versus CAM-CVF (dotted line) spectra of the same sources once the CAM-CVF spectra have been extracted using manual aperture photometry with CIA*

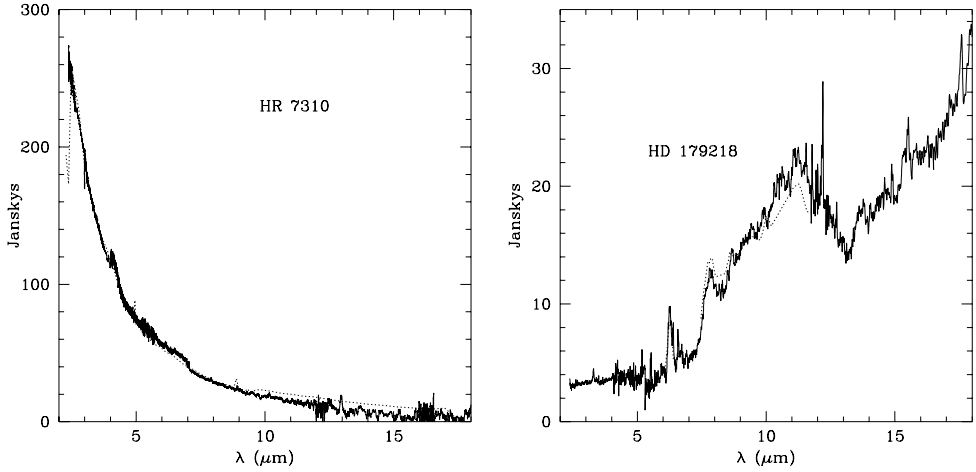

Figure 3.5: *SWS OLP v9.5 (solid line) versus CAM-CVF (dotted line) once the CAM-CVF spectra have been extracted using manual aperture photometry with CIA*

CAM-CVF observation of the faint extended source IC 443 is considered. Figure 3.6 shows the spectrum of IC 443 as obtained from OLP v9.5 with transient correction and as obtained from OLP v8.4 without correction. We can see that the peak strengths are noticeably stronger and the line bases are narrower. At the same time the baseline at short wavelengths has become much closer to the zero emission level.

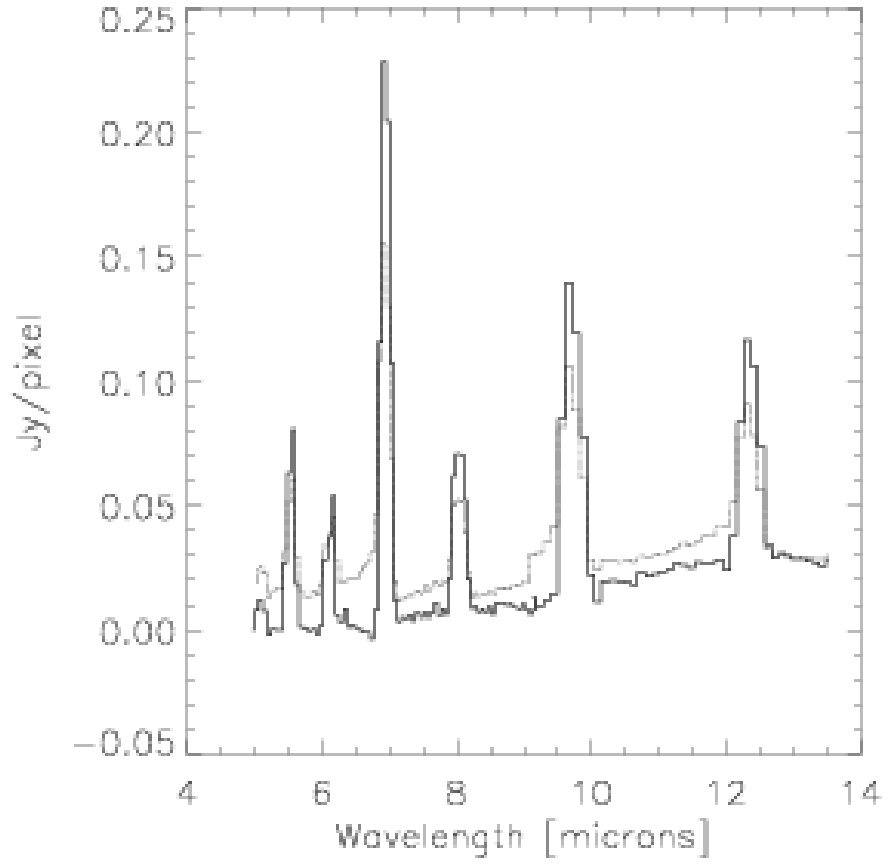

Figure 3.6: *OLP v9.5 spectrum of IC 443, with the Fouks-Schubert transient correction (solid) and without transient correction (dotted) - Diego Cesarsky*

CAM-CVF versus PHT-S

In Figure 3.7 we present the OLP v8.0 CAM-CVF and OLP v8.4 PHT-S spectra of two of the sources in the cross-calibration sample as they were retrieved from the ISO Data Archive. They correspond to the bright star HR 7310 and the faint star HD 207129, which were selected as representative of the general behaviour observed for CAM and PHT data products in OLP v8.

We can see that although a general good agreement in the overall shape exist, there are strong discrepancies in the absolute flux level which can reach more than 20% in some regions of the

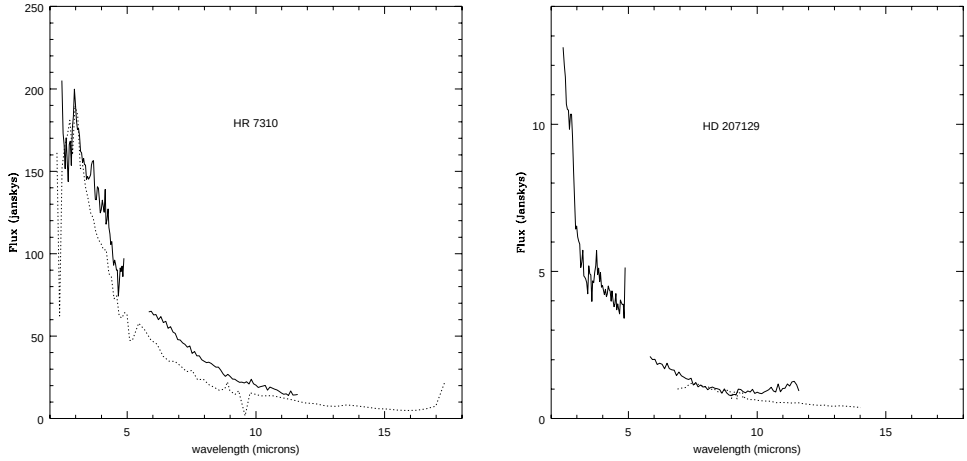

Figure 3.7: *CAM-CVF OLP v8.0 (dotted line) versus PHT-S OLP v8.4 (solid line) OLP v8 spectra of two of the sources in the cross-calibration sample as they were retrieved from the ISO Data Archive*

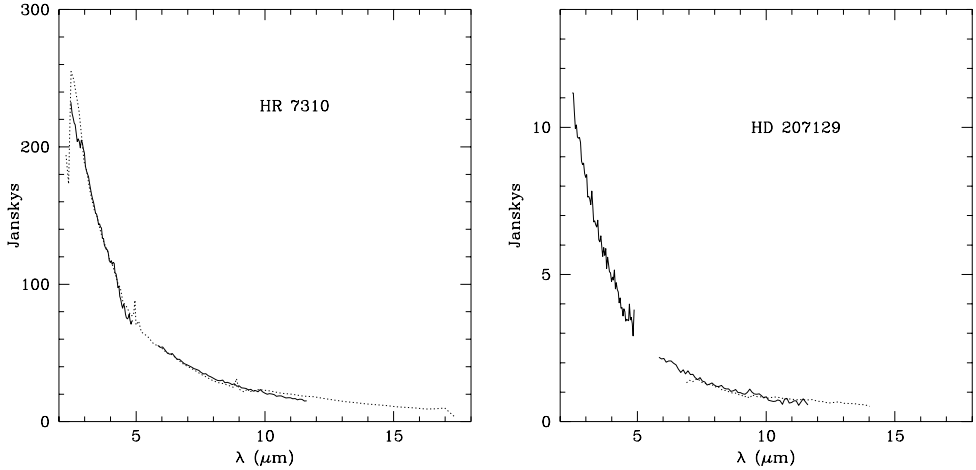

Figure 3.8: *CAM-CVF (dotted line) versus PHT-S (solid line) OLP v9.5 spectra of the same sources, once the CAM-CVF spectrum has been extracted using 'manual' aperture photometry*

spectral range.

The results obtained with OLP v9.5 after the PHT-S spectra are corrected for transients and the CAM-CVF spectra are extracted using 'manual' aperture photometry (shown in Figure 3.8) are excellent.

In the overlapping region between PHT-S and CAM-CVF, there is almost a perfect match both for the bright star HR 7310 and the faint HD 207129.

In both cases the shape of the PHT-S spectrum is considerably improved after the application of the dynamic calibration method to correct for transient effects by the OLP v9.5 pipeline.

For a faint star like HD 207129, the background continuum emission is usually not negligible. In this case, a background measurement available in the ISO Data Archive taken at a position 3 arcmin away from the central source was used to subtract this contribution to the observed OLP v9.5 PHT-S spectrum of this star and the result obtained after subtraction is shown in Figure 3.8, where we can see the excellent agreement between the continuum subtracted PHT-S spectrum and the available CAM-CVF data in the overlapping region.

Direct comparison of lines in CAM-CVF and SWS spectra

Observations of the Orion bar complex made with CAM-CVF and SWS have recently been analysed by Cesarsky et al. (2000; A&A 358, 708).The spectra taken show a combination of strong emission features corresponding to PAHs and amorphous silicate grains together with narrow emission lines coming from an ionized region around the isolated O9.5V star σ^2 Ori A.

The presence of broad and narrow emission features in the mid-infrared spectrum of this region of the sky makes the comparison of the spectra obtained with CAM-CVF and SWS quite interesting for cross-calibration purposes since they constitute an excellent laboratory to test the effect of the presence of emission lines on the internal consistency of ISO calibration.

The CAM-CVF observations employed the 6" per pixel field-of-view of CAM. Full scans of the two CVFs in the long-wave channel of the camera were performed with both increasing and decreasing wavelength. The results of these two scans are almost identical, showing that the transient response of the detector was only a minor problem for these observations.

The raw data were processed using CIA in a standard way and the Fouks-Schubert transient correction was applied to the data resulting in only minor corrections.

A complete SWS (2.4 to 46 μm) spectrum of the HII region surrounding the star σ^2 Ori A was obtained and reduced with SWS IA using version 30 of the CAL_G files.

This SWS spectrum is shown in Figure 3.10 together with the CAM-CVF spectrum obtained co-adding all the pixels falling within the SWS aperture. As we can see, the agreemnent between the spectra is excellent, within 20% for the continuum.

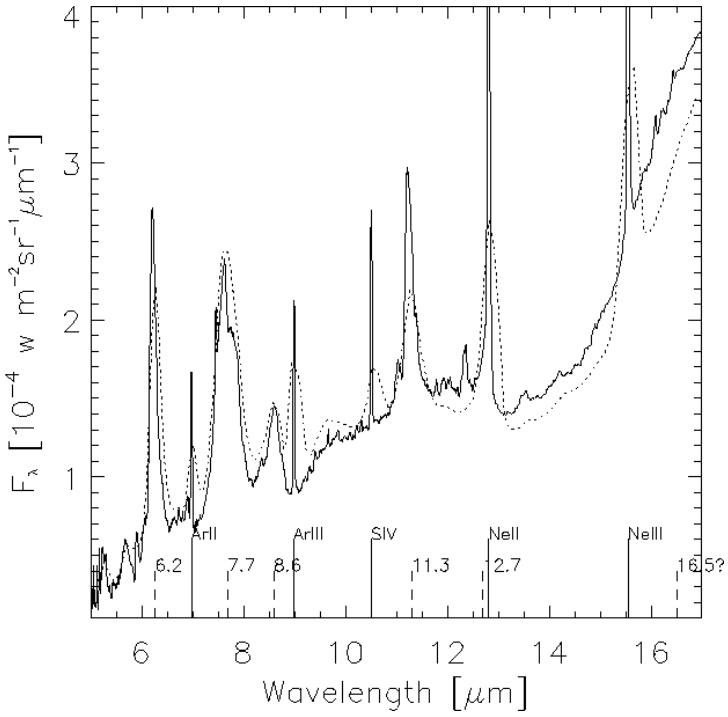

Figure 3.9: *The SWS spectrum (full line) compared to the CAM-CVF spectrum (dotted line). In this latter case, all the CAM pixels falling in the SWS aperture have been co-added. - Cesarsky et al. (A&A 2000, 358, 708)*

3.4.2 Cross-calibration of sources observed with IRAS and ISO SWS

A large number of astronomical sources observed with SWS were also detected by IRAS at the 12 and 25 μm bands and included in the IRAS catalogues, either in the Point Source Catalogue, or in the Catalogue of Low Resolution Spectra (LRS, hereafter). The latter contains low resolution spectral information between 8 and 22 μm of an important number (a few thousand) of IRAS sources detected above a certain brightness limit. Note that these LRS spectra were absolutely calibrated in flux by simple scaling the spectrum with the photometric IRAS flux at 12 μm.

In order to compare the absolute flux calibration of IRAS and ISO SWS we took the full list of sources contained in the IRAS LRS Catalogue (5425 sources) and searched the ISO Data Archive for observations made with ISO at the same positions of the sky allowing for a maximum offset of $1.5'$.

This way, we found 556 different pointings in the ISO Data Archive containing SWS01 observations corresponding to around 400 different sources.

The sample contain sources associated to a wide variety of properties ('red' and 'blue' spectra, faint and bright sources, etc.) and constitutes an ideal database for cross-calibration purposes and evaluate the degree of consistency betwen IRAS photometry and SWS spectroscopy.

Some of the sources in this sample, unfortunately, cannot be used for this cross-calibration analysis, because they are extended sources for which a direct cross-calibration between the SWS flux and the IRAS photometry cannot be made since the SWS calibration is based on point source flux calibration. In addition, many of these extended sources are usually located in areas of the sky with a complex structure at 12 and 25 μm, which complicates even more the problem.

Sources which look extended to SWS are easily recognised because the spectra show strong flux

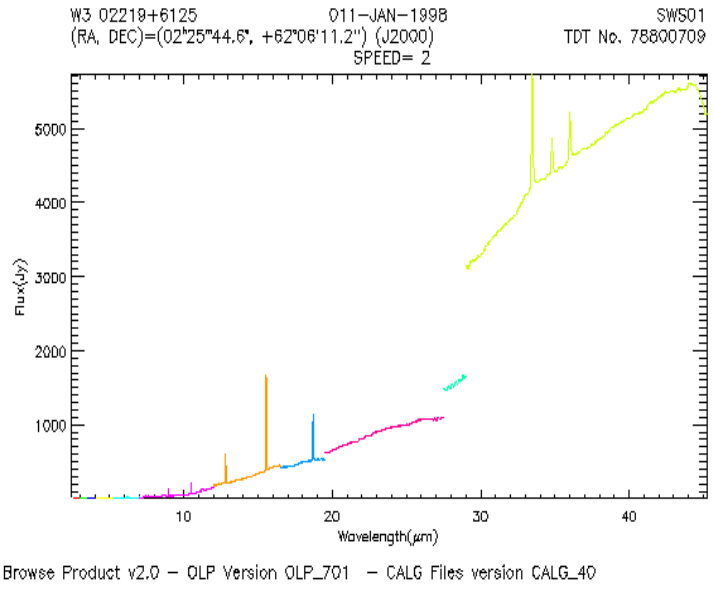

Figure 3.10: *Example of the discontinuities observed in one of the extended sources included in the sample. Jumps between bands in the SWS range are coincident with changes in the aperture size - Pedro García-Lario*

jumps between bands coincident with changes in the aperture size. A good example of this is shown in Figure 3.11.

Another factor which has to be taken into account in this cross-calibration analysis is the intrinsic variability of many of the sources contained in the sample. As we have already mentioned in this document, we know that many of the stars observed by ISO are characterized by their strong variability. They are known to be pulsating stars in the Asymptotic Giant Branch (AGB) phase evolving into planetary nebulae. In some cases, also some young stellar objects might be found variable but usually the amplitude of the variations in this spectral range is not very large. In principle, we only removed from the working sample variable AGB stars well recognized as such in the literature.

This way, we ended up with a list of more than 250 sources. Each of these 250 individual OLP v8.4 spectra were retrieved from the ISO Data Archive and further processed with ISAPv2.0. Basically, bad data points affected by glitches were identified and removed from the spectra using the available tools in ISAP and what we can call 'ISO SWS photometry' was performed at 12 and 25 μm with the help of the 'syn_phot' application in ISAP, which simply convolves the ISO spectrum with the transmission profile of the IRAS filters at 12 and 25 μm and assigns a monochromatic flux at these two wavelengths under the assumption that the source SED shape is of the form $\nu \times f_\nu$ = constant, or equivalently $\lambda \times f_\lambda$ = constant, in the same way as IRAS did.

In Figure 3.11 we show the results obtained from this study at 12 μm for the sources in our sample when OLP v8.4 data products were used. At first sight, the first conclusion that we can extract from our analysis is that there is a clear systematic underestimation of the ISO OLP v8.4 fluxes at 12 μm with respect to the IRAS photometry at the same wavelength. ISO synthetic photometry at 12 μm was found to provide fluxes typically 12% fainter than IRAS (see Figure 3.12). The shift appeared to be constant, independently of the flux level considered. The few obvious outliers towards positive values (ISO fluxes overestimated with respect to IRAS) in this distribution might be unknown variable sources detected close their maximum brightness by ISO while the obvious asymmetry observed in the distribution towards negative values (ISO

fluxes underestimated with respect to IRAS) is interpreted as a combination of unknown variable sources (caught during minimum brightness by ISO) and bad-pointed observations.

Interestingly, a similar behaviour was observed at 25 μm (see Figure 3.13). ISO OLP v8.4 fluxes at 25 μm appeared also systematically underestimated with respect to the IRAS photometry at the same wavelength but in this case the constant shift was only of 8%. Again this value is not flux dependent.

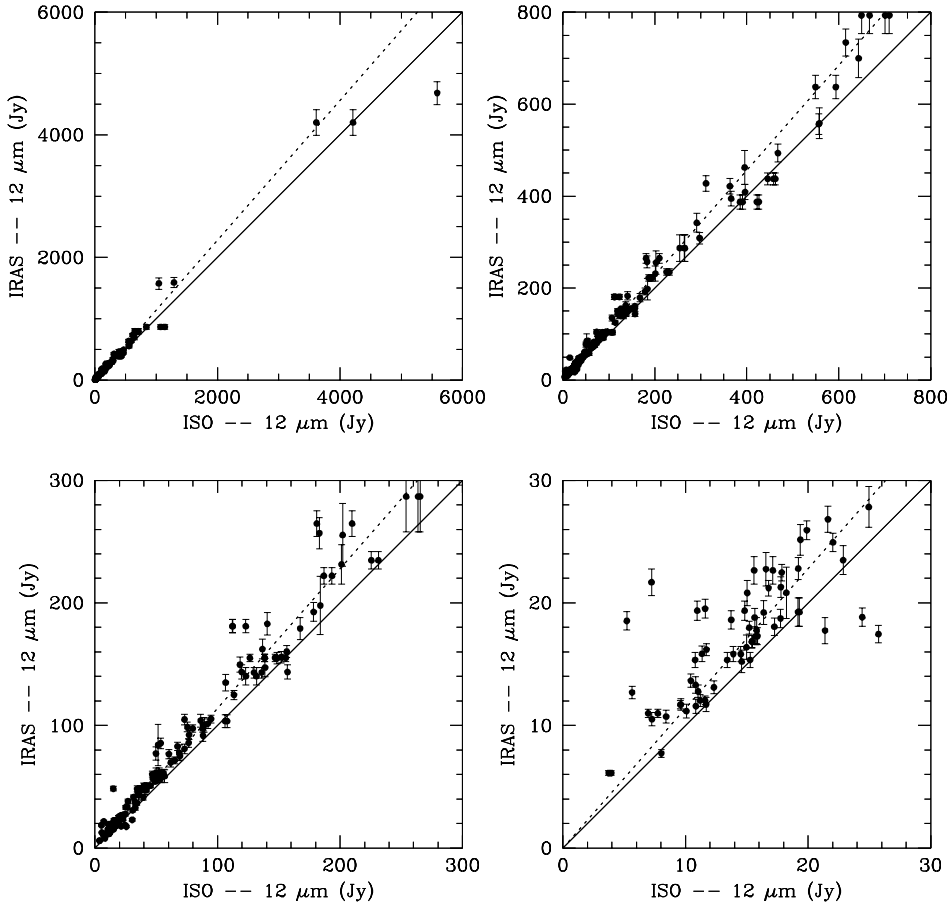

Figure 3.11: *ISO SWS synthetic photometry at 12 μm compared to IRAS photometry at the same wavelength. The dashed red line represents a 12% systematic underestimation of the ISO fluxes with respect to IRAS (see text for details) - Pedro García-Lario*

Figure 3.14 shows the distribution of discrepancies found between the ISO SWS synthetic photometry and IRAS photometry at 25 μm, where we can see the 8% shift clearly. Note, however, that the overall distribution is not asymmetric this time. The number of strongly underestimated fluxes by ISO with respect to IRAS are more or less similar to the number of overestimations. The few obvious outliers at both sides of the distribution are the same sources observed as outliers at 12 μm. Thus, we interpret the symmetry observed as the consequence of the smaller number of bad pointed observations at this wavelength, probably because of the larger apertures used by SWS.

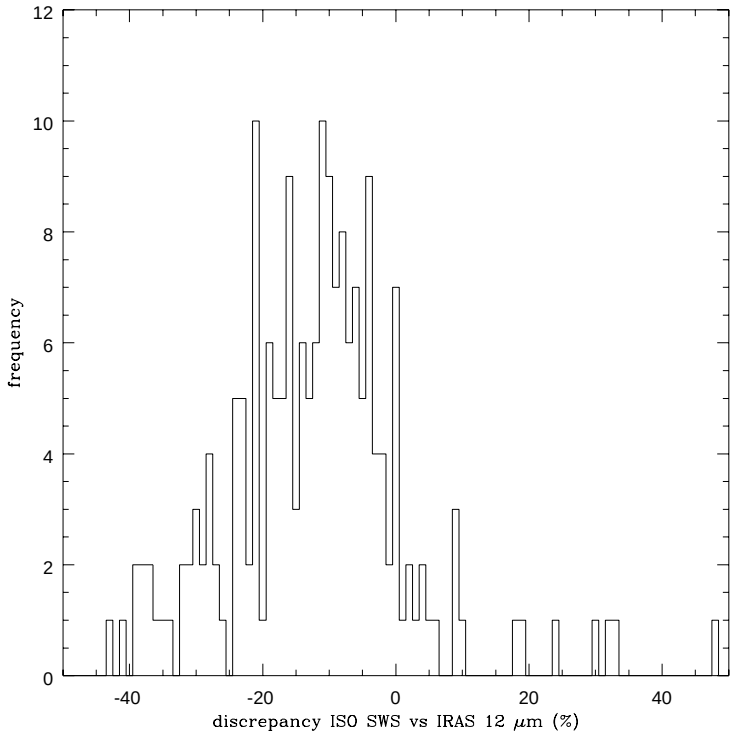

Figure 3.12: *Distribution of discrepancies found between the ISO SWS synthetic photometry at 12 μm and IRAS photometry at the same wavelength - Pedro García-Lario*

It is interesting to note also that, when the constant shifts of 12% and 8% are removed, the fluxes detected by ISO are consistent within 10-15% with those quoted in the IRAS Point Source Catalogue.

Following an investigation by the SWS NDC a bug was found in the way the calibration files were implemented in the pipeline, leading to a systematic underestimation in band 2 data of the order of the discrepancies observed with our cross-calibration exercise. This bug has been corrected in OLP v9.5 and now the absolute flux calibration of SWS should be correct.

Unfortunately, at the time of writing this Status Report it has only be possible to check a few OLP v9.5 test cases (around 20) which were found to be representative of the general behaviour since their corresponding OLP v8.4 products were off with respect to ISO by -9.5% and -5.9in mean at 12 and 25 μm, respectively.

Once the new OLP v9.4 data products for this small data set were analysed we found that the mean absolute fluxes derived by ISO at 12 μm are only -1.9absolute fluxes derived by ISO at 25 μm differ by just $+0.18$with respect to the IRAS ones. For the derivation of this numbers, 4 measurements at 25μm corresponding to sources with an absolute flux level at this wavelength below 10 Jy were excluded. No measurements at 12 μm were excluded.

The preliminary conclusion is that the agreement between ISO OLP v9.5 data and IRAS at 12 μm and 25 μm is now found to be excellent (within the 10-15% level typically) for strong sources (above 50 Jy), although it becomes worse for low flux levels (typically within the 30-40% level for fluxes below 5-10 Jy).

A possibility exists that the remaining discrepancies observed at 12 μm in some of the sources in our sample could be due to the transient effects in band 2 ISO data which are not yet corrected for in OLP v9.5. This might be the case, for instance, of a couple of objects in the short list of

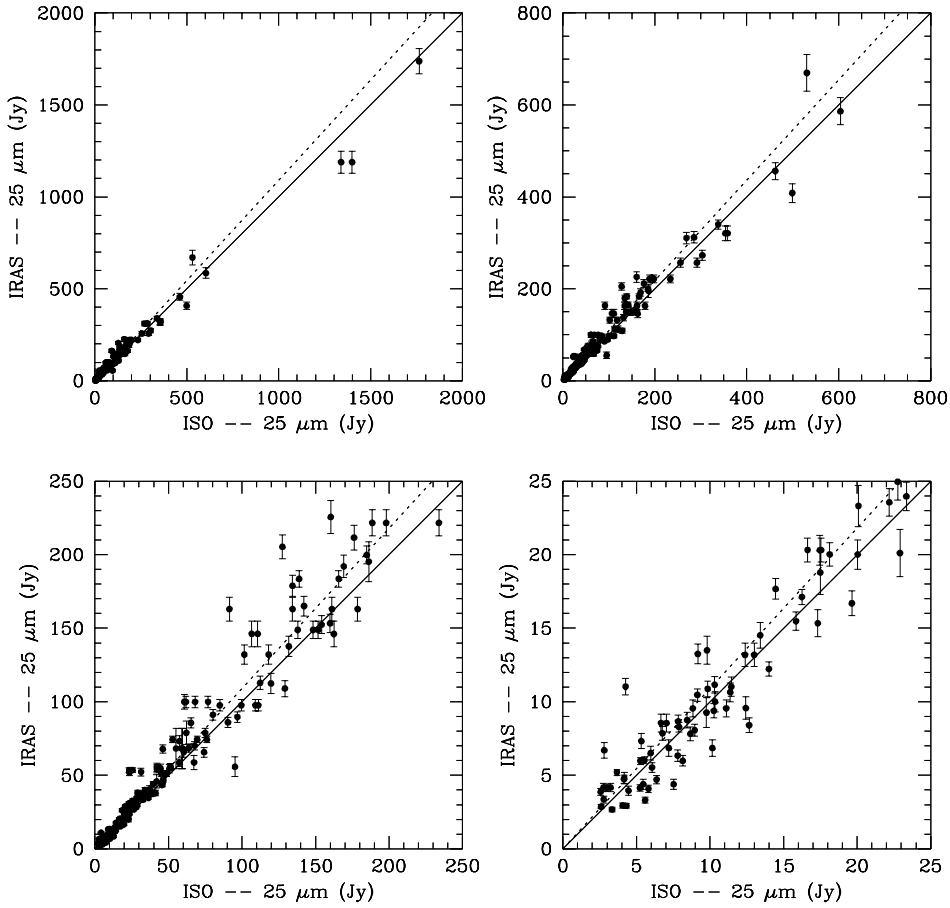

Figure 3.13: ISO SWS synthetic photometry at 25 μm compared to IRAS photometry at the same wavelength. The dashed red line represents an 8% systematic underestimation of the ISO fluxes with respect to IRAS - Pedro García-Lario

test cases showing a strong silicate emision at 10 μm for which the SWS fluxes are 14.9% and 10.9% fainter than the IRAS fluxes at 12 μm.

A similar cross-calibration work will be started soon using the same database of IRAS LRS spectra for comparison with ISO PHT-S spectra. A preliminary search show that there are 232 PHT-S spectra in the ISO Data Archive which can be identified with sources included in the IRAS LRS Catalogue. The intention is to extend the analysis in the future also to CAM-CVF data.

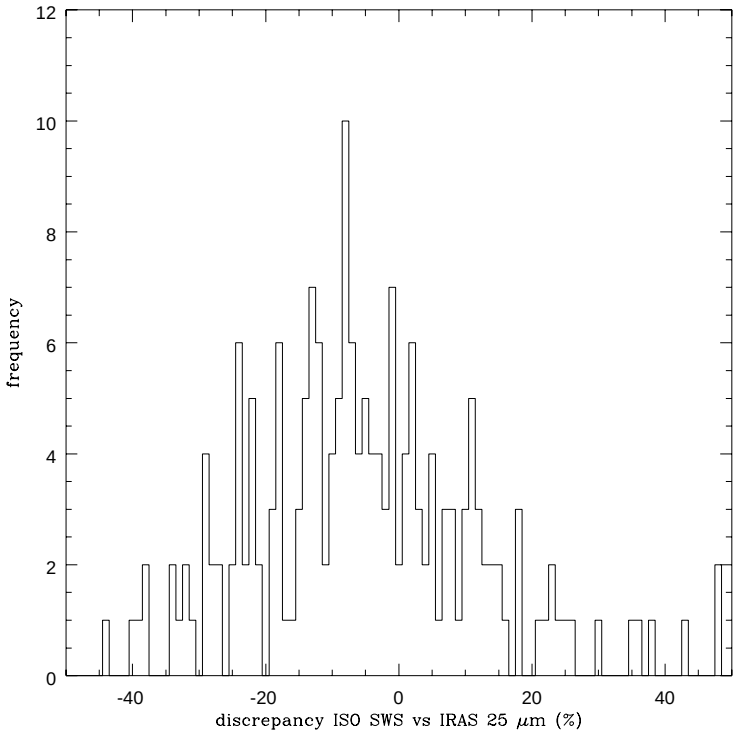

Figure 3.14: *Distribution of discrepancies found between the ISO SWS synthetic photometry at 25 μm and IRAS photometry at the same wavelength - Pedro García-Lario*

3.4.3 Cross-calibration of sources observed with MSX and ISO SWS

In order to better understand the discrepancies found between ISO OLP v8.4 data products and IRAS we decided to extend the cross-calibration analysis of ISO SWS to observations made with other space facilities. Thus, we present here the preliminary results obtained from a cross-calibration comparison of ISO SWS data with photometric data provided by the *Midcourse Space Experiment* (MSX).

Briefly, MSX was a multi-discipline experiment sponsored by the Ballistic Missile Defense Organization. The principal objective of the MSX astronomy experiments was to complete the census of the mid-infrared sky. Experiments were designed to cover the regions either missed by the IRAS and COBE/DIRBE or where the sensitivity of IRAS was degraded by confusion noise arising in regions of high source densities or structured extended emission, including the entire Galatic Plane.

The MSX Point Source Catalogue contains all the point sources detected with signal-to-noise ratio > 3 following criteria very similar to IRAS (detection requires multiple HCON confirmations).

The infrared instrument on MSX was a 35 cm clear aperture off-axis telescope cooled by a single solid H_2 cryostat equipped with Si:As BiB arrays with eight columns of detectors, each with 192 rows of 18".3 square pixels, and a high sensitivity (0.1 Jy at 8.3 μm). Two narrow band filters covered the spectral regions centred at 4.29 (B1) and 4.35 (B2) μm, and four broad band filters covered the spectral regions centred at 8.28 (A), 12.13 (C), 14.65 (D) and 21.34 (E) μm (see Table 3.1).

Table 3.1: *MSX SPIRIT III Spectral Bands*

Band	No active cols.	Isophotal $\lambda(\mu m)$	50% peak intensity	Isophotal BW(μm)	Zero mag flux (Jy)	Abs. Photom. Accuracy	Survey Sens. (Jy)	Effective FOV Ω_{EFOV} ($\times 10^{-9}$sr)
A	8	8.28	6.8−10.8	3.36	58.49	5%	0.1−0.2	10.6
B_1	2	4.29	4.22−4.36	0.104	194.6	9%	10−30	14.0
B_2	2	4.35	4.24−4.45	0.179	188.8	9%	6−18	14.0
C	4	12.13	11.1−13.2	1.72	26.51	3%	1.1−3.1	11.7
D	4	14.65	13.5−15.9	2.23	18.29	4%	0.9−2	11.3
E	2	21.34	18.2−25.1	6.24	8.80	6%	2−6	12.6

In the following analysis we will only consider the broad MSX filters A, C, D and E.

About 100 sources suitable for cross-calibration purposes with an available SWS01 spectrum in the ISO Data Archive have been identified to have their corresponding mid-infrared counterpart in the MSX Point Source Catalogue.

In order to perform a similar analysis using the 'syn_phot' application in ISAP v2.0 to the one performed in the cross-calibration with IRAS data, the MSX filter transmission profiles (kindly provided by Michael Egan, from the MSX project) were implemented in a local version of ISAP (soon these filters will be publicly available in the new version of ISAP v2.1). Again, bad data points affected by glitches were identified and removed from the SWS spectra using the available tools in ISAP and 'ISO SWS photometry' was performed at the A, C, D and E MSX filters with the help of 'syn_phot'. We remind that this tool simply convolves the ISO spectrum with the transmission profile of the A, C. D and E MSX filters and assigns a monochromatic flux for each of these bands under the assumption that the source SED shape is of the form $\nu \times f_\nu =$ constant, or equivalently $\lambda \times f_\lambda =$ constant, in the same way as MSX did.

At the time of writing this Report it was only possible to perform a preliminary analysis on the six sources in the list of SWS OLP v9.5 test cases with MSX data available. As you can see in Table 3.1, appart from a strongly discrepant individual measurement in filter A for source #1, there is a general good agreement at all filters in the absolute mean flux level derived from MSX and ISO OLP v9.5 SWS data (within 5% at all bands with the exception of band A). In most cases, the ISO fluxes are in agreement with the corresponding MSX ones within 10% (see Table 3.2).

In any case, we believe it is still too soon to derive any conclusion from this analysis until we

Table 3.2: *Comparison between MSX photometry and ISO synthetic photometry in a few OLP v9.5 test cases*

MSX photometry (Jy)				SWS photometry (Jy)				Discrepancies MSX vs ISO			
A	C	D	E	A	C	D	E	A	C	D	E
248	1290	1265	2532	720.0	1354	1292	2697	+190%	+5.0%	+2.1%	+6.5%
15.4	25.4	43.4	43.0	9.9	21.7	42.1	45.9	−35.8%	−14.9%	−3.0%	+6.8%
18.1	7.2	5.5	2.9	16.0	7.6	4.9	3.7	−11.6%	+5.2%	−10.9%	+29.2%
15.6	19.8	21.7	41.4	13.3	19.7	19.9	32.1	−14.3%	−0.4%	−8.0%	−22.5%
26.1	95.5	99.0	230.8	26.4	93.0	91.9	209	+1.2%	−2.6%	−7.2%	−9.4%
230	349	242	256.9	216	330	242	248	−6.0%	−5.6%	−0.0%	−3.3%

can extend it to a significant number of sources. Work in this field is on-going.

3.4.4 Cross-calibration of sources observed with IRAS and ISO LWS

Josephine Chan, in collaboration with Bruce Swinyard, is carrying out a similar analysis considering a database of sources observed with ISO LWS for which there is available IRAS photometry at 100 μm.

The purpose of this study is in principle twofold. One is to find the definition of 'faint source' from the point of view of LWS. In other words, we need to find the break down point of the data which is affected by the inaccurate dark current subtraction. The other is the cross-calibration study itself between LWS and IRAS data.

Both of these issues can be addressed at the same time through a systematic study of the LWS data and, for this, we must have a statistically meaningful sample. The selection criteria, and therefore the results, are only preliminary. Some additional criteria may need to be applied. Hence, the number of sources in the sample and the results below presented may change slightly.

The goal is to make a systematic study of the ISO-LWS data as a function of the type of object observed (bright/faint, blue/red, point/extended,...) determining the consistency with IRAS data in each case.

There are 2322 LWS01 GT grating observations corresponding to almost 500 different objects in the ISO Data Archive. In order to compare the absolute flux calibration of IRAS and ISO LWS searched the IRAS Point Source Catalogue (PSC) for counterparts based on the following criteria:

1. Search radius: $2'$; if more than one IRAS source is found the pointing is rejected;
2. IRAS Point source correlation coefficients are A(100 or B(99
3. $F_\nu(100\mu m) < 1000$ Jy – to avoid detector non-linearity
4. $F_c/F_s < 0.5$ where F_c/F_s is the flux ratio of cirrus and source
5. no strong cirrus background is deduced from the CIRR3 value, or visible in the IRAS Sky Atlas Map and/or the LWS Parallel map at 100 μm (LW1 detector).
6. source is not far-infrared variable

This way a total number of around 120 common pointings were found and included in this cross-calibration analysis.

There are some effects for which the data need to be corrected. We know that sometimes 'false strong features' appear at $\sim$53 μm, and $\sim$105 μm on the LWS spectra of some point sources. The origin of these features is believed to be a near-infrared leak in the blocking filters located in front of the detectors. It is necessary to remove these 'false' features because the values of LWS synthetic photometry are strongly affected if this is not done.

The other main problem which affects the data is cirrus, as it is reflected in the selection criteria above listed. At 100 μm, the infrared sky is characterized by emission from instellar dust on all spatial scales. A significant chance exists that any catalogue source is affected by components of this long-wavelength emission on point source scale. While the IRAS photometric fluxes quoted

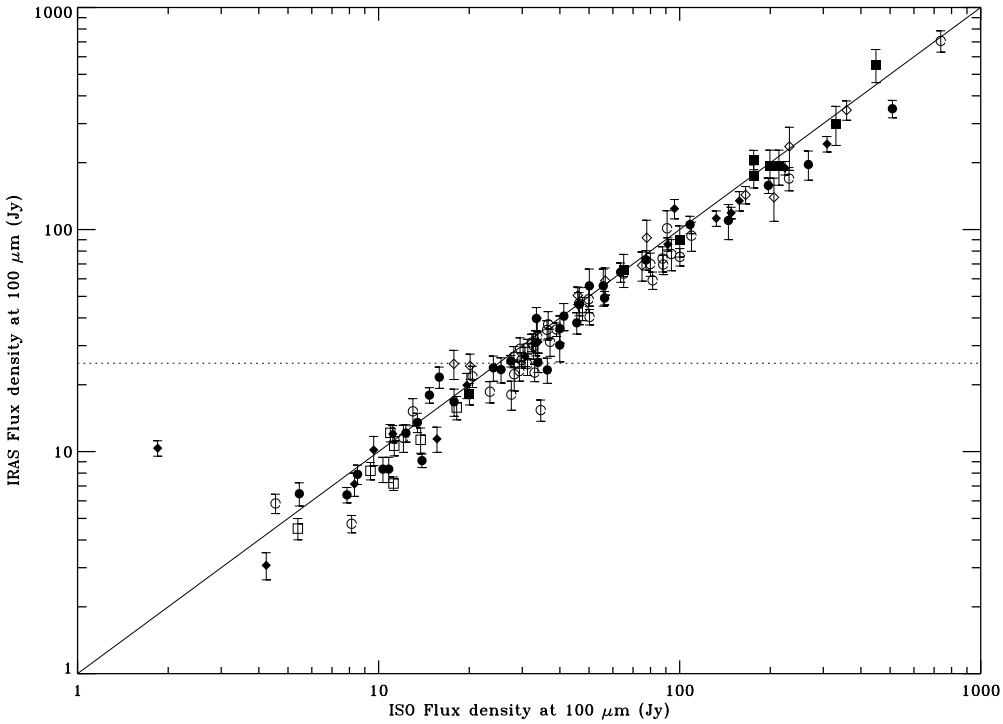

Figure 3.15: *ISO LWS synthetic photometry at 100 μ compared to IRAS photometry at the same wavelength - Josephine Chan*

in the PSC are already corrected for this background 'cirrus' emission, the photometry derived from LWS data contains also this background contribution. Therefore, it is necessary to recover the *uncorrected CIRRUS* flux at 100 μm from the original information contained in the IRAS PSC and derive the uncorrected IRAS flux at 100 μm before making any comparison with LWS synthetic photometry.

Two methods can be applied to perform this 'cirrus correction'. Both recovery procedures are only approximate:

> Method 1 is to recover the 'uncorrected cirrus' IRAS flux in the 100 μm band. It is based on the value of CIRR2 listed in the IRAS PSC which is directly related via an analytical expression to the value of F_c/F_s via the formula listed in the IRAS Supplement V-54.
>
> Method 2 is to 'remove' the cirrus from ISO-LWS synthetic photometry based on the CIRR3 values listed in the PSC. If the F_c/F_s is less than 0.5 and CIRR3 is less than 254 MJy sr^{-1}, the correction is expected to be quite accurate.

Sample objects were divided into six different groups based on the category source provided by the observers and also based on their IRAS associations. This 'classification' is not rigorous. However, one can considered them as homogeneus groups from the statistical global point of view. The following groups were established:

- Group 1: Dust Star;
- Group 2: Dust PN;
- Group 3: Galaxies;
- Group 4: Interstellar Medium;

- Group 5: Young Stellar Objects; and

- Group 6: Vega like stars.

The ISO Spectral Analysis Package (ISAP) v2.0 was used for the spectral analysis of the selected LWS01 spectra. Three main applications 'zip','average' and 'syn_phot' were heavily used for processing the AAR LWS data. The 'ISO LWS photometry', equivalent to the IRAS photometry at 100 μm, of these sources was obtained simply by convolving the ISO spectrum with the transmission profile of the IRAS filters at 100 μm using the 'syn_phot' application again assigning a monochromatic flux at these two wavelengths under the assumption that the source SED shape is of the form $\nu \times f_\nu$ = constant, or equivalently $\lambda \times f_\lambda$ = constant.

Figure 3.15 shows the comparison of the IRAS photometry and ISO synthetic photometry at 100 μm. The photometry distribution has at least 2 different slopes. The first discontinuous 'junction' point is around 20 - 30 Jy. This might be due to an inaccurate dark current subtraction below $\sim$ 25 Jy, which could be the limit for the definition of a 'faint source' for LWS. However, there seems to be a second one at around 100 Jy whose origin is not yet understood.

In general there is a reasonable good agreement, with the data points distributed mainly along or below the diagonal line (ISO fluxes are overestimated with respect to IRAS). In Figure 3.15 each individual group is plotted with a different symbol. There seems to be small differences in the plotted distribution from group to group but, in general, they are all consistent. The small systematic overestimation of fluxes by ISO with respect to IRAS is most likely due to the fact that the current methods of cirrus correction are only approximate. The percentage difference between IRAS flux density and LWS synthetic flux density is $\sim$ 20-30% in most cases. Figure 3.16 shows the distribution of ISO/IRAS flux density ratios at 100 μm as a function of the IRAS flux density at 100 μm.

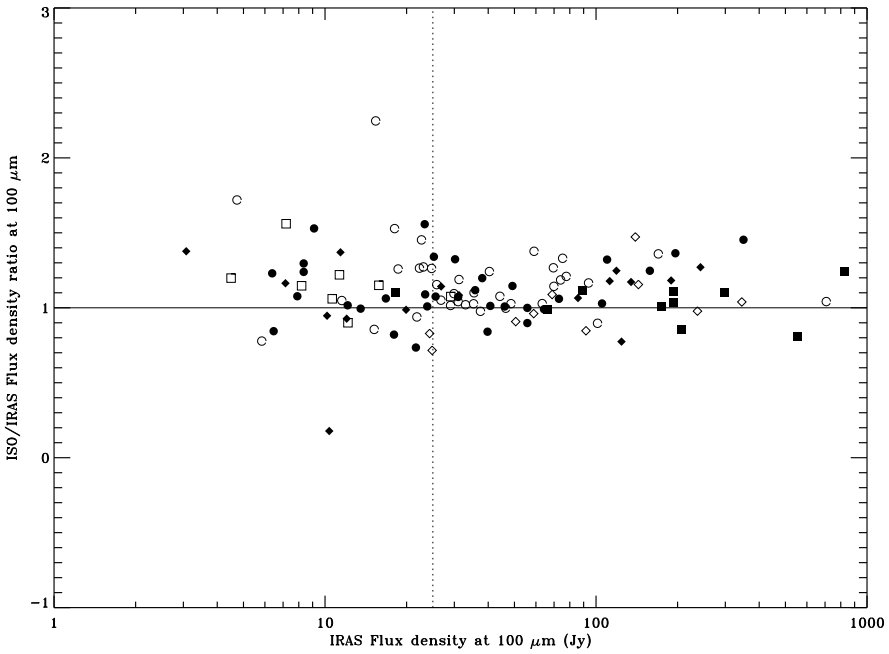

Figure 3.16: *ISO LWS synthetic photometry at 100 μ compared to IRAS photometry at the same wavelength - Josephine Chan*

Additional analysis is still on-going in order to interpret these preliminary results.

3.4.5 ISOPHOT versus COBE/DIRBE

PHT-S OLP v9.0 measurements of the zodiacal background, calibrated with the dynamical calibration indicate that an excellent agreement exist with COBE data (see Figure 3.17).

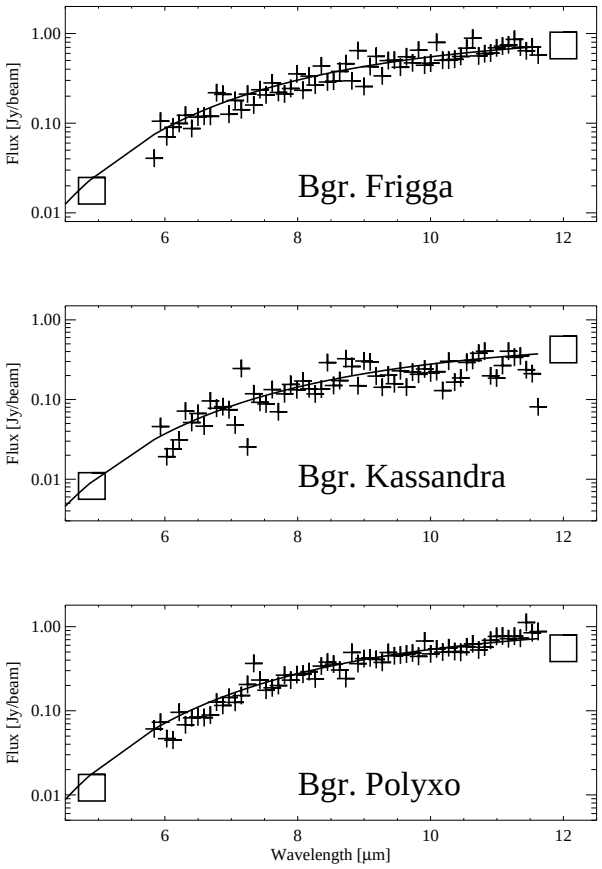

Figure 3.17: *Comparison of PHT-S sky background measurements made in the vecinities of the asteroids Frigga, Kassandra and Polyxo (crosses) with COBE data at 4.9 and 12 μm (squares). The solid line indicates the zodiacal light model prediction - Thomas Müller*

On the other hand, as it was already mentioned in Section 2.2.1 of this report, measurements of the sky background through default apertures with the following detectors: P1 at 12μm (default aperture is 52"), P2 at 25μm (79")and P3 at 60μm (180"), together with FCS measurements were analysed amd compared by Thomas Müller with COBE/DIRBE results.

The COBE/DIRBE values have been calculated from weekly maps, using the median of all DIRBE pixels within 1.5 degrees from the nominal position. The ISOPHOT signal was calibrated with the actual response of the detector. Both, COBE/DIRBE and ISOPHOT values were colour corrected assuming a background blackbody temperature of 275 K. Colour correction values for COBE/DIRBE (ISOPHOT) are: 12.0 μm: 0.93 (0.93), 25.0 μm: 1.31 (1.12), and 60.0 μm: 1.32 (1.09). Since the background temperatures vary between 259 and 292 K (Ábrahám et al. 1999), the colour correction values have uncertainties of up to 3% for both instruments. The COBE/DIRBE values are given with a sigma of less than 1%, the ISOPHOT signal processing uncertainties are 1 to 5%.

All 3 ISOPHOT filtes show considerable systematic offsets with respect to the COBE values: $\sim$ 15% at 12 μm, >40% at 25 μm, and 20−30% at 60 μm (see Figure 3.18).

The flux dependency of the offset seen at 12 and 25 μm in Figure 3.19 can be due to an imperfect signal linearisation. If the COBE-DIRBE values are correct this means that the apparent solid angle of the PHT apertures are considerably larger than the currently used ones. So far, the effective solid angles are set equal to the physical sizes of the apertures.

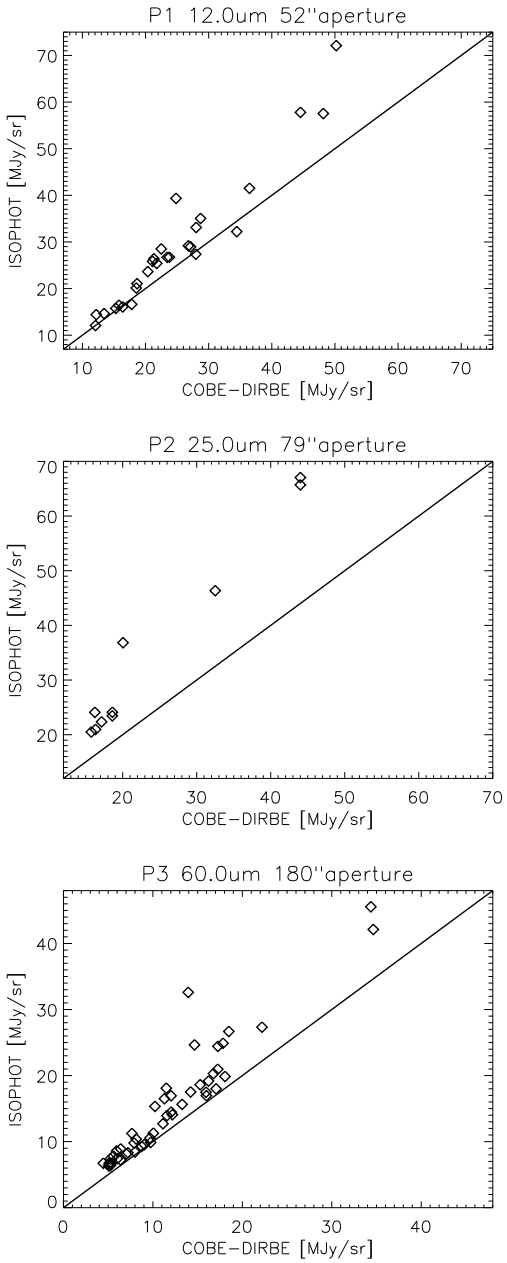

Figure 3.18: *Comparison of ISO P1-12µm, P2-25µm and P3-60µm colour corrected surface brightness of the sky background through default apertures with COBE/DIRBE data - Thomas Müller*

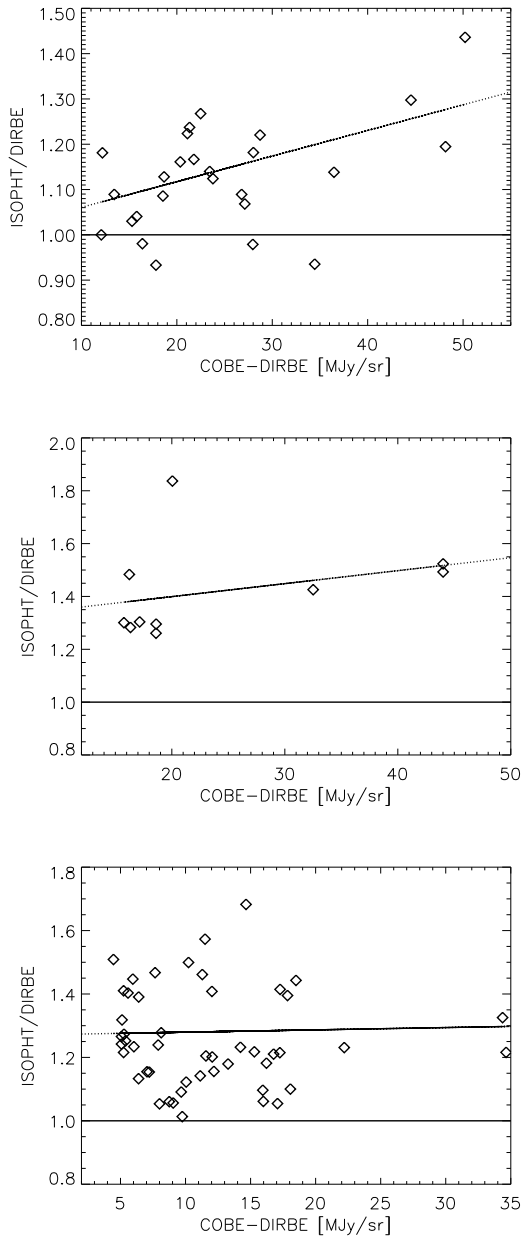

Figure 3.19: *Flux dependency of the offsets shown in Figure 3.18 for P1-12μm, P2-25μm and P3-60μm detectors - - Thomas Müller*

3.4.6 Comparison between ISO and KAO line fluxes

A cross-calibration comparison between ISO observations of a number of compact HII regions with LWS and observations taken with the Kuiper Airborne Observatory (KAO) has been performed by Leticia Martín.

The sample includes 12 different compact HII regions. Three lines, namely [O III] 52 μm, [N III] 57 μm and [O III] 88 μm were analysed with the same results in all cases (see Figure 3.20).

A slightly higher flux is systematically detected by LWS with respect to the KAO line fluxes but the differences found are of less than 30%.

The LWS line fluxes were derived using OLP v8.7. The line fluxes will appear in a catalogue as Peeters et al. (2001), at the moment in preparation.

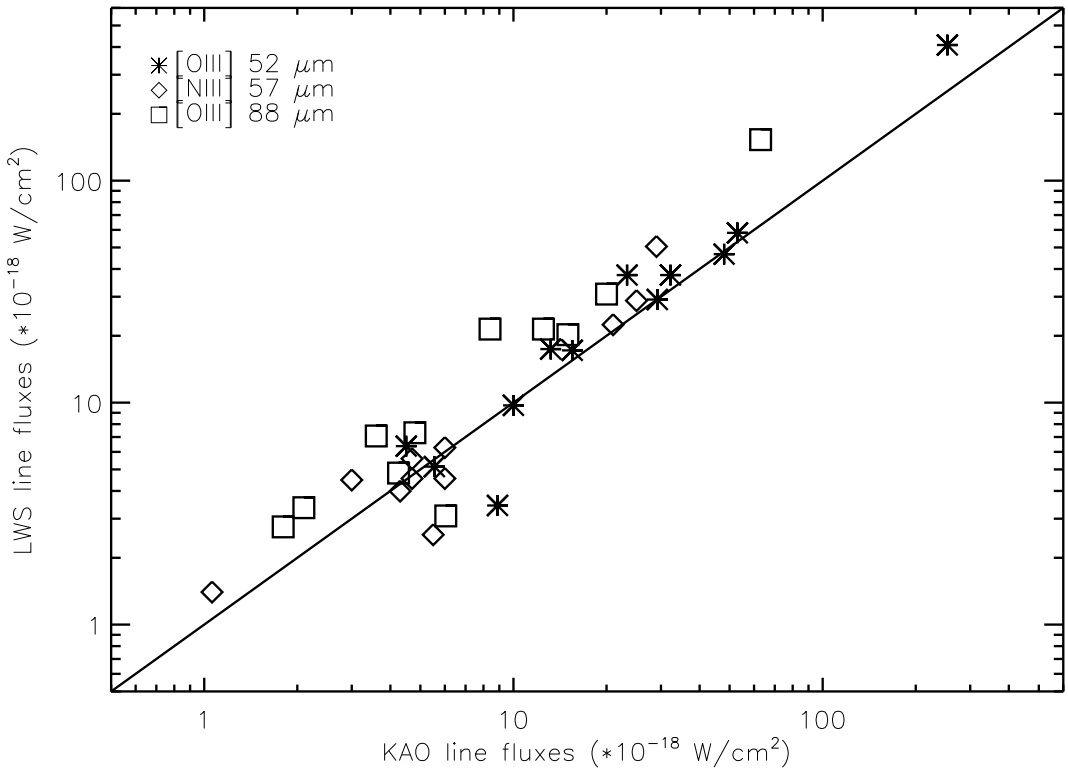

Figure 3.20: *Comparison of forbidden lines detected both with LWS and KAO for a small sample of compact HII regions - Martín et al.*

3.4.7 Cross-Calibration comparisons with models

CAM:

A small sample of Hypparcos Input Catalogue (HIC) stars have been used throughout the ISO mission to calibrate ISOCAM.

In order to determine the consistency between the measurements and the models used to derive the calibration curves, the fluxes determined by OLP v9.5 for these stars as a function of wavelenght obtained with multi-filter or CVF observations have been compared with the fluxes predicted by the models. In many cases, the same star has been observed with various apertures and all the different measurements have also been considered.

Plots have been generated automatically reading the CPSL (CAM Point Source List) file which uses an automatic PSF fitting tool to determine the position and the flux of all the detected point sources in a CAM field.

In general, the results obtained show that most of the flux measurements which can be derived this way are significantly below the model fluxes. If we take the mean value of all the measurements taken per star, the discrepancies range from just a 5% in the case of HIC 67485 to 35% in the case of HIC 69713. The full list of stars analysed and the mean discrepancies found are listed in Table 3.3 compared with the same calculations made for OLP v7.

Table 3.3: Mean discrepancies found in the photometry of some ISOCAM calibration stars with respect to the models

Calibration star	OLP v7	OLP v9.5
HIC 67485	n.a.	−5%
HIC 69713	−36%	−35%
HIC 70218	−29%	−20%
HIC 73005	−32%	−22%
HIC 77277	n.a.	−17%
HIC 85317	n.a.	−11%
HIC 94376	−17%	−17%
HIC 94890	−9%	−8%

In Figure 3.21 we show as an example of the results obtained the case of HIC 77277, where the mean error found is −17%.

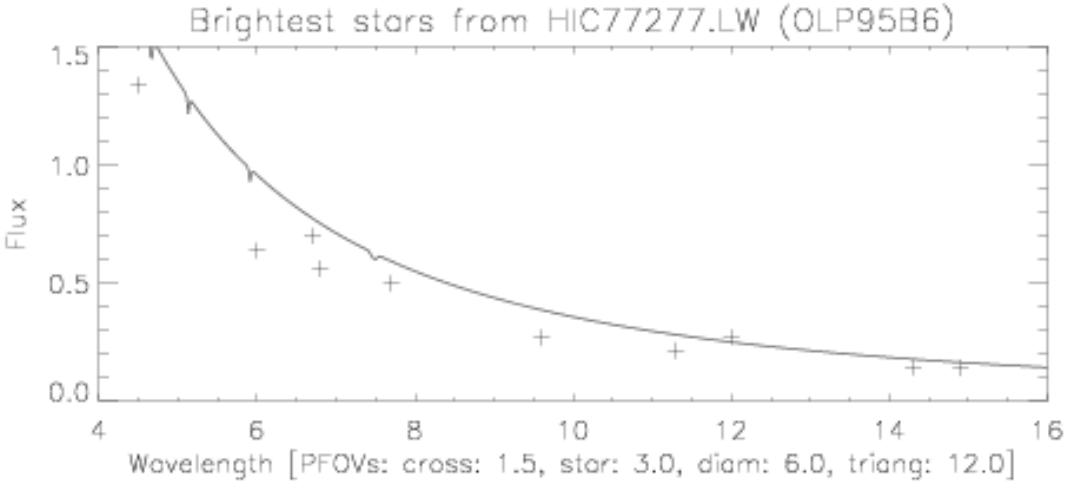

Figure 3.21: *Comparison of CAM OLP v9.5 measurements on HIC 77277 with the calibration model - Diego Cesarsky*

In most cases there is an improvement with respect to previous calculations made with OLP v7 data products. However, it appears that the transient corrector did not bring up the fluxes all the way up to the model level, possibly because the Fouks-Schubert correction is esentially non-operant for point-like sources. A good point however is that the correction did not worsen the flux measurements.

Clearly an upcoming task for the next version of the OLP will be trying to understand this systematic underestimation of fluxes by OLP.

LWS:

A comparison of Uranus observations made with LWS and reduced using OLP v7 with two possible models for this planet was already shown in one of the previous Status Reports.

This time we want to show another cross-calibration comparison made by Thomas Müller based on the analysis of fixed grating observations of Ceres and Uranus reduced with OLP v8.7. The ratio observation/model has been calculated for 15 LWS02 measurements made on Ceres and 12 LWS02 measurements on Uranus.

The agreement of the Ceres model (Müller and Lagerros) and Uranus model (Griffin and Orton) with the observations is found to be excellent (see Table 3.4). For comparison, ratios observation/model for Mars derived by S. Sidher et al. (assuming $\epsilon = 0.95$) are also shown.

Table 3.4: Average ratios between Observations and Models

Detector	Ceres	Uranus	Mars
SW1	1.21	1.25	?
SW2	1.01	1.01	0.91
SW3	0.99	0.99	1.04
SW4	0.98	0.99	0.99
SW5	1.00	1.00	0.89
LW1	1.10	1.04	1.09
LW2	1.01	1.11	1.05
LW3	0.95	1.09	0.95
LW4	1.03	1.05	0.98
LW5	1.17	1.05	0.92
SW1-LW5	1.03	1.04	0.98

The results obtained show an excellent agreement for all detectors between SW2 and SW5. At longer wavelengths the discrepancies are higher (up to 17%) due probably to the fact that Ceres is relatively weak (40-80 Jy at 178 μm), saturation effects from Mars and/or possible features from iron oxide which might be present in the spectrum.

The global difference between observations and models amounts to only 3%. In principle, this strengthens the case of the Orton and Griffin model for Uranus. However, note that the stronger discrepancy occurs at the shortest wavelengths for detector SW1, which is precisely where models by other authors (like the one by Abbas, currently used by PHT) differ with Griffin and Orton's model.

Of special interest is the fact that the ration observation/model for SW1 is very similar both in the case of Ceres and Uranus. The problem clearly deserves further investigation.

PHT:

In the case of PHT a large number of consistency checks with models are available in the *"Report on the PHT Scientific Validation for OLP Version 9.0"* by Ulrich Klaas et al. available at:

`http://www.iso.vilspa.esa.es/users/expl_lib/PHT/phtolp90_scivalrep_v1.ps.gz`

Some of the comparisons made using OLP V9.0 data products are summarised here:

1. Consistency check of PHT-S Dynamic Response Calibration

   PHT-S measurements of some of the calibration stars (HR7001 = Vega, HR2491 = Sirius, HR 5340, HR 7469, HR 7924 and HR 8487) that were used to establish the dynamic relative spectral response function surfaces of Cal-G file PSDYNAMIC were checked in order to determine whether the input model SEDs were reproduced. The results obtained show that the method represents a significant improvement with respect to the static default response function applied in OLP v8.4, up to 10% level of agreement or better at a wide range of flux levels.

2. Consistency check of Chopped PHT-S Relative Spectral Response Function

   Measurements of two calibration stars (HR 6817 and HR 6847) which were used to establish the Relative Spectral Response Function for chopped PHT-S calibration were checked in order to determine whether the input model SEDs were reproduced. Both calibration stars were measured both in rectangular and triangular chopped modes obtaining in all cases an excellent agreement with the models.

3. General revalidation of PHT03 and PHT22 staring modes (multi-filter photometry)

   The composite spectra from 1 to 35 μm extrapolated to 300 μm provided by Martin Cohen for HR 5340 (α Bootes) and HR 6705 (γ Draconis) were compared with observations of these stars taken with PHT-P and PHT-C in the staring modes PHT03 and PHT22 with all the available filters (except the 3.6 and 4.85 μm filters in the case of HR 5340 because the source saturated the detectors).

   The conclusion obtained for HR 5340 is that PHT photometry gives a good representation of the SED from 3.3 to 170 μm (agreement within 10% in most cases), with small improvements (in PHT-P3 photometry) with respect to OLP v8.4 but still some problems at the longest wavelengths where the source flux extraction is more difficult because of the strong background (see Figure 3.22).

   In the case of HR 6705, there is a general good agreement from 3 to 100 μm with the only exception of a measurement at 15 μm probably affected by strong transients. The C100 filters are systematically high by 20 to 45%. Adopting a default responsivity calibration for these filters gives fluxes which are lower than the model in contrast with the fluxes derived from actual responsivity calibration. The exception is the 105 μm filter which is too low both for actual and default responsivity calibration methods. Very likely this is cause by the background subtraction. For C200 filters, no useful resylts were achieved. The fluxes are all too low or even negative.

4. General revalidation of PHT03 and PHT05 staring modes with Sirius (multi-filter and absolute photometry)

   PHT03 (multi-filter) and PHT05 (absolute photometry) measurements of the calibration star HR 2491 (Sirius) out to 25 μm were compared to the model from 1 to 300 μm of this star provided by Martin Cohen. The colour-corrected fluxes were compared also with IRAS photometry and the results are shown in Figure 3.23.

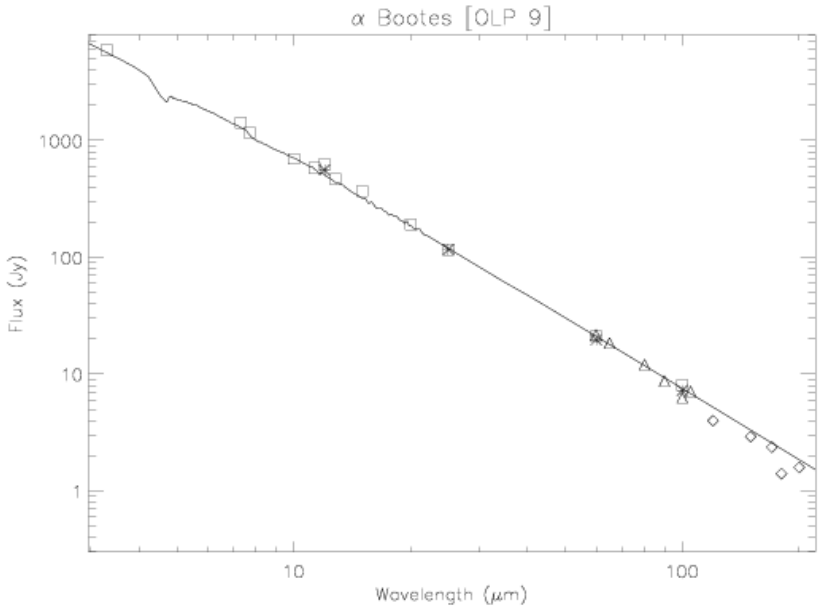

Figure 3.22: *Comparison of PHT-P and PHT-C photometry, using the full ISOPHOT filter set, with the composite spectrum out to 300 μm extrapolated SED of α Bootes (HR 5340) provided by M. Cohen and with IRAS photometry for OLP v9.0 data products. All photometric points are colour-corrected for a 4000 K black-body. The meaning of symbols is the following: solid line: model, asterisks: IRAS, squares: PHT-P (PHT03) measurements, triangles: C100 (PHT22) measurements, diamonds: C200 (PHT22) measurements - Ulrich Klaas*

The accuracy of the absolute photometry of Sirius is found to be better than 5% (for P2 25 μm this is derived estimating the amount of non-subtracted background since this measurement was not taken) while the accuracy of P1 multi-filter measurements is found to be better than 10% absolute and better than 5% relative.

Similar results on absolute photometry (PHT05) were found when the comparison was made using observations of α Ari = HR 617.

5. Revalidation of C200 (PHT25) absolute photometry

   The background subtracted, colour-corrected flux values derived with OLP v9.0 using the C200 absolute photometric mode were compared against the model prediction by Lagerros for Ceres and Abbas for Uranus.

   In Figure 3.24 we show the results obtained for Ceres and in Figure 3.25 the results obtained for Uranus, respectively.

   As we can see, the level of agreement is quite good in both cases. With the exception of the C200 filter measurement of Ceres at 200 μm which is off by 14% with respect to the model, the remaining measurements are all within the 10% level of agreement.

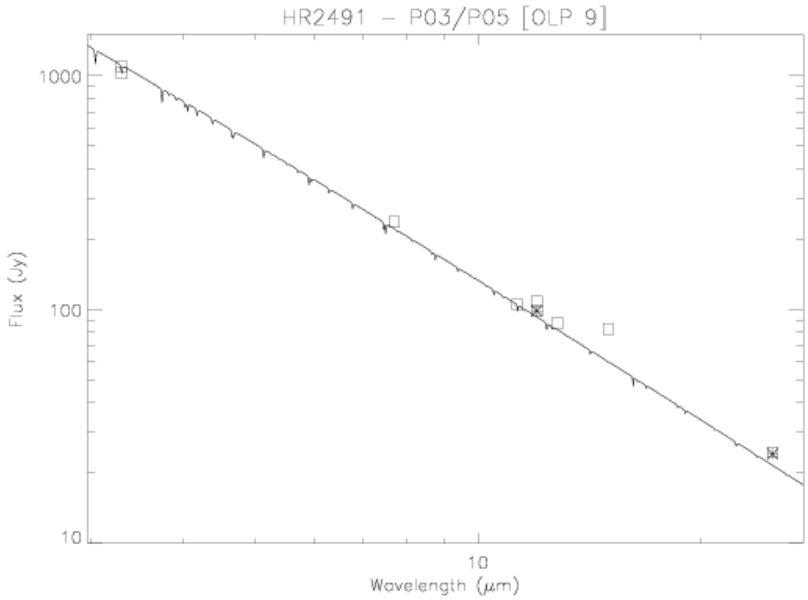

Figure 3.23: *Comparison of PHT-P absolute and multi-filter photometry with the composite spectrum of Sirius (HR 2491) provided by M. Cohen and with IRAS photometry for OLP v9.0 data products. All photometric points are colour-corrected for a 10000 K black-body. The meaning of the symbols is the following: solid line: model, asterisks: IRAS, squares: PHT-P (PHT03 and PHT05) measurements - Ulrich Klass*

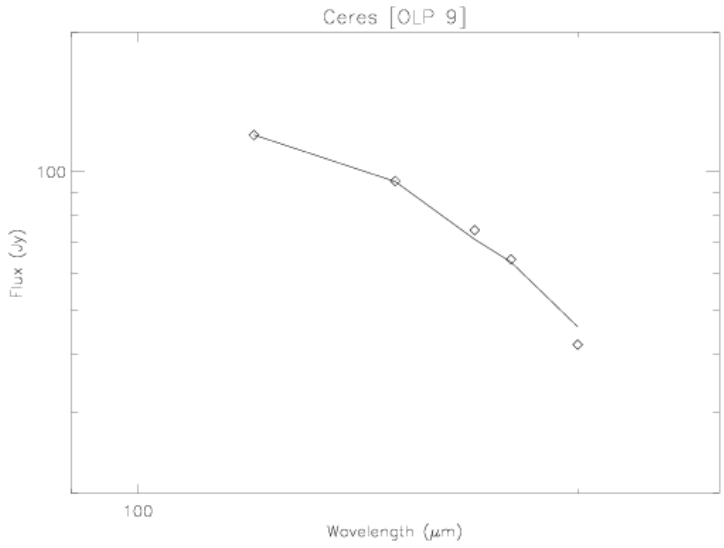

Figure 3.24: *Comparison of C200 absolute photometry of the asteroid Ceres with the thermophysical model by Lagerros for OLP v9.0 data products. All photometric points are colour-corrected for a 240 K black-body. The meaning of the symbols is the following: solid line: model, diamond: C200 (PHT25) measurements - Ulrich Klaas*

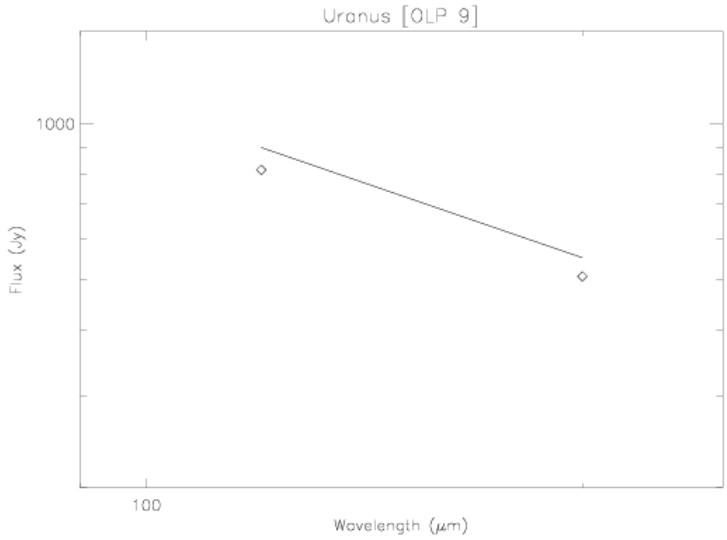

Figure 3.25: *Comparison of C200 absolute photometry of Uranus with the model provided by Abbas for OLP v9.0 data products. All photometric points are colour-corrected for a 60 K blackbody. The meaning of the symbols is the following: solid line: model, diamond: C200 (PHT25) measurements - Ulrich Klaas*

SWS:

Similar comparisons have been made between a few OLP v8.4 spectra of bright stars observed with SWS and their corresponding models (again composite spectra provided by Martin Cohen in most cases).

In general, a very good agreement between observations and models (within 10%) is found at flux levels above 10 Jy, especially at short wavelengths (bands 1 and 2). In bands 3 and 4 stars are quite faint and the noise increases extraordinarily. In Figure 3.26 we show some of the comparisons made.

Note that two of the stars plotted, HR 6705 and HR 6688, were used for determining the absolute flux calibration of SWS. Thus, these cross-calibration comparisons must be considered just as internal consistency checks. The other two stars shown in Figure 3.26, HR 337 and HR 6132, were not part of the small set of stars used for the calibration of SWS. However, the results are also found to be rather consistent with the models.

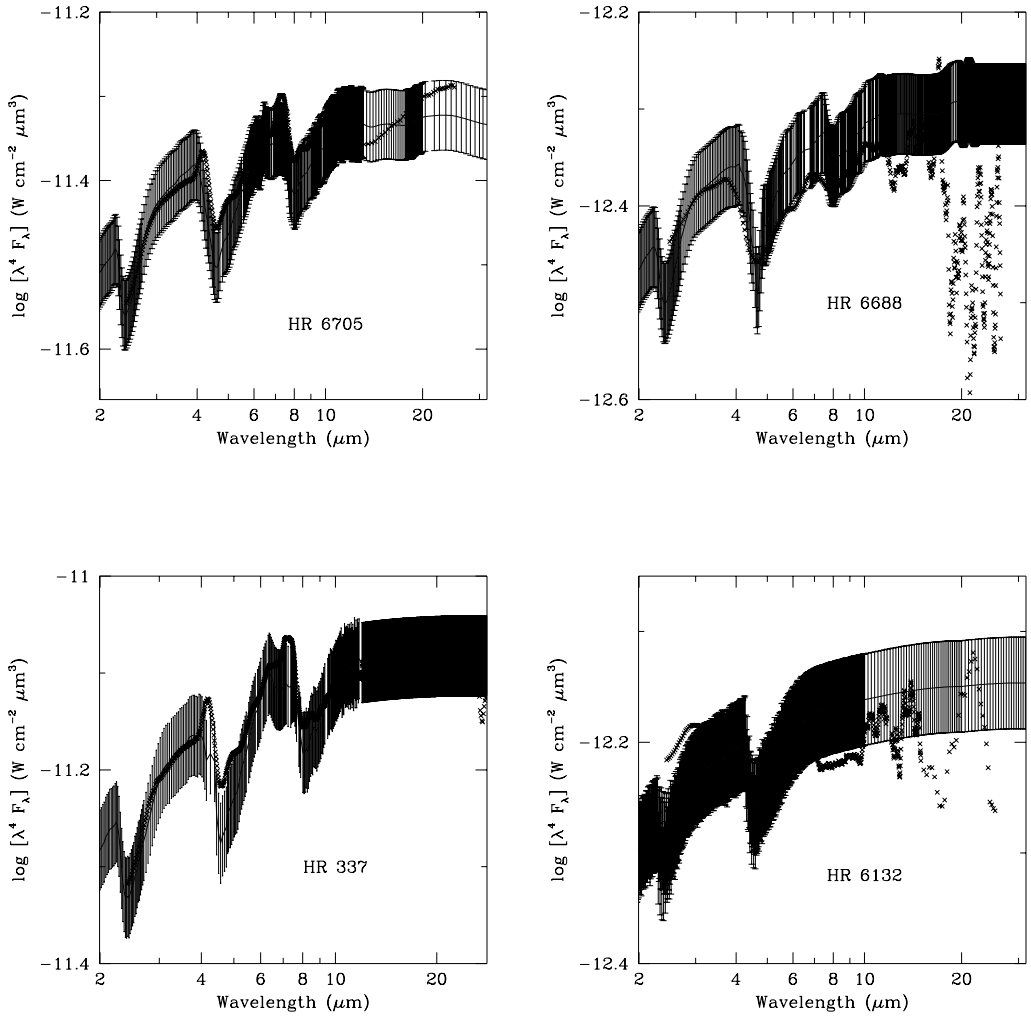

Figure 3.26: The SWS OLP v8.4 spectra (crosses) of the stars HR 6705, HR 6688, HR 337 and HR 6132 are compared to their model SEDs (blue solid line). In red we indicate 10% deviations with respect to the model

Chapter 4

Calibration accuracies and 'Error Budget'

In the following, the 'state-of-the-art' of the calibration of each of the instruments on board ISO as of November 28, 2000 is summarized. Note that this cross-calibration report may not reflect the latest up-to-date information on a specific instrument/observing mode at the time you read this document.

For a revision of the latest information available at any moment we suggest to check the general ISO documentation available in the Web at:

`http://www.iso.vilspa.esa.es/users/expl_lib/expl_lib.html`

4.1 PHT

4.1.1 Improvements in OLPv9.0 for PHT

On July 18, 2000, version 9.0 of the PHT OLP pipeline for automatic data processing was released. Note that this means that, after this release, PHT data retrieved from the ISO Data Archive using the *'Latest Processing'* option will be processed with OLPv9.0.

This is a summary of the main improvements implemented in version 9.0 of the pipeline:

1. **PHT-S dynamic calibration:** *(AOTs affected: PHT40)*

   Probably the most relevant improvement in OLP v9.0. Used to correct staring spectroscopic observations (AOT PHT40) for transient effects, it brings down the errors associated to this observing mode (sometimes as high as 30%) to just a few percent.

   The main idea behind the dynamic spectral response calibration is that a standard star spectrum of similar brightness as the target spectrum suffers the same transient effects. By taking into account the same temporal evolution of the signals for both standard and target spectrum, the transient effects cancel out by dividing the target spectrum by the standard spectrum, without having to derive "infinite values" with a sophisticated transient correction. Since target and standard spectrum can be quite different in shape, a library of standard stars is necessary to calibrate each PHT-S pixel individually in this way. For the automatic approach in the OLP, the transient behaviour with time for the different flux (signal) regimes was characterized by surfaces stored in the new CalG file

PSDYNAMIC constructed from the library of standard stars. The software will determine for each ramp the appropriate transient dependent correction factor.

There are new SPD products, PSSD and PSLD, containing the dark measurements, which precede each sky measurement.

Due to the calibration scheme, which determines directly the flux in Jy, the units of the main SPD products, PSSS and PSLS, changed from V/s to Jy. In order to have consistent data products for all PHT40 submodes, the processing for chopped observations (implemented with OLP 8.4) and raster observations (still using the default RSRF in CalG PSPECAL) had to be adapted, too.

Unfortunately, this calibration method cannot be applied to raster maps, since there is no dark measurement preceding the spectra at each raster pointing (needed for the reproducibility of the transient behaviour as a function of flux). In any case, PHT-S raster maps represent only a minor fraction of the PHT data.

2. **Non-linearity corrections:** *(AOTs affected: all AOTs, except PHT40)*

   Refinements of the flux-dependent signal linearisation have been incorporated in OLP v9.0.

   The signal linearization tables P%%SLINR, introduced with OLP V8.4 have been upgraded with regard to the following aspects:

   a.the new linearisation tables have been re-normalised with respect to the median responsivity per bandpass to avoid filter-to-filter corrections at the signal level.

   b.the shape of the curves among the pixels in the C100 and C200 arrays for a given filter has been homogenized. The curves of the individual pixels have now similar shape based on fine-tuning by eye.

   c.the curves of responsivity as a function of signal smoothly become constant in the extrapolations to very small and very strong signals where no calibration observations are available.

   Due to the re-normalization also the default responsivity values in files P*RESP_01 and P*RESP_02 have been updated.

3. **Refinement of FCS characterization:** *(AOTs affected: all AOTs, except PHT40)*

   The CALG files P%%ILLUM, P%%FCSPOW, P%%FLAT, PPFTOF and PFLUXCONV have been upgraded to reflect the introduction of the new signal linearization corrections (P%%SLINR, see item 2 above). The physical FCS model was refined to give a better relation between the electrical FCS heating power and the FCS/TRS temperature and this was used to determine the extrapolated FCS powers outside the calibrated range.

4. **Chopped mode observations:** *(AOTs affected: PHT03, PHT22 in chopped mode)*

   Some improvements have been implemented in PHT-P and PHT-C chopped photometry calibration.

   Several deficiencies in the CalG files P

   a.signal loss correction for P2 detector

   b.chopper offset (residual signal difference for zero flux difference in both beams) corrections for all detectors

   c.the signal loss corrections were re-derived with the updated signal linearization calibration as described above under item 2.

Chopped observations with the read-out data reduction flag being set are properly processed now. Refinements were also achieved in the chopped pattern processing and a bug omitting the filter-to-filter correction for chopped measurements was fixed.

5. **Handling of different calibration filters for start and end modules in raster maps:** *(AOTs affected: PHT17/18/19 and PHT37/38/39)*

   So far it was assumed in the OLP processing that the FCS measurements of the start and end modules of sparse maps are done in the same filter. This needs, however not to be the case. This led to a mismatch of the responsivity values for the sparse map modules which are interpolated values in time between the two responsivity values from the bracketting FCS measurements. With the new version the correct filter information for the evaluation of both FCS measurements is used.

6. **Complementary flux units for point and extended source products:** *(AOTs affected: all AOTs, except PHT40)*

   Depending on the original observer definition whether the target was a point (P) or extended (E) source, different PHT photometry AAR products are generated, e.g. PPAP and PPAE for PHT-P or PCAP and PCAE for PHT-C pointed observations. P-type products are in unit Jy, E-Type products in unit MJy sr^{-1}. The comparison between both products, needed e.g. for background subtraction, where the on-source measurement may be in Jy while the off-source measurement is in MJy sr^{-1}, is not straight forward, since a conversion using the wavelength dependent effective solid angles and point spread function factors is necessary.

   For these products now complementary flux information in the respective units is provided, i.e. for P-type products in addition the surface brightness in MJy sr^{-1} and for E-type products the flux in Jy/pixel. The same is true for the scan products PPAS and PCAS.

   For the OLP 9 version this additional information is restricted to the data records, corresponding information in the headers has to be postponed to a later version. This made it necessary to define new keyword fields for the AAR products.

7. **Colour correction tables PCCMBBONE and PCCMBBTWO:** *(colour correction factors for modified black bodies)*

   In the *"What's New"* note from 23 December 1999 *"Wrong colour correction Cal-G tables for ISOPHOT"* observers were warned about faulty contents of the CALG files PCCMBBONE and PCCMBBTWO providing the color correction factors for modified blackbodies. From this time to now the correct files were only available via the PIA homepage. The correct files are now available in the IDA with the OLP 9 delivery.

4.1.2 Current calibration accuracies and 'Error Budget' for PHT

The latest report available concerning the updated PHT calibration status as of OLP v9.0 is contained in the document *ISOPHOT Calibration Accuracies* by U. Klaas et al. available at:

`http://www.iso.vilspa.esa.es/users/expl_lib/PHT/calacc_v4.ps.gz`

Table 4.2 gives a summary overview of the currently achieved photometric accuracies as of OLP v9.0.

Note that a number of AOTs are not yet scientifically validated (see Table 4.3) and, thus, no global accuracies can be provided. In addition, the two polarisation modes PHT50 (PHT-P)

Table 4.1: Covered wavelength range and typical aperture sizes of ISOPHOT subinstruments. Note that for PHT–C the first aperture number denotes the pixel size, the second one the array size.

subinstrument	**detector**	**dimension**	**wavelength range** [μm]	**typical aperture size** ["]
PHT–P	P1	1	3 – 17	5 – 180
	P2	1	15 – 29	23 – 180
	P3	1	40 – 130	52 – 180
PHT–C	C100	3x3	40 – 130	43.5 / 138
	C200	2x2	100 – 240	89.4 / 182
PHT–S	SS	1x64	2.5 – 4.8	24
	SL	1x64	5.8 – 11.8	24

and PHT51 (PHT-C) are processed by the pipeline only to raw data level and are not here considered. It is the goal of ISO Post Operations to scientifically validate the OLP processing of all standard AOTs in Table 4.3 for which this is pending.

Currently known limitations and caveats are discussed in Chapter 2 of the already mentioned *"Report on the PHT Scientific Validation for OLP Version 9.0"* by U. Klaas et al. available at:

`http://www.iso.vilspa.esa.es/users/expl_lib/PHT/phtolp90_scivalrep_v1.ps.gz`

Note that a careful interactive analysis using PIA may significantly improve the calibration accuracy numbers given in Table 4.2. One can expect to achieve a higher accuracy using PIA in the following cases:

1) measurements with signal transients which do not stabilise during the measurement time, but which are long enough to perform a reasonable transient fit.

2) flat-fielding of maps, depending on the sampling mode and the dynamic range.

3) correction of non-linear signal drifts in maps.

4) detection of faint sources by refined deglitching and filtering.

5) photometry from mini-maps, through visual determination of sky background

4.1.3 Future plans in PHT calibration

In the next (and last) version of the OLP pipeline v10.0 other calibration problems will be addressed. The main pending calibration issues concern:

1) validation of chopped photometry calibration

2) PHT-P aperture calibration, both for external (sky) and internal (FCS) beams

3) PHT32 (chopped raster maps) calibration

Table 4.2: ISOPHOT Photometric Calibration Accuracy Overview (as of OLP v9.0).

detector	**source type** **p**oint / **e**xtended	**source brightness**	**typical on-source integration** [s]	**absolute accuracy** [%]	**multi-filter accuracy** [%]
P1	p	50 – 6000 Jy	32	< 10	< 20
P1	p	0.1 – 50 Jy	≤ 256	40	
P2	p	10 – 200 Jy	32	< 10	5
P2	p	0.5 – 10 Jy	≤ 256	< 15	
P3	p	0.5 – 25 Jy	32	10	< 10
P3	p	< 0.5 Jy	≤ 256	20	
C100	p	0.5 – 25 Jy	32	15	< 25
C100	p	0.05 – 0.5 Jy	≤ 256	$< 25^*$	
C100	e	5 – 15 MJy sr^{-1}	32	25	20
C200	p	1 – 900 Jy	128	10	20
C200	p	0.2 – 1 Jy	≤ 256	$<20^*$	
C200	e	4 – 10 MJy sr^{-1}	64	20	20
SS staring	p	1 – 6000 Jy	256	< 30	< 20
SS staring	e	30 – 3000 MJy sr^{-1}	256	< 10	< 20
SL staring	p	0.3 – 1500 Jy	256	< 10	< 20
SL staring	e	5 – 10000 MJy sr^{-1}	256	< 10	< 20
SS chopped	p	0.5 – 500 Jy	1024	< 10	< 10
SL chopped	p	0.2 – 200 Jy	1024	< 10	< 10

* for mini-map photometry using PCAS products

While issue 1) is in good track with good confidence to be finalized for OLP v10.0, the other two issues are still open with regard to what results can be finally achieved. The likelihood of implementation in OLP v10.0 is very low, due to the complexity of the tasks and manpower limitations.

Concerning assessment of chopped observations with P2 filters, a report has recently been prepared by R. Laureijs and M. Jourdain de Muizon on *Processing of ISOPHOT chopped photometry at 25 μm* available at:

`http://www.iso.vilspa.esa.es/users/expl_lib/PHT/report_25chop.ps.gz`

This document presents the results derived from a refined analysis of a homogeneous sample of more than 80 main sequence stars which were observed with PHT03 at 25 μm in chopped mode. After comparison of the ISOPHOT photometry with estimates of the stellar fluxes at 25 μm derived from photometric data in the optical from Hipparcos it is found that the current ISOPHOT calibration can be strongly improved by assuming a default responsivity for the P2 detector corrected for orbital dependence. In addition, a relationship is derived which corrects for the effect that in chopped mode the fluxes of bright objects (> 1 Jy) are undererstimated whereas the fluxes of fainter stars (< 300 mJy) are overestimated. The large deviations from the predictions found using OLP processing justify the conclusion that these results cannot yet be scientifically validated.

Table 4.3: Status of scientific validation of PHT OLP AOT processing

AOT	**submode**	**scientifically valid since**	**next upgrades**	**foreseen in OLP Vx.y**
PHT03	staring point source	V6	non-lin R/FCS	10.0
	staring extended source	no	non-lin R/FCS	10.0
			beam	10.0
	nodding	V6	non-lin R/FCS	10.0
	chopped point source	no	chop & non-lin R/FCS	10.0
	raster map	no	map cal	10.0
PHT04	staring point source	no	non-lin R/FCS	10.0
			beam	10.0
			norm. source flux	10.0
	staring ext. source	no	non-lin R/FCS	10.0
			beam	10.0
			norm. source flux	10.0
	chopped point source	no	chop & non-lin R/FCS	10.0
PHT05	staring point source	V6	non-lin R/FCS	10.0
	staring extended source	no	non-lin R/FCS	10.0
			beam	10.0
PHT17/9	staring point source	V6	non-lin R/FCS	10.0
	staring extended source	no	non-lin R/FCS	10.0
			beam	10.0
PHT22	staring point source	V7	non-lin R/FCS	10.0
	staring extended source	V7	non-lin R/FCS	10.0
	nodding	V7	non-lin R/FCS	10.0
	chopped point source	no	chop & non-lin R/FCS	10.0
	raster map	V8.4	flat-field	10.0
PHT 25	staring point source	V7	non-lin R/FCS	10.0
	staring extended source	V7	non-lin R/FCS	10.0
PHT32	chopped mapping	no	map cal	10.0
			de-glitch & flat-field	10.0
PHT37/9	staring point source	V7	non-lin R/FCS	10.0
	staring extended source	V7	non-lin R/FCS	10.0
PHT40	staring point source	V5		
	staring extended source	V6		
	chopped point source	V6		
	raster map	V6		

Meaning of calibration upgrades:

non-lin R/FCS	: refinement of flux dependent signal linearization and FCS power files
beam	: comparison with COBE/DIRBE photometry and empirical determination of effective solid angle
chop	: chopper signal correction, including correction of chopped FCS measurements
flat-field	: improvement of flat-field correction using actual sky measurement
map cal	: Assessment of accuracy of photometry from maps
de-glitch	: improved de-glitching method
norm. source flux	: normalized source flux relative to 180 arcsec aperture to determine relative source profile

With respect to the problem of the determination of aperture profiles in PHT-P detectors, aperture calibration will be focused on the 180″ aperture in order to safe the wide beam absolute sky measurements for the Legacy Archive. The status is the same for both OLP and PIA, since the implementation limitation is due to the still lacking calibration assessment.

A recent study of the problem, including an assessment of PHT-P extended source calibration vs COBE/DIRBE (see Section 3.4.5) made by Thomas Müller is contained in the document: *"PHT Apertures and Absolute Photometry"*, available at

`http://www.iso.vilspa.esa.es/users/expl_lib/PHT/TM_aperture.ps.gz`

This means that the following modes remain non-validated:

- point source photometry in non-standard apertures
- extended source photometric calibration with PHT-P
- multi-aperture photometry in both cases

Note that the first of these items, point source photometry in non-standard apertures, may only be critical for the largest apertures. It is unlikely that for P1 and P2 point source photometry these large apertures were used (for P3, 180″ is the standard aperture and hence calibrated).

Finally, concerning point 3) in the list of pending items for OLP v10.0, and as already mentioned in Section 2.2.6, a PHT32 processing prototype including full transient modelling has been developed by Richard Tuffs within PIA. The solution found requires a high degree of interactivity and, thus, there is no possibility to implement it as part of any pipeline. It is still too early to conclude on possible final calibration accuracies for point sources and slightly extended sources. For OLP v10.0 at least a calibration accuracy assessment will be performed.

Appart from other general calibration areas, like de-glitching or transient corrections, to be improved for all modes, another big issue which will probably be addressed in OLP v10.0 is a consistent error propagation handling and display in the products. In the current pipeline version the uncertainty information is restricted to statistical errors which are minimal errors.

Other calibration improvements, some of them flagged in Table 4.2, to reduce limitations on data quality are:

- FCS straylight contamination for C200 measurements (this is a byproduct of FCS calibration)
- correction for flat-field residuals in P22 raster maps (PIA already offers several methods for improved flat-fielding)
- baseline drift corrections in nodding and raster map observations (PIA already offers median methods to flatten baselines).
- calibration of multi-aperture measurements of slightly extended sources in order to provide the users with a method to distinguish between a pure point source and a possible contribution by a slightly extended component.

Of course, ISOPHOT polarisation observations are not processed by OLP. The current scheme to process up to signal level (intensities) per polarizer and derive polarization parameters within a dedicated FORTRAN routine may be upgraded to have the full processing within PIA. There is one open calibration and processing item, namely that for extended sources (can be compact) the four C200 pixels give discrepant polarization parameters.

From the above calibration status overview it is clear that some tasks can only be performed in a period of time which extends beyond the end of the Post-Operations Phase. The goal in any case, as we have already mentioned, will be to increase the amount of validated data products as much as possible in order to avoid a fair amount of unvalidated products in the ISO Legacy Archive.

With OLP 10, we envisage that about 80% of the ISOPHOT OLP data will be scientifically valid and milder caveats will apply. By the end of the Post Operations Phase 90% of the ISOPHOT data should be sufficiently reducible within PIA with regard to available calibration schemes. The remainders need ongoing efforts into an Active Archive Phase to achieve further completion and improved data quality for inclusion into the ISO Legacy Archive.

4.2 SWS

4.2.1 Improvements in OLPv9.5 for SWS

On November 28, 2000 version 9.5 of the SWS OLP pipeline for automatic data reduction was released. This means that, at the present time, when SWS data is retrieved from the ISO Data Archive and the *'Latest Processing'* button is selected the user gets the data processed with OLPv9.5.

The main area of change for users is in the Derive-SPD section, which has been extensively modified. Derive-AAR was only slightly changed (see point 6 below).

The change in programming language from Fortran to IDL, while the major difference between versions for the developers, is invisible to the users. It was carried out in order to make the Derive-SPD part of the OLP software available for general users OSIA. The conversion also allows a better development enviroment for improvements. The entire Derive-SPD pipeline has been reviewed during the re-coding process and a number of minor bugs have been identified and fixed.

Improvements in the data reduction over OLP 8.4 are:

1. **Correction for reset pulse effects:**

   'Correction for reset pulse effects' is now done after 'Correction of the integration ramp for the RC time constant' rather than before.

2. **Pulse-shape correction:**

   Small detector voltage jumps are visible at SPD level which affect the calibration of SWS spectra leading to flux shifts of up to 10 Jy in the worst cases. They might have an important effect in faint sources. A correction tool has been implemented in OLP v9.5 which correct for these jumps.

   It was first believed that the pulse-shape could be corrected for with a single set of pulse-shapes (one for each detector). This was implemented for OLP Version 4.3 (using calfile 02B), but deactivated for later versions, and assumed that the effect of the after-reset pulse was constant. Since then it was learned that this is not the case and that the pulse-shape can change from observation to observation and sometimes also change within one observation.

OLP 9.5 corrects for the pulse-shape on an observation to observation basis and in some cases also on individual parts within one observations. Consequently it does not rely on a fixed type of calibration but use the data itself to do the calibration.

3. **Glitch handling:**

   Glitch handling is improved, helped also by the above modification. However, this has excacerbated the problem of glitch detection confusing gltches with spectral lines in fast AOT1 observations. This can effect both the wings and the center of the line. This effect depends on the strength of the line as well as the resolution of the grating at the wavelength of the line. An examination of the FLAG of the data product will indicate if a particular wavelength has been treated for a radiation hit ('Glitch').

   Users are recommended to read the note at:

   `http://www.iso.vilspa.esa.es/users/expl_lib/SWS/AOT1-lines.html`

4. **Slope calculation:**

   Slope calculation is improved in the case of glitches by using a model for fitting and an 'intelligent' sample skipping algorithm. For cases where the slopes contain no glitches, the slope calculation remains unchanged.

5. **Post-helium observations:**

   The post-helium observations are correctly wavelength calibrated, although not flux calibrated.

6. **Correct application of the internal calibrator data to flux calibration:**

   The application of the internal calibrator data to the flux calibration in the pipeline has been corrected to match the internal calibrator data used in the derivation of the absolute flux calibration. The net result is higher fluxes in bands 2, 3, 4 and the FP bands on the order of ∼10%, ∼5%, ∼5% and ∼5%, respectively.

In addition, the new beam profile calibration files are now available in the SWS IA and also in OSIA v2.0. The SWS pointing correction tool will be implemented as a new module later in OSIA v3.0.

4.2.2 Current calibration accuracies and 'Error Budget' for SWS

A document describing the *SWS Calibration Status* as of March 1999, still esentially valid for OLP v9.5 data products is available at:

`http://www.iso.vilspa.esa.es/users/expl_lib/SWS/SWS_Cal_Accuracy.html`

For SWS the goals originally set before the mission (an accuracy of 30% or better) have, in general, been achieved for well-behaved data sets. By well-behaved data sets we understand point sources in the several hundred to several thousand Jansky flux density range that were observed with correct pointing and suffered no instrumental or operational problems.

In Table 4.4 an overview of flux calibration accuracies of SWS OLP products as of OLP v9.5 is given as a function of the SWS band considered. The quoted 'worst' uncertainties are primarily valid for the edges of the bands, representing the maximum product of the absolute and relative spectral responsivity uncertainties.

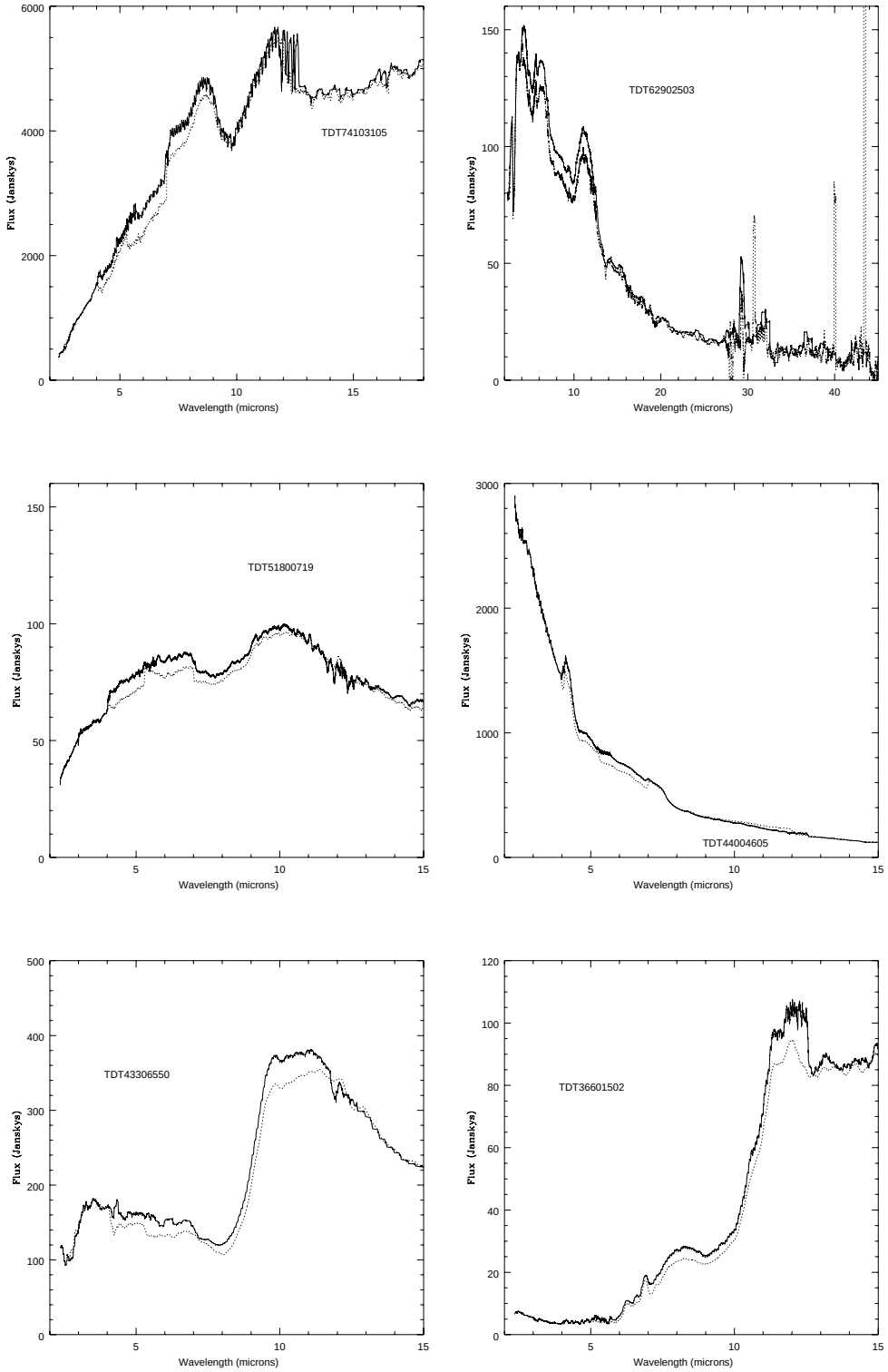

Figure 4.1: A few examples in which SWS OLP v9.5 data (solid line) is compared to SWS OLPv8.4 (dotted line). Note the systematic increase of flux around 10 microns in the new OLP calibration.

Table 4.4: Overview of the SWS bands and flux calibration accuracy as of OLP v9.5

	Band	Key wavel. μm	Grating order	Aperture number/area $''$	Detector type	Wavelength range μm	Accuracy key - worst
SW	1A	2.48	SW4	1 / 14x20	InSb	2.38 - 2.60	5% - 7%
	1B	2.87	SW3	1 / 14x20	InSb	2.60 - 3.02	5% - 7%
	1D	3.08	SW3	2 / 14x20	InSb	3.02 - 3.52	5% - 7%
	1E	3.80	SW2	2 / 14x20	InSb	3.52 - 4.08	5% - 7%
	2A	4.50	SW2	2 / 14x20	Si:Ga	4.08 - 5.30	7% - 12%
	2B	5.90	SW1	2 / 14x20	Si:Ga	5.30 - 7.0	7% - 15%
	2C	7.70	SW1	3 / 14x20	Si:Ga	7.0 - 12.0	11% - 25%
LW	3A	14.0	LW2	1 / 14x27	Si:Ga	12.0 - 16.5	11% - 25%
	3C	17.0	LW2	2 / 14x27	Si:Ga	16.5 - 19.5	11% - 20%
	3D	24.0	LW1	2 / 14x27	Si:Ga	19.5 - 27.5	12% - 20%
	3E	28.5	LW1	3 / 20x27	Si:Ga	27.5 - 29.0	20% - 30%
	4	32.0	LW1	3 / 20x33	Ge:Be	29.0 - 45.2	30% - 35%
	5A	11.8	LW3	1 / 10x39	Si:Sb	11.4 - 12.2	11% - 25%
	5B	14.8	LW2	1 / 10x39	Si:Sb	12.2 - 16.0	11% - 20%
	5C	17.0	LW2	2 / 10x39	Si:Sb	16.0 - 19.0	11% - 20%
	5D	24.0	LW1	2 / 10x39	Si:Sb	19.0 - 26.0	12% - 30%
	6	27.0	LW1	3 / 17x40	Ge:Be	26.0 - 44.5	30% - 35%

The flux reproducibility was checked during the mission by regular observations of the calibration star HR 6705. The various measurements agreed to within 6% for band 1 and 2 to 15% for bands 2 to 4.

Unfortunately, an 'error-recipe' for the combination of all the known individual error contributions to a useful overall error estimate for SWS data products does not exist yet.

The problem is that the relevance of the various error contributions depends strongly on the properties of the observed source as well as on the type of scientific analysis that is aimed for.

Thus, no 'error budget' in the true sense can be given, although it is possible to provide the user with an indication of the currently known error contributors.

Some of the known sources of error are:

Detector memory effects: Band 2 (Si:Ga) and band 4 (Ge:Be) are specially affected. Strong sources are more seriously affected (up to the 20% level). A transient correction based on the Fouks-Schubert model applicable to band 2 data will be implemented in OLP v10.0 which will bring the errors (sometimes up to 20%) down to the few percent level. The signature of memory effects is that the up- and down-scans are different in flux level. The down-scan normally succeeds the up-scan in the AOT and appears to be already 'accustomed' to the flux level. No working solution has been found yet for SWS band 4 memory effects.

Dark current problems: dark currents corrupted by memory effects or glitches usually result also in systematic differences between the up- and down-scans. For large errors in the subtracted dark current, the final spectra will resemble the spectral responsivity. Unfortunately, small dark current problems and memory effects have a similar signature in the final spectra.

Fringes: Bands 2 and 3 can be affected. The amplitude and frequency of the fringes depend on the source morphology, brightness and position in the SWS entrance aperture. Fringe amplitudes of about 5% of the continuum level are seen in band 2 and up to 20% in band 3. Fourier filtering or sine fitting can be used to remove the fringes 'manually'.

Pointing Offsets: As a consequence of the non-uniformity of the detector material and small internal misalignments, the signals in the different AOT bands are reduced by band-dependent

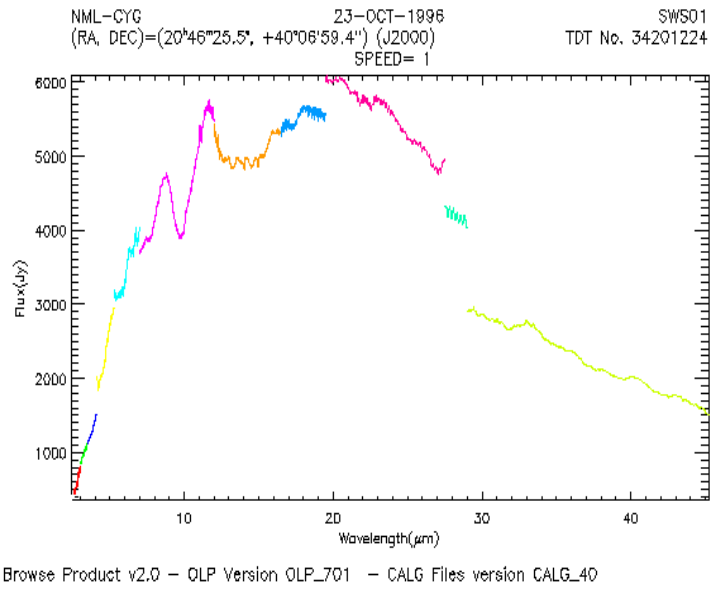

Figure 4.2: Example of the discontinuities observed in one of the bad pointed sources included in the sample. Jumps between bands are not correlated with the aperture size - Pedro García-Lario

factors when a point source is observed with a pointing offset with respect to the centre of the SWS aperture. Corrections for this effect is possible now that the detailed beam profiles have been determined and the actual satellite pointing is known with sufficient accuracy. A pointing correction tool will be available soon in SIA and later in OSIA v3.0. Pointing offsets are recognized by jumps in the continuum level at band edges in AOTs 1 and 6. In AOT 2 data the effect is very difficult to see. In some cases small offsets of just a few arcseconds can lead to 20% flux deviations.

Glitches: All SWS detector data suffer from cosmic ray hits. Some of them are removed automatically, but especially in the long wavelength bands, usually more strongly affected, the removal is far from complete. Tails following a cosmic ray hit are usual in these bands. Currently, they can only be removed manually within OSIA.

Extended sources: SWS calibration is based on point source emission. As a result, the fluxes derived are not appropriate for extended sources (partially) filling the SWS aperture. At the band edges, jumps in the signal level are seen, which are due to changes in the effective size of the detectors. To obtain reliable flux densities for extended sources, the SWS detector beam profiles should be convolved with the source structure at the appropriate wavelength. As a first order correction, the ratio of the aperture sizes can be taken.

Very weak sources: For very weak sources careful inspection of the data is required to be able to filter out data affected by glitches and determine the true dark current level, while fringes are normally insignificant. Proper calibration and analysis of such data is only possible with much manual labour.

Very bright sources: Very bright sources suffer mainly from memory effects and fringes. The data may also be affected by detector saturation which starts to become important at the several 10000 Jy level. Again, manual labour is needed to deal with such observations.

Generally, for well-behaved data sets, the use of OSIA's tools does not lead to strong improvements in the calibration with the exception of data affected by the presence of interference fringes in band 3 and, to a lesser degree, in band 2.

For data sets that are not well-behaved the quoted accuracies are not reached with standard OLP processing. However, often manual processing using OSIA tools allow to reach the same level of accuracy.

4.2.3 Future plans in SWS calibration

The correction for memory effects in band 2 based on the adapted Fouks-Schubert model, initially planned for implementation in OLP v9.5 has been defered to OLP v10. The method is able to decrease up to the few percent the error contribution for this effect.

There are also plans to update or add a large list of other modules in the SWS pipeline processing.

They are related to improvementes in: midbit correction, reset cutout length, de-biasing in band 4, AC correction, glitch treatment (including a higher order polynomial fit in the glitch detection algorithm, the extension of the search to the full reset interval and the use of a fit slope+step function) and cross-talk corrections.

Most of these changes will basically lead to a better linearization of SWS integration ramps.

Additional analysis of pre-saturation, improved error calculation and a complete re-derivation of band 2 RSRFs consistent with 'dynadark' are also foreseen, as well as improvements in de-fringing.

It is obvious that the quality of all these improvements can only be judged at the time they are implemented.

In some cases, the corrections, if available, will only be implemented as part of OSIA, but not in the pipeline. This is the case of memory effect corrections in band 4 or the point-to-extended flux conversion.

4.3 CAM

4.3.1 Improvements in OLPv9.5 for CAM

The new version 9.5 of the OLP pipeline for automatic data reduction of ISOCAM data was released on November 28. Note that this means that, as of this date, CAM data retrieved from the ISO Data Archive using the *'Latest Processing'* option will be processed either with OLP v9.5.

It contains two major changes:

1. **Fouks-Schubert correction for transients:**

   The Fouks-Schubert transient correction improves the accuracy of the photometry by correcting the LW data for transient effects. Note that the correction is very good for low contrast illumination (extended sources and/or faint sources over a high background) but still fails on point sources and strong gradient illumination.

2. **Multiresolution Median Transform Method:**

   The deglitching is now performed by using the Multiresolution Median Transform method. This method is useful to deal with glitch structures of different sizes, and particularly for structures with large dynamics and perform an efficient automatic detection (see Section 2.2.2 for a more detailed description). As the glitch structures can have different sizes, we need a multiresolution tool in order to perform efficient automatic detection. The old 'wavelet transform' used in the pipeline for de-glitching is not well adapted to treat this kind of data, due to the linearity of the transform. At a glitch position, a structure would

be detected at all scales. This is due to the high intensity of the glitch. The Multiresolution Median Transform (MMT) [Starck et al. 1998a] is an alternative to this wavelet transform.

Other algorithms remain for the time being only available under CIA, like the variable flat-field correction, various sophisticated de-glitchers, the code SLICE to remove long-term transients in CAM redundant data. or the so-called 'Faint Source treatment', a S/W package especially intended to deal with faint sources, which improves significantly the detection and photometry of sources at very low flux level.

4.3.2 Current calibration accuracies and 'Error Budget' for CAM

The latest report on CAM accuracy is contained in the *ISOCAM Calibration Accuracies Document* by Joris Blommaert and Diego Cesarsky (November 1998) which refers to OLP v7 data products (but it is still esentially valid for OLP v9.5) and it is available at:

`http://www.iso.vilspa.esa.es/manuals/CAM/accuracies/cam_accur/`

An overview of the flux accuracy of the different CAM OLP data products is given in Table 4.5 for two different brightness levels. The numbers in this Table are based on the analysis of standard stars observed in the central part of the array. Note that although polarisation observations (CAM05) are handled by the off-line software, this mode is not implemented in the standard way (i.e. not via an AOT). Then for this mode the concept of scientific validation does not apply.
A description of the known sources of error affecting CAM calibration and the corresponding 'error budget' is contained in *The ISOCAM Calibration Error Budget Report* by Andrea Biviano (November 1998), available at:

`http://www.iso.vilspa.esa.es/users/expl_lib/CAM/errdoc.ps.gz`

The following sources of error are identified:

- **Transients:** in general, the dominant error source in CAM images are transients, for which a correction has now been implemented in the pipeline based on the Fouks-Schubert model, which is only valid for extended sources (low background contrast). In general, the photometric fluxes derived in the pipeline for point sources are still found to be systematically lower than the stellar model fluxes. In particular, most of the CVF observations are usually performed after a discrete filter observation, thus implying a large decrease in the incident flux on the detector. This can introduce important transient effects that last several readouts and hence several wavelength steps which are not yet corrected for in the pipeline. The result is a larger than true flux for the first wavelength steps. We also know that transients are more important for weak sources than for bright sources and this is the most important reason for the differences in the uncertainties quoted in Table 4.5.

Table 4.5: ISOCAM Photometric Calibration Accuracy Overview.

CAM AOT	> 100 mJy key	> 100 mJy worst	<100 mJy
CAM01	10%	20%	30%
CAM03	10%	20%	30%
CAM04	15%	40%	40%
CAM05	n.a.	n.a.	n.a.

- **Glitches:** the contribution of glitches to the overall noise of CAM images is also important. 'Common' glitches are associated to impacts of cosmic ray electrons while the so-called 'faders' and 'dippers' are linked to impact of protons or α particles. Tipically, 'common' glitches are easy to remove while the rare 'faders', followed by a slow decrease of the signal, and 'dippers', followed by a reduction in the sensitivity of the affected pixel, have a long lasting effect more difficult to remove. Unfortunately, only a fraction of them are detected in the pipeline and automatically removed and manual processing with CIA is needed.

- **Point Spread Function:** the fluxes for point sources in the CPSL (CAM Point Source List) FITS file are derived by PSF-fitting in the image. This photometry can be affected by larger errors than stated in Table 4.5 if the fitting is incorrect. The observed PSF is generally quite close to the theoretical one if the ghost contribution is not significant (see below). However, the accuracy of the PSF does not allow deconvolution yet.

- **Ghosts:** CVF observations might be affected by the existence of 'ghosts' generated by multiple reflections between the detector and the CVF surface. Ghosts can appear away from the source image but may as well fall onto (and surround) the sky image, depending on the actual position of the source on the detector. In some cases, the photometric accuracy can be affected up to 35% by the presence of ghosts, and straylight from sources outside the theoretical field of view can also affect CVF images so that sources with a flux below 10% of the background might not be detectable.

- **Flat-field:** because of wheel-jitter the 'library' flat-field may not cover the same detector region as the sky image does. The effect is small in the central region of the array where the uncertainty is less than 1%. The uncertainty becomes, however, very large in the edges (up to a factor of 5 in extreme cases), where vignetting is important (for example in the case of a $6''$ p.f.o.v. measurement). Incomplete stabilization is another issue to consider. A large part of the small residual error in the flat-field observations is probably due to this effect. In any case, the noise levels reached are lower than expected pre-launch (1% in LW and 3% in SW).

Other error contributors like saturation, read-out, gain accuracy, dark current stability are also discussed in the 'error budget' document above refered. A summary of the main conclusions is displayed in Table 4.6.

Regarding flux reproducibility, repeated photometric observations on HIC 89474 throughout the whole ISO lifetime give a standard deviation of around 2% for both LW and SW detectors. Similar observations on a larger set of absolute flux calibration standards give an r.m.s. of around 5%. It was also found that the LW detector is very linear over a very large range of flux levels from a few mJy up to the saturation level. From CVF observations the derived r.m.s. is 3% for the SW part and 4% for the two LW CVF segments.

Significant improvements in the photometric accuracy of ISOCAM data can be achieved by making use of the software tools implemented in CIA, the Interactive Analysis software package for ISOCAM data reduction.

Deglitching routines are available under CIA although they only mask the frames corresponding to the glitches. Thus, a visual inspection of all pixels histories is needed for a proper masking. The impact of 'faders' and 'dippers' is related to the general problem of the transient behaviour of the CAM detectors and can be corrected using transient correction algorithms implemented in CIA, based on the so-called 'IAS method' (for LW detectors).

Manual elimination of ghost images, which can in some cases lead to errors up to 35% in aperture photometry, is also possible with CIA, as well as the elimination of inaccuracies introduced by

Table 4.6: ISOCAM photometric calibration error budget.

Noise origin	magnitude	after correction
Stabilization (random)	10 x sky noise	2 x sky noise
Stabilization (systematic)	40% of source flux	15% of source flux
Saturation	≥30% decrease in responsivity	
Read-out noise	LW: 0.7 ADU/g	
	SW: 2 ADU/g	
Gain	0.15% output current	
Dark current	LW: 0.5 ADU/g	0.25 ADU/g
	SW: 0.5 ADU/g	
Flat-field	LW: 0.5% (high background)	
	SW: ≤ 1%	
Conversion signal→flux	5%	
Point Spread Function	20%	few%
CVF RSF	3%	
Ghosts	≤35%	
Straylight	10% of sky flux	

inaccurate flat-fields, at least in the case of rasters with sufficient background and redundancy (not possible, however, for staring observations yet).

In summary, the magnitude of all the above effects compared to pre-launch expectations are generally in good agreement. Note that in Table 4.5 the 5% accuracy quoted as error induced by the conversion factor from ADU/g/s to Jy is worse than the pre-launch value (2%) because the measured photometry is PSF corrected, so this error estimate includes also the uncertainty in the PSF.

The CVF Spectral Response Function (SRF) is very well constrained. Typically the accuracy is at the 3% level on average in the absence of ghosts and straylight.

4.3.3 Future plans in CAM calibration

The expected accuracies of ISOCAM's final OLP data products will strongly depend on whether ways are found to transfer into the pipeline some of the calibration tools which are currently under development and/or only available under CIA.

In many cases, this will probably not be possible, either because there is no time left for coding the new calibration results (transients in point sources, ghosts model) or because they are tools which require a high degree of interactivity and, thus, it is not easy to make them available in an automated pipeline (mostly those currently available in CIA, such as the various de-glitchers or the SLICE S/W package mentioned above).

Concerning calibration issues which are still under investigation like the transient correction for point sources or the recognition of ghosts and the creation of a ghosts correction matrix, it is assumed that any progress will come too late for its inclusion into OLP v10.0. Should these algorithms become available in time, then their inclusion will become a high priority item but, in principle, they are foreseen only for implementation in CIA at a later stage.

Concerning the tools which are at the present time only available under CIA, it is well known, for instance, that several de-glitching methods under test could also improve significantly the calibration accuracy of CAM maps and point/extended source detection, as well as PSF fitting, which may affect the photometry substantially. And it is also well known that the SLICE S/W

package is giving excellent results when applied to extended faint sources in highly redundant CAM raster maps reducing the errors up to the limits imposed by read-out and photon noise equivalent to 100-200 μJy. Again, the problem here basically resides in how to make all these tools available in the CAM pipeline.

There are several areas where improvements are expected in version 10.0 of the CAM pipeline, like: inclusion of final sensitivity Cal-G files, sensitivity errors, a refined version of the 'faint source treatment' package, astrometric correction, flat-field corrections taking the lens-wheel jitter into account, treatment of flat/dark observations and mosaic generation.

4.4 LWS

4.4.1 Improvements in OLPv8.7 for LWS

As of December 1999, a new version (v8.7) of the LWS OLP pipeline for automatic data reduction was released. Currently, when LWS data is retrieved from the ISO Data Archive and the *'Latest Processing'* button is selected, the user gets the data processed with OLPv8.7. Note that in the case of LWS there will be not an OLP v9 version of the pipeline, the next version to be released being the final OLP v10, on which all efforts are now concentrated.

One of the most important changes introduced in version 8.7 of the pipeline was that data products were derived using a new Uranus model in the LWS calibration files. The effect of the new model is that for a source decreasing in flux from short to longer wavelengths, the spectrum of this source is now 'flatter' in detectors SW1 and SW2. With the new model, both the RSRF and photometric calibration have been re-derived.

The photometric calibration of SW1, however, has been slightly degraded in the centre of the detector i.e. this is 10% higher than before as more of the detector was used to set the level. The photometric level of SW1 will be updated soon to replace it back to the OLP v7 level. The photometric levels of the other nine detectors remains the same as for OLP v7.

On checking all observations of Uranus against the model, a 'problem' has been found in the data. This has the effect that detectors SW1 and SW2 appear tilted down at short wavelengths and up at long wavelengths. This tilt has been noted for all observations after the LWS was switched off in the period corresponding to revolutions 380−442. Before this period the slope follows the model. This may indicate a change to the RSRF of these detectors during the switch off period but further investigation is needed before definitive conclusions can be made.

In addition, the OLPv8.7 LWS Fabry-Pérot products from AOTs LWS03 and LWS04 show a marked improvement in the flux calibration in comparison to their OLP v7 counterparts. As a consequence of this, the LWS04 mode was scientifically validated.

In OLP v7 the Fabry-Pérot LSAN file gave the flux per spectral resolution element (in units of W cm^{-2}). In OLP v8.7 the units will be W cm^{-2} μm^{-1}, where the throughput correction (i.e. the Fabry-Pérot transmission multiplied by the Fabry-Pérot resolution element) has been performed using Mars as calibrator.

The other noteworthy change in OLP v8.7 is that fixed dark currents are subtracted for all Fabry-Pérot observations, rather than those measured during the observations themselves. These fixed set of detector dark currents originate from a series of dedicated measurements made in revolution 650.

Other minor changes were just oriented to ensure that LWS data will be Y2K compliant.

4.4.2 Current calibration accuracies and 'Error Budget' for LWS

A document describing the *LWS Calibration Status* as of November 1998 is available at:

Table 4.7: Flux calibration accuracy of LWS OLPv8.7 data products per AOT

		LWS01 Grating	LWS02 Grating	LWS03 Fabry-Pérot	LWS04 Fabry-Pérot
Point sources	Bright	30%	30%	Unvalidated	n.a.
	Medium	10%	10%	Unvalidated	n.a.
	Faint	50%	50%	Unvalidated	n.a.
Extended sources	Bright	50%	50%	Unvalidated	n.a.
	Medium	30%	30%	Unvalidated	n.a.
	Faint	50%	50%	Unvalidated	n.a.

`http://www.iso.vilspa.esa.es/users/expl_lib/LWS/LWS_Cal_Accuracy.html`

Although this report is based on OLPv7 data products, most of its content is still valid for OLP v8.7 data.

A summary of the main accuracy numbers is displayed in Table 4.7 as a function of the AOT and the brightness of the source observed. Note that the concept of 'bright', 'medium' and 'faint source depends on the observing mode. For the grating modes a 'bright' source means typically more than 1000 Jy at 120μm, while 'faint' could be a source with a flux density in the order of 10−50 Jy at 120μm. For the Fabry-Pérot modes these numbers have to be multiplied by a factor of 10 at least.

Some of the known sources of error affecting LWS grating observations are:

Dark current subtraction and memory effects: this especially affects spectra of faint sources. There is evidence that observation of a bright source before a faint one caused the dark current to be higher than expected and to be decaying during the subsequent observation. In addition, dark current variations have been observed within Fabry-Pérot measurements which are presently not fully understood.

Fringes: channel fringing is seen on the measured spectra of extended or off-axis point sources. Extensive modeling of the response of the instrument has been carried out using the ASAP optical design software showing that the fringes are produced by the interference between the reflecting surface of the LWS field mirror and its support structure as the diffraction pattern of the source falls off the edge of the field mirror itself. A quantitative model, however, is not yet available that would allow the removal of the fringes given knowledge of the spatial structure of the source. Instead, a method has been developed which performs a fit for the period, amplitude and phase of the sinusoid and removes it from the spectrum by division or subtraction.

Beam profile: the pipeline processing of LWS data makes no attempt to correct for the beam shape of the instrument. A model for the core of the beam profile has been obtained using spectra of Mars located at different positions with respect to the axis of the LWS as a function of wavelength. The observations show that the FWHM of the esentially gaussian beam profiles obtained are ∼20% narrower than expected and assymetries and fringes are present in the wings. With the availability of the new model, it is now possible to convert from point source fluxes (Jy) to extended source fluxes (MJy sr^{-1}).

Non-linearity effects: Bright sources cause some of the detectors to become non-linear. The problem is complicated by photon curing of the detectors; this, in turn, causes the responsitivity of the detectors to change. An empirical method has been developed and implemented in the pipeline for the derivation of the photocurrent, and hence flux, from the voltage ramps which fits a first or second order polynomial automatically with no *a priori* assumptions about how the detectors respond, reducing the noise in the output spectra.

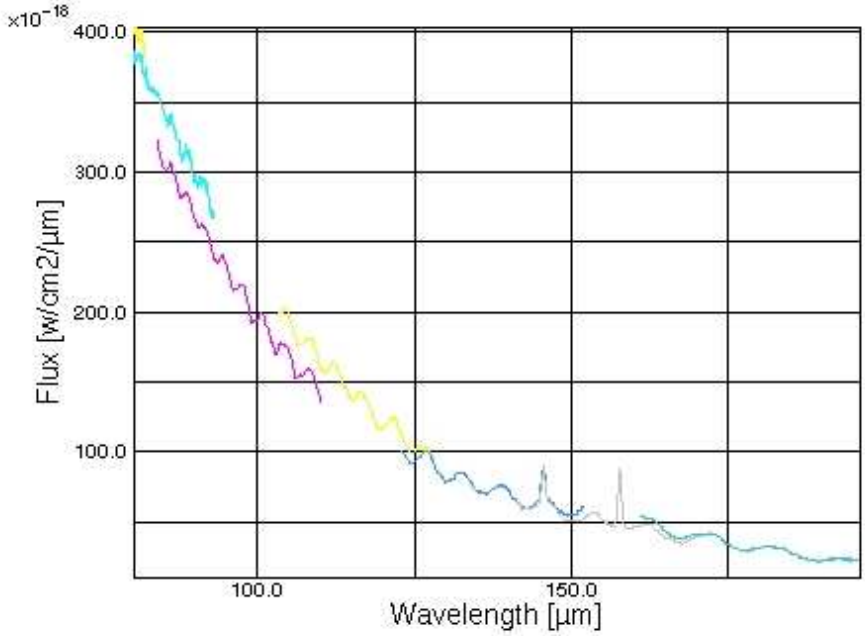

Figure 4.3: *Example of fringes detected in the LWS spectrum of a bright extended source*

Time constants: The time constants of the detectors cause the shape of the spectrum (both lines and continuum) to be distorted under certain illumination conditions.

Poor order sorting: Spectra below 50 μm and between 83 and 90 μm might suffer from contamination owing to poor order sorting. An instrument model is required that will allow the determination and removal of the contamination.

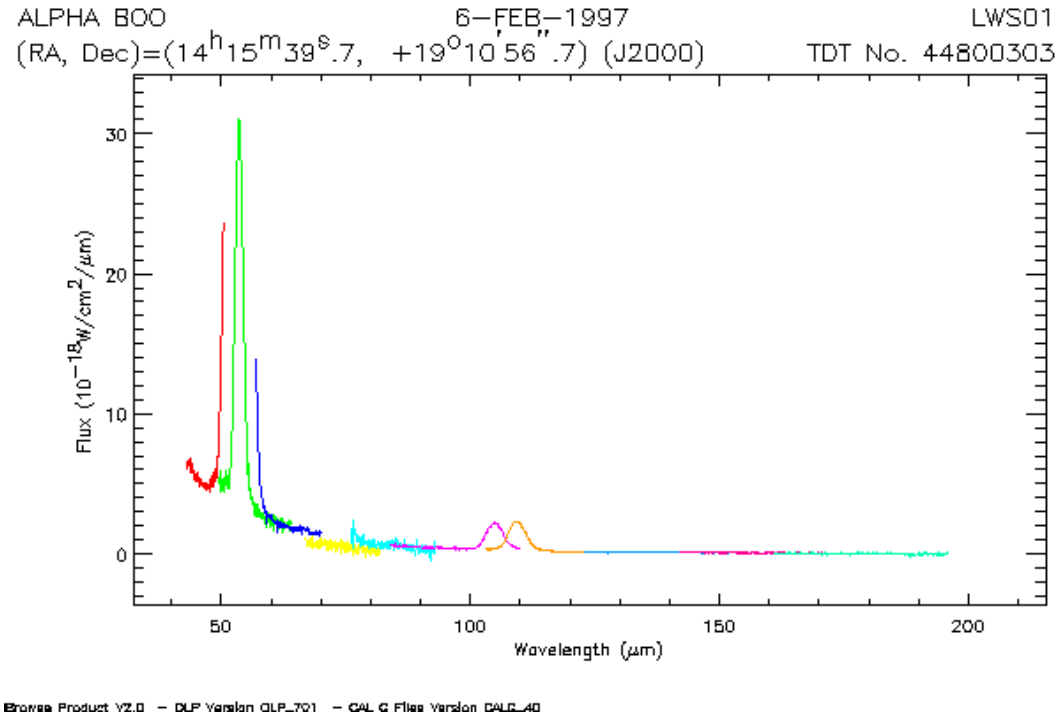

Figure 4.4: *Example of near infrared leaks in the LWS spectrum of Arcturus*

Despite the significant advances achieved in the understanding of the Fabry-Pérot modes, some problems still remain to be addressed. These include:

Line asymmetry: The line profiles observed using AOT LWS04 are generally asymmetric, with the long wavelength wing at a higher level than the short wavelength one. This phenomenon is partially attributed to memory effects, also present in grating spectra. Various methods for removal of transient effects are being investigated. The effect on line flux depends on the line-to-continuum ratio. For example, for a line with no continuum, the line flux can change by as much as 30%. The effect on the velocity shift is relatively small (about ± 3 km s^{-1}). It is also possible that some of the profile asymmetry observed may well be due to loss of parallelism as the Fabry-Pérot line is scanned.

Velocity shifts: There appears to be a discrepancy in the measured and expected velocity shifts in LWS04 lines of up to ± 30 km s^{-1}, depending on the actual line being observed. At present the cause for this discrepancy is not known and is under investigation.

Removal of grating profile: Note that in the Fabry-Pérot modes, the problem with the underlying grating profile is not yet still fully solved. Removal of the grating response profile is complicated by the fact that the grating position is not known sufficiently accurately. This can result in a skewed spectrum. The user is recommended to refer to FP_PROC, the LWS Interactive Analysis (IA) Fabry-Pérot processing tool which removes the grating profile. For LWS04 spectra the user can remove the skewness interactively, thereby deducing the actual grating position. For LWS03 observations, a least-squares fitting algorithm which minimizes the residuals in the overlap regions of spectra at adjacent grating positions is employed. The effect of not removing the grating profile on Fabry-Pérot line fluxes from LWS04 observations is likely to be very small, and this is why this mode was scientifically validated in v8.7 of the pipeline. However, for continuum fluxes in LWS03 observations the effect may not be negligible and is expected to be a function of the Fabry-Pérot scan extent.

The calibration accuracy of products manually processed with LIA does not strongly improve for the grating observing modes LWS01 and LWS02 for well-behaved data sets. The only changes expected concern LWS03 and LWS04. For bright sources observed with these AOTs there is an excess component in the signal that is most likely due to straylight.

A discussion on the individual contribution to the LWS photometry 'error budget' coming from the different steps involved in LWS data processing is contained in the document: *In-orbit performance of the ISO Long Wavelength Spectrometer* by Bruce Swinyard et al. (October 1998), available at:

`http://www.iso.vilspa.esa.es/users/expl_lib/LWS/HAWAII.PS`

Assuming a mean uncertainty in the Uranus model of $\sim$5% and a statistical error on the RSRF better than 0.01, for observations where the dark current is not a significant contribution to the signal, the uncertainty contributed to the measurement by the calibration process is estimated to be of the order of 7% for most detectors. In the case of faint sources, when the dark current becomes significant, the uncertainty in the measurement of the dark current begins to dominate.

Long term monitoring has shown that the reproducibility of the flux calibration is within 10% for all objects not influenced by the uncertainty in the dark current measurement.

For LWS the goals originally set before the mission (an accuracy of 30% or better in the grating mode and 50% in the Fabry-Pérot mode) have in most cases been achieved for well-behaved data sets. In some areas, however, problems remain and they are the subject of further investigation.

4.4.3 Future plans in LWS calibration

In the case of LWS, as it has already been mentioned, it was decided that there will be no more pipeline version releases until the final one (OLP v10.0), expected in February 2001.

Meanwhile, the flux calibration accuracy of LWS is expected to improve significantly during the remaining post-operational phase.

Among the areas where improvements are expected in LWS calibration are:

- Drift correction
- RSRF changes before/after switch-off in revolutions 380−442
- Illuminator flash processing (new functionality)
- Strong source correction
- Intelligent Dark Current Subtraction (new functionality)
- Uranus/Mars models
- Glitch detection
- Fabry-Pérot wavelength calibration (velocity correction)
- LWS03 Fabry-Pérot observations
- Beam profile Cal-G files
- Uncertainty calculation
- Dark Current fixed values

Solutions to other calibration problems are expected to be implemented only in LWS IA, like for:

- Transient correction
- Defringing
- Fabry-Pérot RSRF
- Straylight correction in Fabry-Pérot modes
- Grating profile removal from LWS03

Other LWS calibration items will only be documented, like the known problems with spurious features, filter leaks or the ghosts observed in Fabry-Pérot spectra.

Acknowledgements: Many people working at the ISO Data Centre and at the National Data Centres have contributed to the results here presented. They are too numerous to name individually but the improvements in ISO calibration would have never been possible without their enthusiastic dedication to the Project.